

University of Windsor

Scholarship at UWindor

Electronic Theses and Dissertations

Theses, Dissertations, and Major Papers

1-1-1974

Inelastic collisions of excited atoms at thermal energies: Studies of sensitized fluorescence of rubidium and cesium using a pulsed dye laser.

Paul W. Pace
University of Windsor

Follow this and additional works at: <https://scholar.uwindsor.ca/etd>

Recommended Citation

Pace, Paul W., "Inelastic collisions of excited atoms at thermal energies: Studies of sensitized fluorescence of rubidium and cesium using a pulsed dye laser." (1974). *Electronic Theses and Dissertations*. 6114.

<https://scholar.uwindsor.ca/etd/6114>

This online database contains the full-text of PhD dissertations and Masters' theses of University of Windsor students from 1954 forward. These documents are made available for personal study and research purposes only, in accordance with the Canadian Copyright Act and the Creative Commons license—CC BY-NC-ND (Attribution, Non-Commercial, No Derivative Works). Under this license, works must always be attributed to the copyright holder (original author), cannot be used for any commercial purposes, and may not be altered. Any other use would require the permission of the copyright holder. Students may inquire about withdrawing their dissertation and/or thesis from this database. For additional inquiries, please contact the repository administrator via email (scholarship@uwindsor.ca) or by telephone at 519-253-3000ext. 3208.

INELASTIC COLLISIONS OF EXCITED ATOMS AT THERMAL
ENERGIES: STUDIES OF SENSITIZED FLUORESCENCE OF
RUBIDIUM AND CESIUM USING A PULSED DYE LASER

by

Paul W. Pace

A Dissertation

Submitted To The Faculty of Graduate Studies Through
The Department of Physics In Partial Fulfillment of The
Requirements For the Degree Of Doctor of Philosophy At

The University of Windsor

Windsor, Ontario

1974

UMI Number: DC52695

INFORMATION TO USERS

The quality of this reproduction is dependent upon the quality of the copy submitted. Broken or indistinct print, colored or poor quality illustrations and photographs, print bleed-through, substandard margins, and improper alignment can adversely affect reproduction.

In the unlikely event that the author did not send a complete manuscript and there are missing pages, these will be noted. Also, if unauthorized copyright material had to be removed, a note will indicate the deletion.

UMI®

UMI Microform DC52695

Copyright 2009 by ProQuest LLC.

All rights reserved. This microform edition is protected against unauthorized copying under Title 17, United States Code.

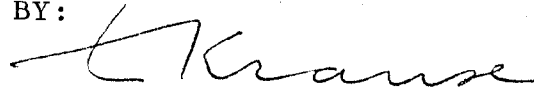
ProQuest LLC
789 E. Eisenhower Parkway
PO Box 1346
Ann Arbor, MI 48106-1346

ABH 8553

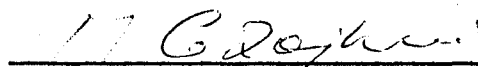
© Paul W. Pace 1974

531900

APPROVED BY:



Dr. L. Krause



Dr. M. Czajkowski



Dr. J.B. Atkinson (Chairman)



Dr. R.N. Zare (External Examiner)

ABSTRACT

An organic dye laser has been employed to investigate the $^2P_{1/2} \leftrightarrow ^2P_{3/2}$ excitation transfer processes in the second excited states of the alkali metals rubidium and cesium induced by collisions with ground state atoms of the same type. In preparation for the investigation, a study of various dye laser systems is made. The rate equations for the dye laser molecular state densities and mode photon densities are set up for a flashlamp and a nitrogen laser pumped tunable dye laser. These are solved numerically and the results are compared with the experimental measurements. A method is presented for measuring the intensities of resonance and sensitized fluorescence using a pulsed nitrogen laser pumped dye laser. The alkali vapour densities were kept sufficiently low to enable the cross sections for the mixing processes to be determined under single collision conditions and to ensure that radiation trapping and quenching effects were negligible.

The alkali vapour was irradiated with each component of the 2P doublet in turn and measurements of the relative intensities of the fluorescence yielded the following cross sections:

$$\begin{aligned} \text{Rb: } Q_{12} (^6^2P_{1/2} \rightarrow ^6^2P_{3/2}) &= 245 \pm 39 \text{ \AA}^2 \\ \text{Rb: } Q_{21} (^6^2P_{1/2} \leftarrow ^6^2P_{3/2}) &= 163 \pm 26 \text{ \AA}^2 \\ \text{Cs: } Q_{12} (^7^2P_{1/2} \rightarrow ^7^2P_{3/2}) &= 121 \pm 15 \text{ \AA}^2 \\ \text{Cs: } Q_{21} (^7^2P_{1/2} \leftarrow ^7^2P_{3/2}) &= 107 \pm 13 \text{ \AA}^2 \end{aligned}$$

These results are consistant with the empirical relationship between the magnitude of the cross sections and the fine structure splitting that has previously been determined for the alkalis. Measurements indicate that the dye laser excitation system produces high signal-to-noise ratios and much improved sensitivity over previous methods.

ACKNOWLEDGEMENTS

I am most grateful to Dr. J.B. Atkinson for his supervision of this work and for his reading of this dissertation in manuscript. I should also like to express my gratitude to Dr. L. Krause for his advice and support throughout the course of this work.

Special thanks are due to Mr. B. Masse and to Mr. D. Clarke for their expertise in designing and in maintaining the necessary electronic equipment and for valuable technical advice. Acknowledgements are due to Mr. R.G. Campbell for his skill in construction of the glassware, to Mr. A. Buzzeo for his assistance in the preparation of some of the diagrams found in this dissertation and to Mr. W. Grewe and the machine shop staff who constructed the intricate pieces of the apparatus.

To the National Research Council of Canada I am grateful for financial assistance in the form of a graduate scholarship.

To my fellow graduate students and to the postdoctoral fellows and staff of the physics department with whom I have been associated, I express thanks for many stimulating and instructive discussions.

TABLE OF CONTENTS

	PAGE
ABSTRACT	iii
ACKNOWLEDGEMENTS	v
LIST OF FIGURES	viii
LIST OF TABLES	x
I. INTRODUCTION	1
II. ORGANIC DYE LASERS	5
1. Properties of Organic Dyes	8
2. The Dye Laser Rate Equations	11
3. Tuning Mechanisms	16
4. Calculated Results	19
(a) Long Pulse Excitation Results (Flashlamp-Pumped)	21
(b) Short Pulse Excitation (Laser-Pumped)	26
5. The Flashlamp-Pumped Dye Laser	30
(a) The Flashlamp Circuit	33
(b) The Optical Pumping Cavity	37
(c) The Flashlamp-Pumped Dye Laser Configuration	40
(d) Experimental Data	41
6. The Nitrogen Laser	44
(a) The Rate Equations For The Nitrogen Laser	45
(b) General Description Of The Nitrogen Laser	49
(c) Mechanical Construction Of The Laser	50
(d) Electrical Construction Of The Laser	53
(e) Operation And Performance	57

	page
7. The Nitrogen Laser Pumped Dye Laser	60
(a) General Description	62
(b) The Dye Laser Amplifier	64
(c) Output Mirror And Beam Expansion Telescope	65
(d) The Diffraction Grating	67
(e) Operation And Experimental Data	68
III. TRANSFER OF ELECTRONIC EXCITATION BETWEEN THE $6^2P_{3/2}$ AND THE $6^2P_{1/2}$ STATES OF RUBIDIUM AND THE $7^2P_{3/2}$ AND THE $7^2P_{1/2}$ STATES OF CESIUM INDUCED BY COLLISIONS WITH GROUND STATE ATOMS OF THE SAME TYPE	71
1. Theoretical	71
2. Experimental	83
(a) Description Of The Apparatus	83
(b) The Pulse Counting System	88
(c) Counting Limitations	93
(d) Experimental Procedure	97
3. Results And Discussion	102
IV. CONCLUSIONS	113
APPENDICIES	
A Experimental Data	117
BIBLIOGRAPHY	120
VITA AUCTORIS	128

LIST OF FIGURES

	PAGE
1. The Dye Laser Energy Levels	9
2. The Tuned Dye Laser Lineshape At Different Times During The Laser Pulse	22
3. The Tuned Dye Laser Normalized Lineshape	23
4. The Dye Laser Linewidth As A Function Of The Peak Output Power	24
5. The Untuned Dye Laser Lineshape At Different Times During The Pulse	27
6. Lineshape Of The Laser Pumped Dye Laser	29
7. Circuitry Of The Flashlamp Pumped Dye Laser	35
8. The Flashlamp And Dye Laser Configuration	38
9. Flashlamp Pumped Dye Laser Output	42
10. Energy Levels Of The Molecular Nitrogen Laser	46
11. The Nitrogen Laser Charging And Firing Circuit	51
12. The Molecular Nitrogen Laser	52
13. Circuitry Of The Thyatron Pulser	54
14. The Thyatron Pulser Power Supply	55
15. The Nitrogen Laser Output Pulse	58
16. Nitrogen Laser Output Power As A Function Of The Nitrogen Pressure	59
17. The Nitrogen Laser Pumped Tunable Dye Laser	63
18. Nitrogen Laser Pumped Dye Laser Temporal Lineshape	70
19. Energy Level Diagram For Rubidium And Cesium	72
20. Schematic Diagram Of The Experimental Apparatus	84
21. The Detection And Counting Apparatus	90
22. The Power Supply, AND Gate and Timer Circuitry	91

23. Plot Of The Intensity Ratios Against Density For Rubidium	103
24. Graph Of The Intensity Ratios Against Density For Cesium	104
25. Variation Of The Alkali-Alkali Cross Sections With Energy Splitting ΔE	109
26. Fluorescence Lines Using The Pulsed Dye Laser Excitation	111

LIST OF TABLES

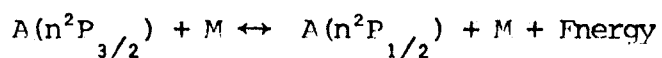
	page
1. The Alkali-Alkali Collision Cross Sections	108

I. INTRODUCTION

In recent years, collisionally induced excitation transfer between various atomic and molecular states has been the subject of a number of experiments. These inelastic processes are of a fundamental and practical nature, as they directly influence the understanding of systems such as gas lasers, stellar atmospheres, the earth's atmosphere and gas plasmas. In these systems, atoms and molecules are continually being excited and de-excited by the absorption and the emission of radiation and by atomic and molecular collisions. To understand such systems it is essential to have a knowledge of the cross sections for the various collisional processes. Such a knowledge also provides a basis for the testing of various theoretical models of the collisions.

Among the many possible atomic and molecular systems, collisionally induced excitation transfer between the fine-structure doublets of the alkali metals has probably been studied the most thoroughly. The 2P fine structure states of the alkalis are particularly suitable for the study of energy transfer collisions since they are connected to the ground state by optically allowed transitions. In addition, the energy splitting between the states ranges from essentially zero in the higher excited states to 554 cm^{-1} in cesium. This allows the influence of the energy splittings on the excitation transfer processes to be evaluated.

The collisional energy transfer process may be represented by the following:



where A is an alkali atom and M the collision partner, may be an atom or a molecule. Basically the experimental procedure consists of selectively exciting one of the alkali fine-structure states and then measuring the relative intensities of the fluorescence emitted from various excited states. The fluorescence component having the same frequency as the exciting light is called the resonance fluorescence, while the other frequency components emitted by states populated by collisional excitation transfer constitute sensitized fluorescence. The ratio of the intensities is a measure of the population ratio and by solving the collisional rate equations, the cross sections for the collisional processes may be extracted from the measurements. Previous measurements of the cross sections for the first excited states has been accomplished in the cases where M is an inert gas (Krause 1966, Pitre and Krause 1967, Gallagher 1968), a diatomic or a polyatomic molecule (Stupavsky and Krause 1968, Stupavsky and Krause 1969, McGillis and Krause 1968, Baylis et al 1973) or a ground state alkali atom of the same or different type (Krause 1966, Pitre and Krause 1968, Hrycyshyn and Krause 1969).

Collisionally induced excitation transfer between fine-structure states higher than the first resonance states has also begun to be studied experimentally. For the cases where M is an inert gas the cross sections have been measured for the second excited states of

cesium (Siara et al 1974, Cuvellier et al 1973), the third excited states of cesium (Pimbert 1972) and the second excited states of rubidium (Siara et al 1972). Cases where M is a molecule have been measured for the second excited states of rubidium (Siara and Krause 1972a) and the third excited states of cesium (Rocchiccioli 1972), and cases where M is a ground state atom of the same type for the third excited states of cesium (Pimbert 1972). These processes have been studied theoretically by a number of authors and agreement with the experimental results depends mainly on the colliding partner.

In all cases except the experiments of Cuvellier and Pimbert the excitation of the fine-structure levels has been by optical absorption from a radio-frequency or a micro-wave frequency excited lamp containing the alkali of interest together with an inert buffer gas. A detailed description of this type of lamp is given by Phaneuf (1970). For the third excited states of cesium, there is a fortuitous overlap of the cesium resonance line and the 388.8 nm line of helium, while a flashlamp pumped dye laser was used to excite the second excited states of cesium in the studies of Cuvellier et al (1973). The technical difficulties associated with these measurements have been discussed by Pimbert (1972) and Cuvellier (1973). Work with higher excited states using previous techniques is even more difficult for three reasons. Firstly, the intensities of the exciting spectral lines from the resonance lamps are much lower than the intensities of the first excited state resonance lines. Secondly, the absorption coefficients for the transitions to the higher excited states

are much smaller than that for the first excited states. Both these factors give rise to much smaller excited state populations than that for the first excited states. Thirdly, the smaller spectral separation of the lines increases the problems of adequate spectral resolution. The decrease in the absorption coefficient does delay the onset of radiation trapping to higher alkali densities, but care must still be taken to avoid radiation trapping.

In the present investigation, excitation transfer between the $6^2P_{1/2}$ and the $6^2P_{3/2}$ fine-structure states of rubidium atoms and the $7^2P_{1/2}$ and the $7^2P_{3/2}$ fine-structure states of cesium atoms, induced by collisions with ground state atoms of the same type, has been studied using the method of sensitized fluorescence. To excite the alkali atoms to the second excited states, a nitrogen laser pumped organic dye laser was used.

The first section of this report will discuss the theory and practice of constructing a suitable dye laser system and the second section will discuss the theoretical and the practical considerations necessary when using the dye laser as an excitation source for a sensitized fluorescence experiment. The results of the measurements indicate that the good spectral resolution and improved intensity of the dye laser over resonance lamp sources allows the accurate measurements of extremely low sensitized to resonance intensity ratios which exist when M is a ground state alkali atom of the same type as A. The results of the cross section measurements will be presented and suggestions for further research are given.

II. ORGANIC DYE LASERS

Many organic compounds exhibit very efficient luminescence, making their use as laser materials very attractive. Initial experiments proved disappointing and as a result, interest declined. However within the past few years the production of coherent, visible and near infra-red radiation by fluorescent organic dyes in solution has been demonstrated. The device based upon this phenomenon is called the organic dye laser. The purpose of this section will be to discuss the theory of dye laser operation and to review flashlamp-excited and laser-excited organic dye lasers.

The organic dye laser is to be distinguished from the inorganic liquid laser which is based upon the rare earth ions in liquid solvents. The properties of the inorganic liquid laser have been reviewed by Lempicki and Sammelson (1966) and by Heller (1968,1968a).

The earliest suggestions that organic materials could be made to lase were proposed by Brock et al (1961) and by Rautian and Sobel'mann (1961). They proposed that triplet state phosphorescence could serve as the mechanism for the organic laser. In 1964 Stockman et al advanced the idea of a laser process based upon the singlet state fluorescence. The first laser action from organic dyes was reported by Sorokin and Lankard (1966). These authors used a giant pulse ruby laser to excite solutions of chloroaluminum phthalocyanine and 3,3' diethylthiadacarbocyanine iodide (DTTC) placed in an optical cavity. Similar results were obtained by Schäfer et al (1966) and by Spaeth and Bortfield (1966) using cyanine dyes

with structures similar to DTTC.

Using the results from these laser-pumped dye lasers, Sorokin et al (1967) suggested that a flashlamp could also be used to excite organic dye lasers and estimated the flashlamp requirements. A suitable flashlamp was built and laser emission from solutions of several dyes of the xanthene class was reported by Sorokin and Lankard (1967a) and by Schmidt and Schäfer (1967). Flashlamp excited dye lasers have since been studied in many laboratories.

Continuous wave operation of organic dye lasers was first achieved by Peterson et al (1970) using rhodamine 6G excited by an argon-ion laser. A summary of CW dye laser configurations is given by Hercher and Pike (1971). Laser excited dye lasers have also been reported using a frequency doubled neodymium:glass laser as the excitation source (eg. Bradley et al 1971). Pulsed molecular nitrogen lasers have also been used as dye laser excitation sources by Capelle and Phillips (1970), Broida and Haydon (1970) and by Myer et al (1970, 1970a).

One of the most useful properties of the organic dye laser is its tunability. This occurs because the spectral width of the fluorescence is large enabling the lasing wavelength to be tuned to any desired value within a reasonably wide range. Furthermore, the number of fluorescent dyes is large and compounds may be selected for emission in any given region of the visible spectrum and near IR spectrum. Thus the dye laser is truly the first tunable laser to operate throughout the entire visible spectrum.

As a result of these developments, the organic dye laser is

proving to be one of the most powerful tools available in atomic and molecular spectroscopy. In particular, the techniques of fluorescence and saturation spectroscopy have permitted precision spectral measurements to be made on atomic sodium (Hänsch et al 1971a), and an accurate determination of sodium concentrations in the laboratory (Hänsch et al 1972) and in the atmosphere (Kuhl and Marowsky 1971) has been accomplished. In these experiments, as in all experiments involving optical excitation, a knowledge of the lineshape of the excitation source is necessary for a correct interpretation of the data. A theoretical model that predicts the spectral and temporal lineshapes of the organic dye laser will be presented. This model will then be used to calculate the expected results for a typical flashlamp pumped dye laser and for a nitrogen laser pumped dye laser. The results of these calculations will then be compared with the experimental data.

1. PROPERTIES OF ORGANIC DYES

An energy level diagram, characteristic of an organic dye molecule, is shown in figure 1. The electronic ground state of the molecule is a singlet state, designated as S_0 , which spans a range of energies determined by the quantized vibrational and rotational excitation of the molecule. The energy between the vibrational states, indicated in figure 1 by heavy horizontal lines, is typically 1400 to 1700 cm^{-1} (Snively 1969). The energy spacing between the rotational levels is smaller by a factor of 100. The collisionally broadened rotational levels, therefore, essentially provide a near continuum of states. Each excited state of the molecule consists of a similar broad continuum of states, and optical transitions between all these states give rise to the characteristic broad absorption spectra. Allowed radiative transitions can occur between the singlet pair and between the triplet pair. A disallowed radiative transition between the lowest triplet state, which is metastable, and the ground singlet state may also occur, although for dye used in dye lasers, the metastable triplet state usually decays through collisional effects. Generally, nonradiative transitions occur between the singlet states and the triplet states. They are discussed more fully by Bass et al (1971) and by Birks (1970) and apart from the transition between the first excited singlet state and the metastable triplet state they are generally neglected in modelling the dye laser.

The dye laser behaves in many respects like a four level laser system, with all four levels in the singlet system. These levels

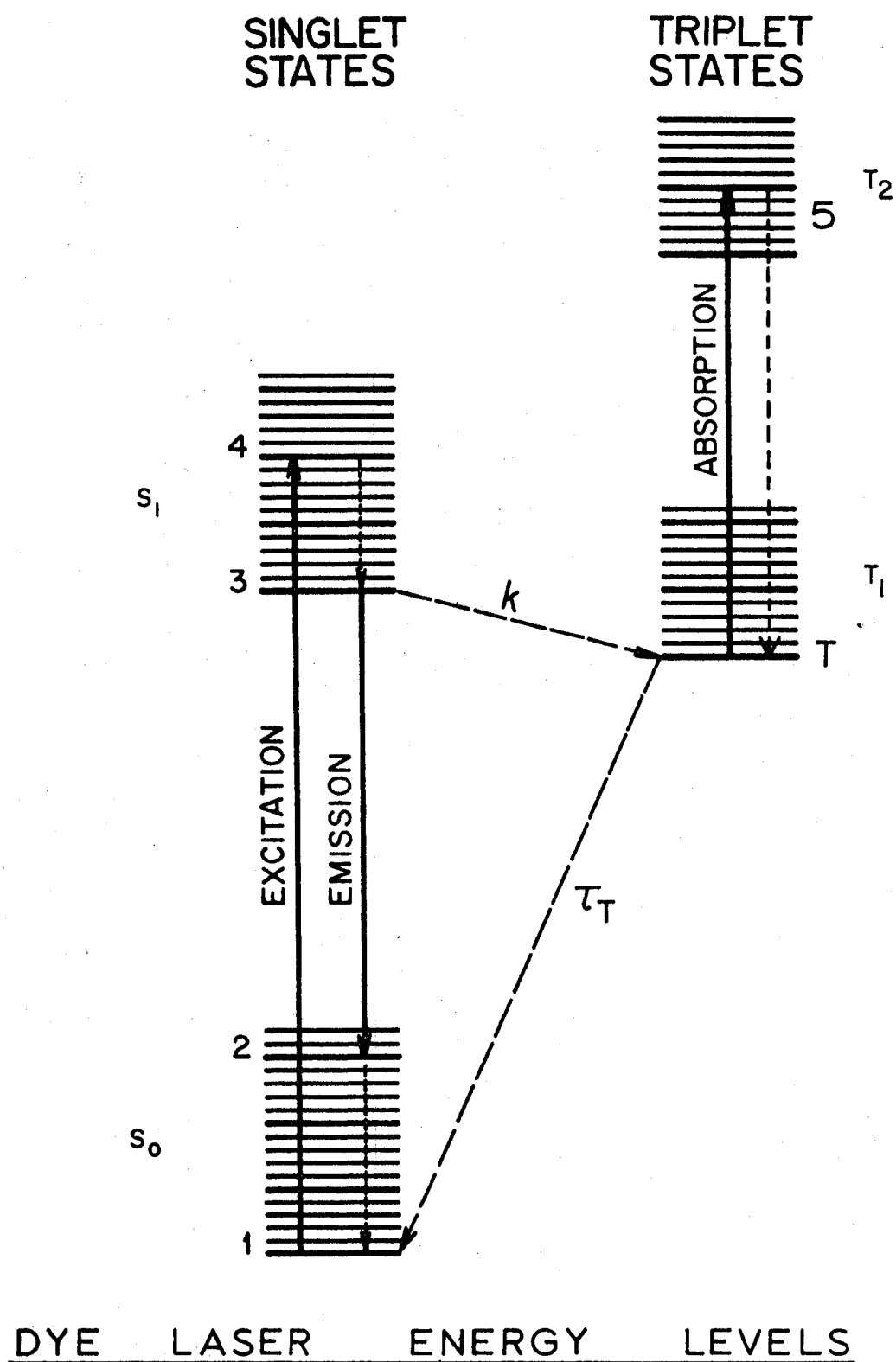


FIG. 1

are labelled 1 through 4 in figure 1. The populations of the sublevels follow a Boltzmann distribution due to the rapid thermalization. The presence of the triplet system introduces complications to the simple operation and in all but a few families of dyes prevents laser operation. The dye molecules are first optically excited to the various vibrational sublevels of the upper singlet state. They then rapidly decay nonradiatively to the thermal distribution in a time shorter than 10^{-11} second (Bass et al 1971). From this state they can make a radiative transition to any of the various vibrational sublevels of the ground state to give rise to a broadband fluorescence spectrum. The decay of these vibrationally excited sublevels of the ground state to a Boltzmann distribution is also characterized by a time constant of less than 10^{-11} second. Since the lifetime for the radiative transition is more than 10^{-9} second, we have in principle a very efficient four-level laser system. The transition from the upper singlet state to the metastable triplet state has two deleterious effects. Firstly, it reduces the number of upper state molecules that can decay radiatively, and secondly, the triplet molecules usually absorb light at the fluorescence wavelengths in a transition to the upper triplet states. All these processes can be described by simple rate equations and the approach will be a phenomenological one starting with the spontaneous emission term.

2. THE DYE LASER RATE EQUATIONS

In a dye laser, the dye molecules form a broadband amplifier and noise generator, while the optical cavity selects a few modes with high Q from the free-space mode spectrum. The total rate of increase of photons in all modes in the wavelength range λ to $\lambda + d\lambda$ due to spontaneous emission is $N_3 E(\lambda) d\lambda / \tau$, where N_3 is the population in the lowest vibrational sublevel of the upper singlet state, τ is the lifetime of this state and $E(\lambda)$ is the lineshape function that is related to the quantum efficiency ϕ by the relationship $\int E(\lambda) d\lambda = \phi$. If the total mode volume of the cavity is V , then the number of modes in the wavelength range λ to $\lambda + d\lambda$ is given by $8\pi\eta^3 V d\lambda / \lambda^4$ where η is the refractive index of the dye solution. Therefore the rate of increase of photons in one cavity mode due to spontaneous emission is $dN_m / dt = N_3 \lambda^4 E(\lambda) / 8\pi\eta^3 \tau V$ where N_m is the total number of photons in mode m . From the theory of stimulated emission, it is well known that the rate of stimulated emission into a cavity mode is equal to the product of the spontaneous emission rate into the mode and the number of photons in that mode. We therefore add the spontaneous and stimulated emission rates to give the total rate of increase of photons in cavity mode m :

$$dN_m / dt = N_3 \lambda^4 E(\lambda) (N_m + 1) / 8\pi\eta^3 \tau V \quad (1)$$

It is convenient to define a cross section $\sigma(\lambda)$ given by $\sigma(\lambda) = \lambda^4 E(\lambda) / 8\pi\eta^2 \tau$ where c is the velocity of light.

Birks (1970) indicates that we can write $1/\tau = \eta^2/\tau_0$, where τ_0 is the lifetime of the upper state in a medium whose refractive index is unity and therefore a more general definition of $\sigma(\lambda)$ would not contain the η^2 factor. Since the lifetime values quoted later were measured in a solution, the factor η^2 is retained for ease of comparison. It will also be seen later that factors of the order of η^2 do not significantly affect the results. Then $dN_m/dt = N_3 \sigma(\lambda) c(N_m + 1)/\eta V$. We define the fraction of mode volume occupied by the dye molecules to be F and, since the mode volume is V , the total population of the excited state N_3 can be related to the population density n_3 by $N_3 = FVn_3$. Thus $dN_m/dt = Fn_3 \sigma(\lambda) c(N_m + 1)/\eta$. This assumes that the densities are uniform throughout the active medium. Analogous terms can be written for the rate of loss of photons from cavity mode m due to singlet-singlet and triplet-triplet absorption. Thus we get:

$$dN_m/dt = -\{n_T \sigma_{TT}(\lambda) + n_1 \sigma_{SS}(\lambda)\} c F N_m / \eta \quad (2)$$

where n_T , n_1 are the molecular densities in the triplet state and the ground state and $\sigma_{TT}(\lambda)$, $\sigma_{SS}(\lambda)$ are the respective triplet and singlet absorption cross sections. Note that the factor is N_m instead of $N_m + 1$ since there is no spontaneous absorption. The cross sections are related to the experimental absorption coefficients by the usual relationships:

$$\alpha = \alpha_{TT}(\lambda) + \alpha_{SS}(\lambda) = n_T \sigma_{TT}(\lambda) + n_1 \sigma_{SS}(\lambda) \quad (3)$$

where α is the absorption coefficient. Finally there is the rate of loss of photons from cavity mode m due to the transmission losses in the optical elements of the cavity and to mode diffraction losses. This is written in the form $dN_m/dt = -N_m/\tau_m$, where τ_m is the cavity lifetime for the mode m . The variation of τ_m with mode will be discussed in the section on tuning mechanisms. Collecting together all the terms for the rate of change of photons in cavity mode m gives:

$$\begin{aligned} dN_m/dt = N_m \{ (n_3 \sigma(\lambda) - n_T \sigma_{TT}(\lambda) - n_1 \sigma_{SS}(\lambda)) Fc/\eta \\ - 1/\tau_m \} + cF n_3 \sigma(\lambda)/\eta \end{aligned} \quad (4)$$

The rate equations for the populations of the upper laser level N_3 , the ground state N_1 , and the triplet states N_T and N_5 are:

$$\begin{aligned} dN_3/dt = W_{31} N_1 - N_3/\tau - \sum_m N_3 N_m \sigma(\lambda) c/V\eta \\ + \sum_m N_1 N_m \sigma_{SS}(\lambda) c/V\eta \end{aligned} \quad (5)$$

$$\begin{aligned} dN_T/dt = k N_3 - N_T/\tau_T \\ - \sum_m N_T N_m \sigma_{TT}(\lambda) c/V\eta + N_5/\tau_5 \end{aligned} \quad (6)$$

$$dN_5/dt = N_T N_m \sigma_{TT}(\lambda) c/V\eta - N_5/\tau_5 \quad (7)$$

$$N = N_1 + N_3 + N_T + N_5 \quad (8)$$

In (5) the first term is the optical excitation term, the second

is the decay rate due to spontaneous emission and the nonradiative transition to the triplet state, the third is the decay rate due to stimulated emission caused by the photons in all cavity modes and the final term is due to singlet-singlet absorption repopulating the upper singlet state. In (6), k is the singlet to triplet crossing rate, τ_T is the metastable triplet decay time, and τ_s is the excited triplet state decay time. Equation (8) simply states the conservation of molecules.

These absolute populations can be converted to the more common population densities. The active volume of the dye molecules is FV where F and V have previously been defined. In many dye lasers the cavity length is much greater than the dye cell length. Providing the mode cross section does not vary appreciably within the cavity F can be taken as the ratio of dye cell length to cavity length. Substituting into equations (4) to (8) gives:

$$\begin{aligned} \frac{dn_m}{dt} = n_m \{ (n_3 \sigma(\lambda) - n_T \sigma_{TT}(\lambda) \\ - n_1 \sigma_{SS}(\lambda)) Fc/\eta - 1/\tau_m \} + Fcn_3 \sigma(\lambda)/\eta V \end{aligned} \quad (9)$$

$$\begin{aligned} \frac{dn_3}{dt} = W_3 n_1 - n_3/\tau - \sum_m n_3 n_m \sigma(\lambda) c/\eta \\ + \sum_m n_1 n_m \sigma_{SS}(\lambda) c/\eta \end{aligned} \quad (10)$$

$$\frac{dn_T}{dt} = kn_3 - n_T/\tau_T - \sum_m n_T n_m \sigma(\lambda) c/\eta + n_s/\tau_s \quad (11)$$

$$\frac{dn_s}{dt} = \sum_m n_T n_m \sigma(\lambda) c/\eta - n_s/\tau_s \quad (12)$$

$$n = n_1 + n_3 + n_T + n_s \quad (13)$$

These equations resemble the rate equations that have been derived and solved by Sorokin et al (1968) and by Snavely (1969) to obtain the time dependence of the laser output power. However, in this case, all the cavity modes have been taken into account and the triplet absorption has also been included. Keller (1970) has done some calculations for typical flashlamp-pumped dye lasers assuming that the time derivatives of the populations can be set equal to zero since the relaxation rates are rapid compared to the time variation of W_3 , the optical excitation term, and all the populations are in dynamic equilibrium with values depending only on the instantaneous value of W_3 . If more than one cavity mode is oscillating, it is easy to see that this is not valid for the photon populations in each mode, even though it may be true for the molecular state populations. In addition, the solutions of Keller are not valid for the short pulse laser-pumped dye lasers, as the time variation of W_3 (Ali 1969) is the same order of magnitude as the relaxation rates of the dye molecules.

In the equations it is assumed that all spatial inhomogeneities due to the standing wave nature of the cavity modes can be neglected as has been done by Sorokin et al (1968), Snavely (1969) and Huth et al (1970). This assumption considerably reduces the complexities of solving both the time and the space variations of the populations and the photon densities.

3. TUNING MECHANISMS

A number of different schemes for tuning dye lasers has been used including prisms, diffraction gratings, Faraday rotators, Lyot filters and tilted Fabry-Perot etalons. The diffraction grating and the Fabry-Perot etalon will be described here as they are the most common means of producing narrow lines. We shall start by discussing the Fabry-Perot etalon. In order to tune the dye laser the etalon is placed within the optical cavity and the tuning is accomplished by altering the angle of the etalon. The etalon was mounted in a precision angular orientation device with an angular resolution of 0.02 arc-second. The transmission of the etalon is given by Born and Wolf (1970) with the result:

$$T = T_0 / \{1 + \zeta \sin^2(2\pi d \cos\theta/\lambda)\} \quad (14)$$

where T_0 is the peak transmission, d the etalon plate separation, θ the angle with the optical axis and $\zeta = 4R/(1 - R)^2$ where R is the reflectivity of the etalon plates. For values of ζ corresponding to reflectivities of 60 percent or higher, this transmission function may be approximated by the Gaussian:

$$T = T_0 \exp\{-4(\lambda - \lambda_0)^2 \ln 2 / (\Delta\lambda)^2\} \quad (15)$$

where $\Delta\lambda$ is the full width at half maximum (FWHM) and where λ is the wavelength for peak transmission. The cavity lifetime is related

to the laser mirror reflectivities and the transmission of the dye cell windows and the Fabry-Perot etalon transmission T by:

$$\tau_m = -2L\{1 + F(\eta - 1)\}/c \ln(t_1^2 t_2^2 T^2 R_1 R_2) \quad (16)$$

where t_1 and t_2 are the dye cell window transmissions and R_1 and R_2 are the laser mirror reflectivities. In general the reflectivities and window transmissions are wavelength independent over the region of interest, so that the wavelength or mode dependence of τ_m arises only from the wavelength variation of T .

Another means of tuning the dye laser was first demonstrated by Soffer and McFarland (1967) and Sorokin et al (1967) who replaced one mirror of a dye laser with a diffraction grating. The grating was mounted in a Littrow arrangement and was adjusted to the angle for which the desired wavelength was reflected back upon itself along the axis of the optical cavity. In effect a mirror with a highly peaked reflectance spectrum is provided; the wavelength of the peak is altered by rotating the grating. Hänsch (1972) has calculated the linewidth of the diffraction grating when used in a nitrogen laser pumped dye laser. This will be presented in section II.7(d). For the present, it will be assumed that the selective reflectivity can be given by equation (15) such that:

$$R = R_0 \exp\{-4(\lambda - \lambda_0)^2 \ln 2 / (\Delta\lambda)^2\} \quad (17)$$

where R_0 is the peak reflectivity and $\Delta\lambda$ is the FWHM as given in

section II.7(d). With this assumption equation (16) becomes:

$$\tau_m = -2L\{1 + F(\eta - 1)\}/c\ln(t_1^2 t_2^2 R_1 R_2) \quad (18)$$

where R_1 is the reflectivity of the output mirror and R is given by equation (17).

The region in which the laser is tunable is determined by the fluorescence and absorption spectrum of the dye. The short wavelength extreme of the tunable region is determined by the loss associated with singlet-state absorption. At the long wavelength extreme the gain of the laser becomes too small for oscillation as a result of the decreased quantum yield.

For dye lasers with no tuning element in the cavity, the output depends on the wavelength dependence of the cross sections and on the dye concentration. The wavelength can be altered by changing the dye concentration (Sorokin et al 1967). Many other methods of tuning the dye laser have been reported, the results of which are summarized by Snavely (1969).

4. CALCULATED RESULTS

The differential equations were solved numerically using an Euler integration routine (Collatz 1966) on an I.B.M. 360 computer for typical flashlamp-pumped and nitrogen laser-pumped rhodamine 6G dye lasers. The cross sections for this dye are well known and there are several published results with which to compare the calculations. The cross sections were derived from the results given by Snively (1969). The photon density is related to the power output by $P = hcV(\sum_m n_m)/\tau_p$, where τ_p , the output coupling lifetime, is given by $\tau_p = -2L(1 + (\eta - 1)F)/c \ln(1 - T_p)$, where T_p is the transmission of the output mirror. The optical pumping term W_3 , was assumed to be of the form $W_3 = W_{30}t \exp(1 - t/2)/2$, where t was measured in microseconds. This is in good agreement with typical flashlamp outputs. The term W_3 was assumed to be a Gaussian for the nitrogen laser-pumped dye laser. This is also in good agreement with the actual shape of the nitrogen laser pulse. (Ali 1969). The total optical pumping pulse length was about 10 microseconds for the flashlamp-pumped dye laser and about 10 nanoseconds for the nitrogen laser-pumped dye laser. The etalon and the grating parameters were chosen to have a peak at 5896 Å corresponding to one of the sodium resonance lines. The following parameters were used in the calculations:

FLASHLAMP PUMPED

LASER PUMPED

$$t_1 = t_2 = 0.96$$

$$t_1 = t_2 = 0.96$$

$$R_1 = 0.97$$

$$R_1 = 0.04$$

$$R_2 = 0.87$$

$$T_p = 0.93$$

$$T_p = 0.10$$

$$L = 30\text{cm}$$

$$L = 50\text{cm}$$

$$F = 0.03$$

$$F = 0.30$$

$$\tau_T = 0.9 \times 10^{-7} \text{ sec (Snively 1969)}$$

$$\tau = 5.5 \times 10^{-9} \text{ sec (Mack 1968)}$$

$$k = 2.8 \times 10^{-7} \text{ sec (Snively 1969)}$$

$$\tau_5 = 5.0 \times 10^{-9} \text{ sec}$$

$$V = 5 \text{ cm}^3$$

$$V = 1.36 \times 10^{-3} \text{ cm}^3$$

$$n = 1.2 \times 10^{17} \text{ cm}^{-3}$$

$$n = 3.0 \times 10^{18} \text{ cm}^{-3}$$

$$(2 \times 10^{-4} \text{ M concentration})$$

$$(5 \times 10^{-3} \text{ M concentration})$$

$$\eta = 1.33 \text{ (methanol as solvent)}$$

The lower order axial modes have a spacing of approximately 0.0004 nm. It was found that the modes could be grouped together to give an effective mode spacing of many times the fundamental mode spacing and still accurately preserve the envelope of the mode photon densities as a function of the wavelength. For the case of the etalon whose FWHM was 0.25 nm, an effective mode spacing of 0.002 nm was found to give a good compromise between accuracy and computing time and for the laser-pumped laser, the FWHM of the grating (see section II.7(d)) was 0.01 nm and the effective mode spacing used was 0.001 nm. The peak transmission of the etalon (or reflection of the grating)

was assumed to be 0.70 except where noted and the value of W_3 was adjusted to give a suitable output power.

4(a). LONG PULSE EXCITATION RESULTS (FLASHLAMP-PUMPED)

Figure 2 shows the laser output lineshape or envelope of the mode photon densities at different times during a typical laser pulse. The left-hand side of figure 3 shows the same results with the peak photon densities normalized to unity, while the time-integrated lineshape is shown on the right-hand side of figure 3. The lineshape is symmetrical about the peak and at any instant has a Gaussian shape. The time-integrated lineshape is symmetrical but it does not have a Gaussian shape since it is due to the integration of Gaussians of different widths and heights. Figure 3 clearly shows how most of the narrowing occurs before the onset of laser action at 1.75 microseconds and that the rate of narrowing decreases when the laser is saturated. The peak output for this laser was 1.05 kw. Figure 4 shows the linewidth as a function of peak output power, obtained by varying W_{30} . The curves are given for $T_0 = 1.0$ and 0.7 and $\sigma = 2.14 \times 10^{-16} \text{ cm}^2$. Curves are also given for the case where σ is twice the above value. The solid lines in figure 4 indicate the instantaneous values at the peak of the laser pulse, while the dashed lines show the time integrated linewidth for two values of T_0 and for a laser cross section of twice the measured value. This value of σ is larger than the value obtained by neglecting the η^2 term that was discussed in the definition of the cross section. The results show that the linewidth decreased slightly with increasing laser power output.

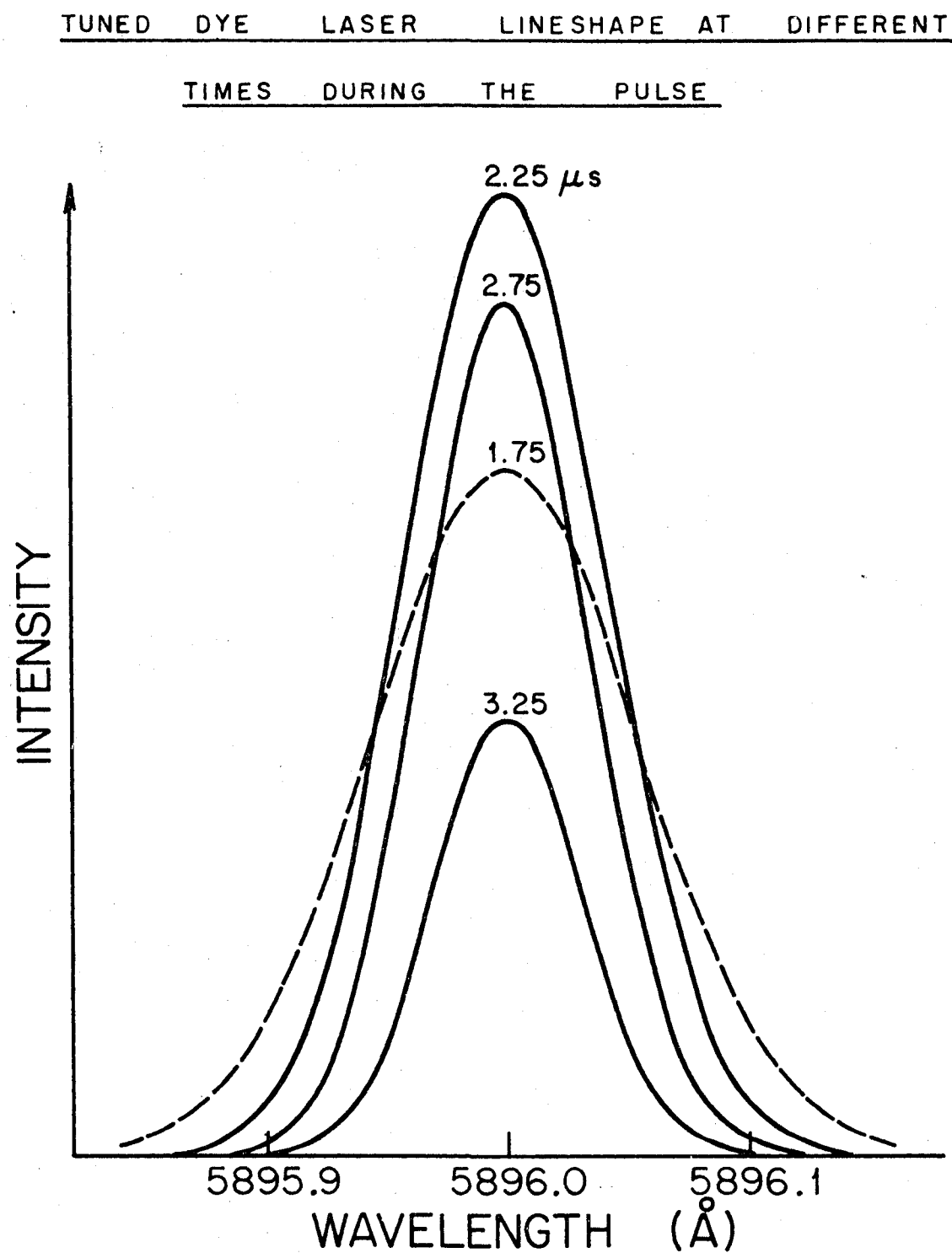


FIG. 2

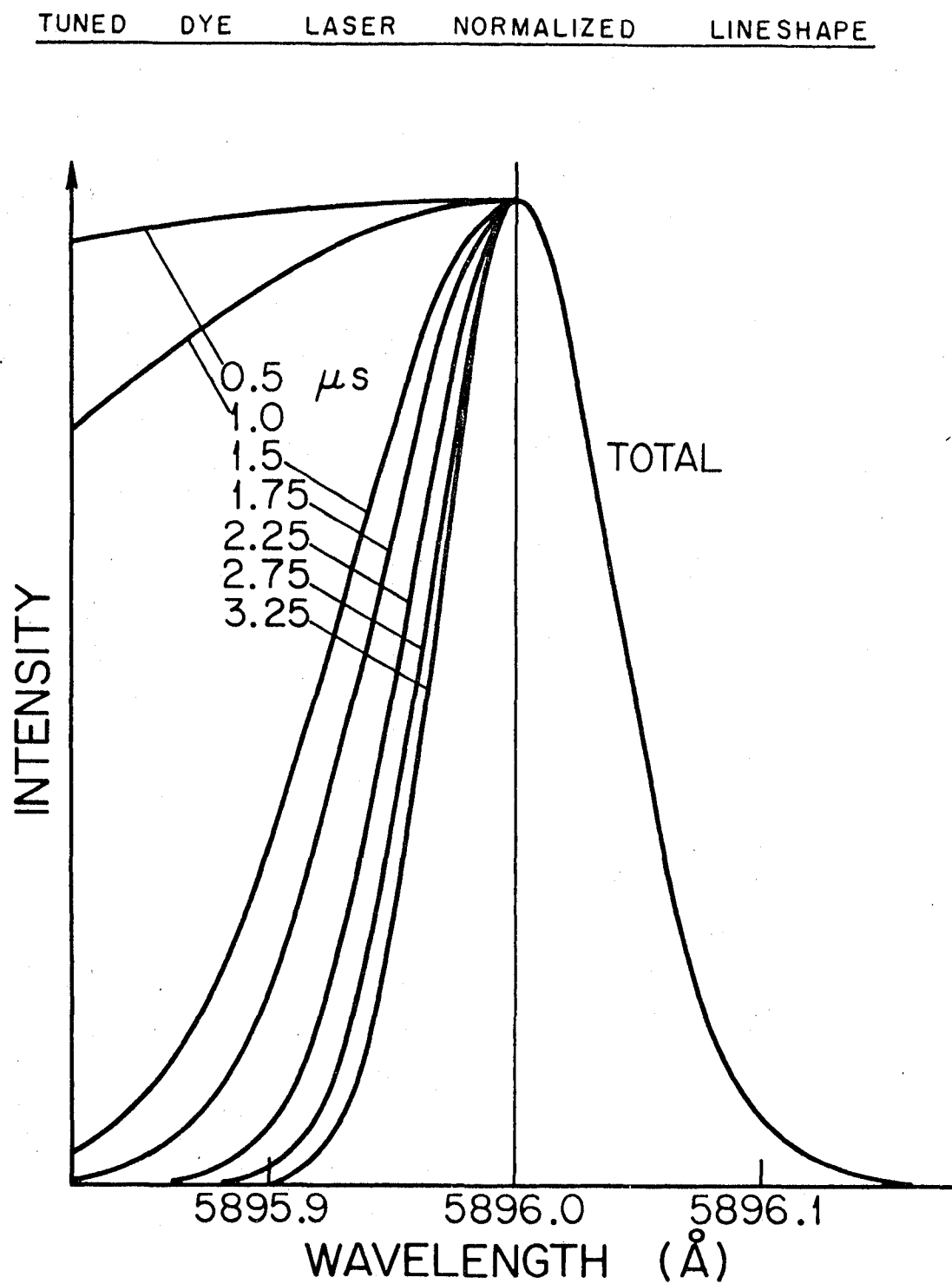


FIG. 3

DYE LASER LINEWIDTH AS A FUNCTION OF PEAK
OUTPUT POWER

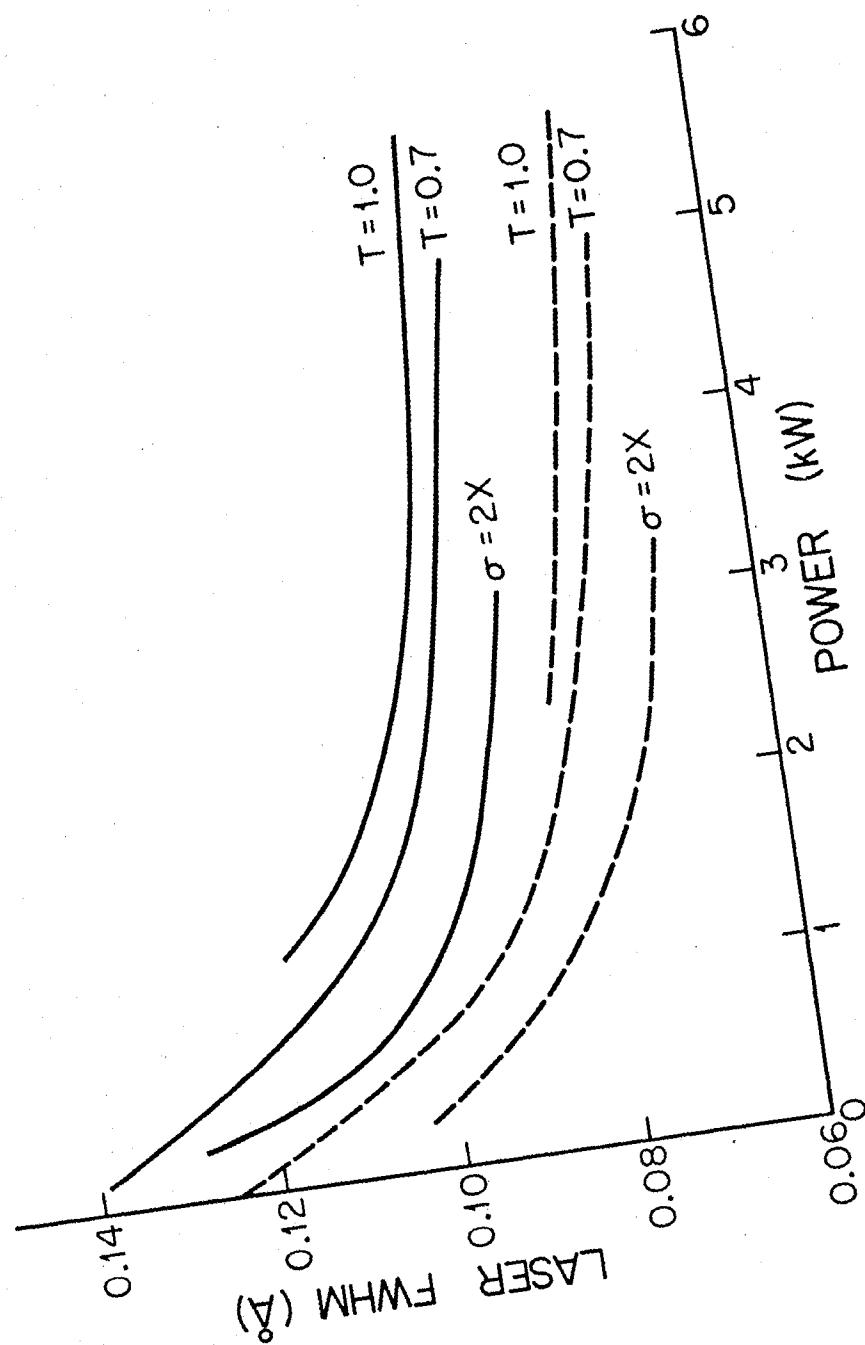


FIG. 4

The increase in the laser cross section, $\sigma(\lambda)$, decreased the threshold pump power by a factor of two as expected; however, the linewidth at a given peak power output was smaller by only 10 to 15 percent and had a very similar dependence on peak power, as can be seen in figure 4. The increase in T_0 also decreased the threshold pump power, but the linewidth increased by less than 5 percent for the same output power.

The effects of the variation of τ_5 , k and τ_T were also studied. The changes in instantaneous lineshape and linewidth were less than 1 percent for values of τ_5 as large as 5×10^{-3} second, while the change in the integrated lineshape was less than 3 percent, the optical pumping conditions being identical to those shown in figure 2. The peak power of the laser pulse was unchanged for values of τ_5 less than 5.0×10^{-8} second, but showed an increase of 10 percent for $\tau_5 = 5.0 \times 10^{-7}$ second and a further increase of 10 percent for $\tau_5 = 5.0 \times 10^{-6}$ second. Thereafter it remained constant as τ_5 was increased further. Since τ_5 is not expected to be larger than 5.0×10^{-6} second (Birks 1970), the results as given should be satisfactory. Furthermore, the results obtained by neglecting the excited triplet state (state 5 in figure 1) were identical to the results shown in figures 2, 3 and 4. Changes in k and τ_T changed both the output power and the linewidth for a given optical pumping term, but in such a way that the graph of figure 4 was reproduced. A change in the spontaneous emission term by a factor of 10 did not change the results by more than 1 percent.

From the differential equations, it is clear that, provided the cross sections are constant over the laser linewidth,

the ratio of the linewidth of the Fabry-Perot etalon to the final laser linewidth is a constant and the results indicate that for rhodamine 6G under the previously mentioned conditions this ratio is about 100:3. For wider filters the wavelength variation of the cross sections will distort the output lineshape towards the peak of the untuned dye laser.

The output of the laser with no tuning elements in the cavity was also computed. The wavelength dependence of the laser output is now due to the wavelength dependence of the cross sections. Similar calculations have been performed by Vreken (1971). However, Vreken does not explicitly introduce the wavelength variation of the cross sections. Figure 5 shows the computed output for a simulated power of 4.5 kw. The integrated linewidth is 2.6 nm and the peak of the laser pulse exhibits a sweep to longer wavelengths with time of about 1.2 nm, with most of this occurring during the risetime of the pulse. Results for a simulated power of 1.5 kw were almost identical, the linewidth being larger by 0.2 nm and the sweep smaller by 0.4 nm. A small shift in the absolute value of the laser cross section shifted the peak of the laser wavelength, but did not change either the width or the sweep.

4 (b). SHORT PULSE EXCITATION (LASER-PUMPED)

It has been shown in the above section that a substantial 'gain narrowing' occurs in flashlamp-pumped dye lasers with a

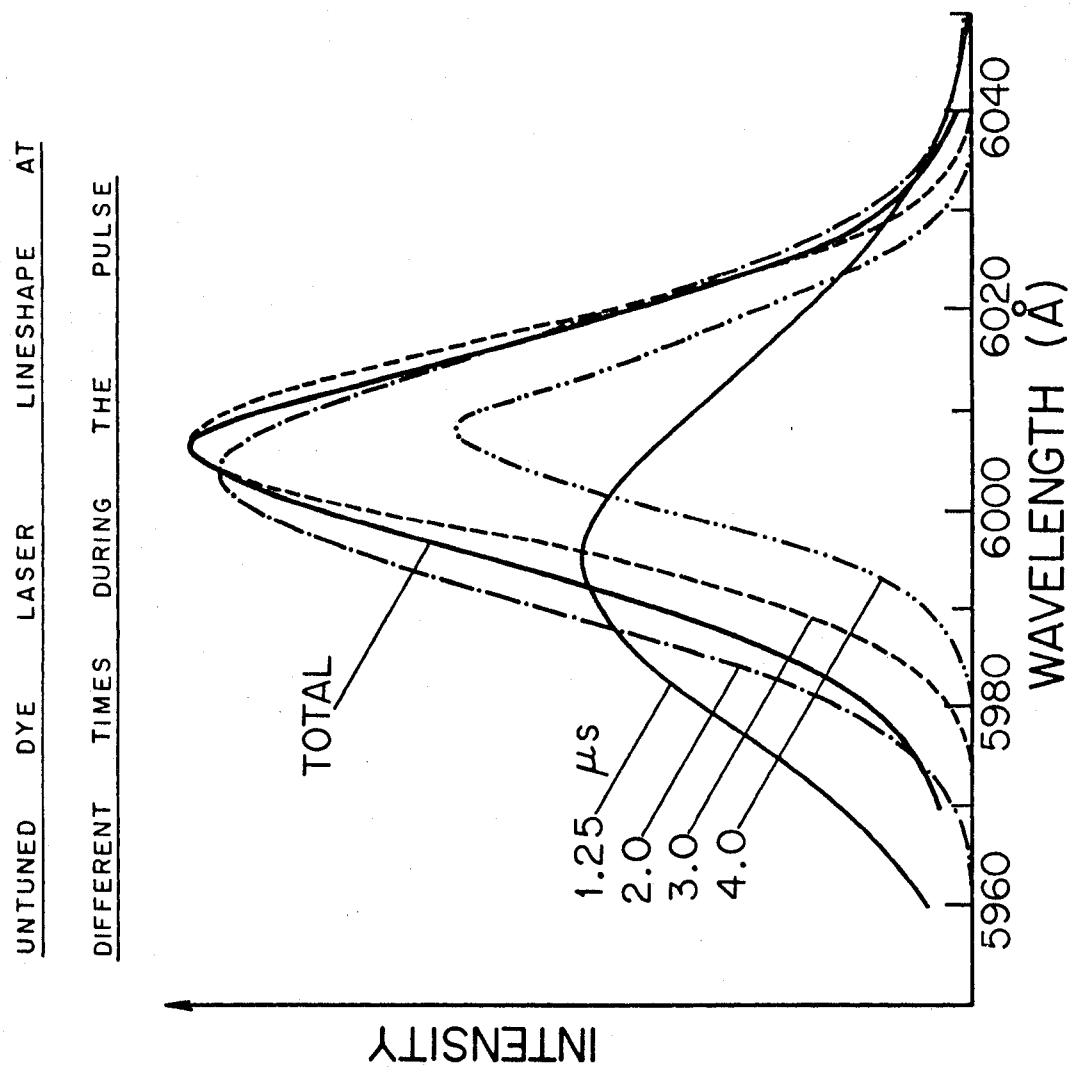
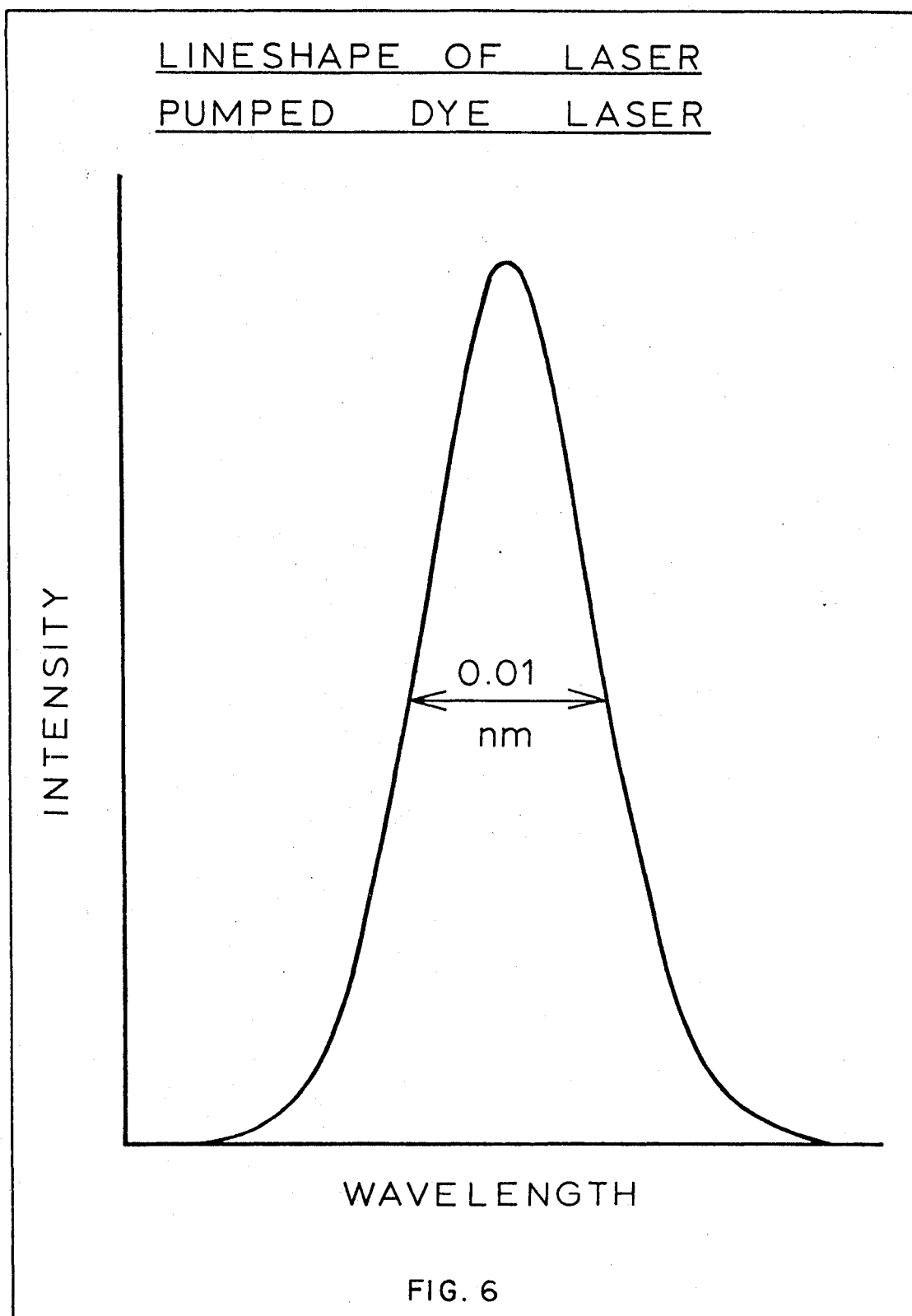


FIG. 5

wavelength selector of low dispersion. In dye lasers pumped by a nitrogen laser, the short pulse duration (10 nsecond) severely limits the number of light passes and there will not be sufficient time for much 'gain narrowing'. Also, if the cavity length is of the order of the coherence length of the light, no discrete axial mode structure is expected (Hänsch 1972). This means that the summation over the various modes in the rate equations should be replaced by the integral over the wavelength. In addition, Sorokin et al (1967) have shown that the effects of the triplet system can be ignored under short pulse excitation.

The rate equations were solved under these assumptions using an Euler integration routine, with essentially the same dye solution parameters as the flashlamp pumped case. The results indicate that essentially no line narrowing occurs during the duration of the laser pulse. This means that the output linewidth of the nitrogen laser-pumped dye laser will be essentially identical to the bandwidth of the tuning element. In this case the filter consisted of a diffraction grating and a beam expansion telescope (see section II.7(c) and II.7(d)). The FWHM of this filter was about 0.01 nm and the calculated output linewidth was 0.01 nm indicating no 'gain narrowing'. Figure 6 shows the integrated output lineshape assuming the filter has a Gaussian shape 0.01 nm FWHM and the peak output is 10 to 20 kw.



5. THE FLASHLAMP PUMPED DYE LASER

By studying the solutions to the rate equations for various excitation pulse lengths, triplet decay and intersystem crossing rates, the importance of using a rapidly rising flashlamp to overcome the effects of the intersystem crossing becomes obvious. Thus in the early flashlamp excited dye laser work, the emphasis was placed on the design of a suitably fast excitation source. The first reported flashlamp-excited dye laser (Sorokin and Lankard 1967a) utilized a lamp which discharged 100 joules in a pulse with a risetime to peak intensity of about 0.3 microsecond and a duration of 1 microsecond. The lamp used by Sorokin and Lankard was similar in design to that of Claesson and Lindqvist (1958). In this arrangement the inductance was kept at a minimum by using a coaxial arrangement for the discharge and the electrical connections and by mounting the lamp in the centre of the energy storage capacitor. The discharge took place in an annular region between two quartz tubes, the inner of which served as a dye cuvette. The outer tube was surrounded by a metal sleeve which provided the electrical connections between the capacitor and the lamp, and also provided a reflector for the lamp. In the experiments of Sorokin et al (1968) no advantage was found in using anything but air at low pressure in the annular region.

Schmidt and Schäfer (1967) obtained similar risetimes with a conventional xenon flashlamp driven by a low inductance capacitor. They used a coaxial arrangement for the lamp and the electrical connections in order to minimize the inductance, and a spark gap in series with the lamp to permit operation at voltages higher

than the lamp breakdown potential.

Under certain conditions the risetime requirements for the flashlamp are not as severe as previously supposed. Snavely and Schäfer (1969a) showed that air-saturated methanol solutions of rhodamine 6G and rhodamine B can be maintained above laser threshold for periods as long as 50 microseconds while the excitation energy remains constant. Recently Peterson et al (1970) have obtained CW operation of a rhodamine 6G laser using an argon laser to pump the dye. A summary of other CW dye lasers is given by Hercher and Pike (1971). Thus by using the proper dyes, conventional flashlamps and flashlamp circuitry can be utilized to excite a dye laser. This is only possible however for dyes in which the triplet lifetime is short or in which a quenching agent can be added to quench the triplet state. A comprehensive survey of most of the dyes capable of flashlamp excitation has been published by Warden and Gough (1971).

It has been found in the experiments of Snavely and Schäfer that laser emission can be terminated while the excitation source is above threshold. This termination was found to be due to refractive index inhomogeneities caused by nonuniform excitation of the dye. The effects produced by nonuniform heating of a liquid laser have been discussed by Winston and Gudmundsen (1964). Results indicate that the optical cavity degraded to the point of terminating laser action in 20 to 30 microseconds.

The excitation produced by a linear flashlamp is nonuniform and the dye closest to the lamp receives the most energy. As the temperature of the solution increases, the refractive index changes.

This hotter dye solution near the flashlamp causes the active medium to bend the laser beam. The length of the laser pulse will be determined by the time during which the beam remains within the optical cavity. This indicates that the cavity should remain short for longer laser pulse lengths. In the case of the coaxial lamp with cylindrically uniform excitation, the heating produces a lenslike active medium. The hotter dye near the cuvette wall will have a lower refractive index and thus a positive lens is produced. This positive lens reduces the effective radius of curvature of the mirrors that make up the cavity. The system will continue to oscillate until the effective radius of curvature of the mirrors decreases to a value for which the cavity is no longer stable (Kogelnik and Li 1966). Accordingly, the longest period corresponds to the shortest cavity.

Long term heating effects are also observed and produce thermal schlieren which may persist for many minutes in a stagnant dye solution. These effects are easily eliminated by circulation of the dye solution through the cuvette. Sorokin et al (1968) observed that without circulation the pulse repetition rate was limited to about one pulse per ten minute interval. By circulating the dye, a repetition rate of about one pulse per second was obtained and Loth et al (1972) obtained repetition rates up to 20 per second.

In the design of a dye circulation system care must be taken to avoid materials that will react with the dye solvents. These problems can be overcome by using a magnetically coupled teflon pump or stainless steel pump and polypropylene tubing for the circulation system.

5(a). THE FLASHLAMP CIRCUIT

In the approach to the design of the flashlamp system, one must consider the conditions imposed by the explosion limits of the flashlamp envelope, the voltage on the capacitor and the geometrical constraints on the size of the lamp. Knowing the voltage-current relationships for the flashlamp, one can write the loop equations for the single mesh driving circuits and find their solutions. These solutions together with the constraints mentioned above can be used to determine the best methods of constructing the flashlamp system. The equations characterizing the voltage-current relationships have been solved by Holzrichter and Schawlow (1970) with the following results.

The initial capacitor voltage should be as large as possible and the circuit impedance should be as small as possible. However, the self inductance of the lamp is proportional to its length and its ability to dissipate energy is also proportional to the length. Consequently one cannot arbitrarily increase the capacitor voltage V_0 and with it the total energy dissipated in the lamp and also decrease the inductance L . These relationships must be optimized subject to additional restraints.

The design of the circuitry is also dependent on whether or not the dye is subject to triplet state effects. If the triplet state can be neglected, the output power of the laser depends only on the discharge power, until the heating effects discussed earlier terminate the laser action. If the triplet state does quench the laser

output, high peak discharge power must be sacrificed to achieve fast rise times. In many cases of interest it appears that the triplet state quenching is relatively unimportant and peak power is often more important than rate of rise of the excitation pulse. This is true for the rhodamine and the coumarin dyes.

Using the results of Holzrichter and Schawlow (1970) a simple continuously evacuated linear flashlamp was constructed. The design of the flashlamp was similar to that proposed by Ferrar (1969). The lamp was made of quartz tubing with a wall thickness of 1 mm and a 3mm inside diameter. A diagram of the lamp is shown in figure 7 along with the electrical circuitry used to operate the lamp. The rubber tubes shown absorb the shock and prevent damage to the ends of the lamp. They also provide a vacuum seal. The electrodes were made of stainless steel. The lamps were continuously evacuated to enhance the risetimes and to minimize internal explosive shock. Energy storage was provided by a 1 microfarad capacitor, triggered by a spark gap. The arrangement of the circuit and construction of the spark gap are also shown in figure 7.

The equation given by Holzrichter and Schawlow for the explosion energy E_x is:

$$E_x = \gamma \ell d (LC)^{1/4} \quad (19)$$

where γ is a constant, ℓ is the length of the lamp, d the diameter, L the circuit inductance and C the circuit capacitance. The value of γ depends on the lamp and is estimated to be about 6×10^4 (Ferrar 1969).

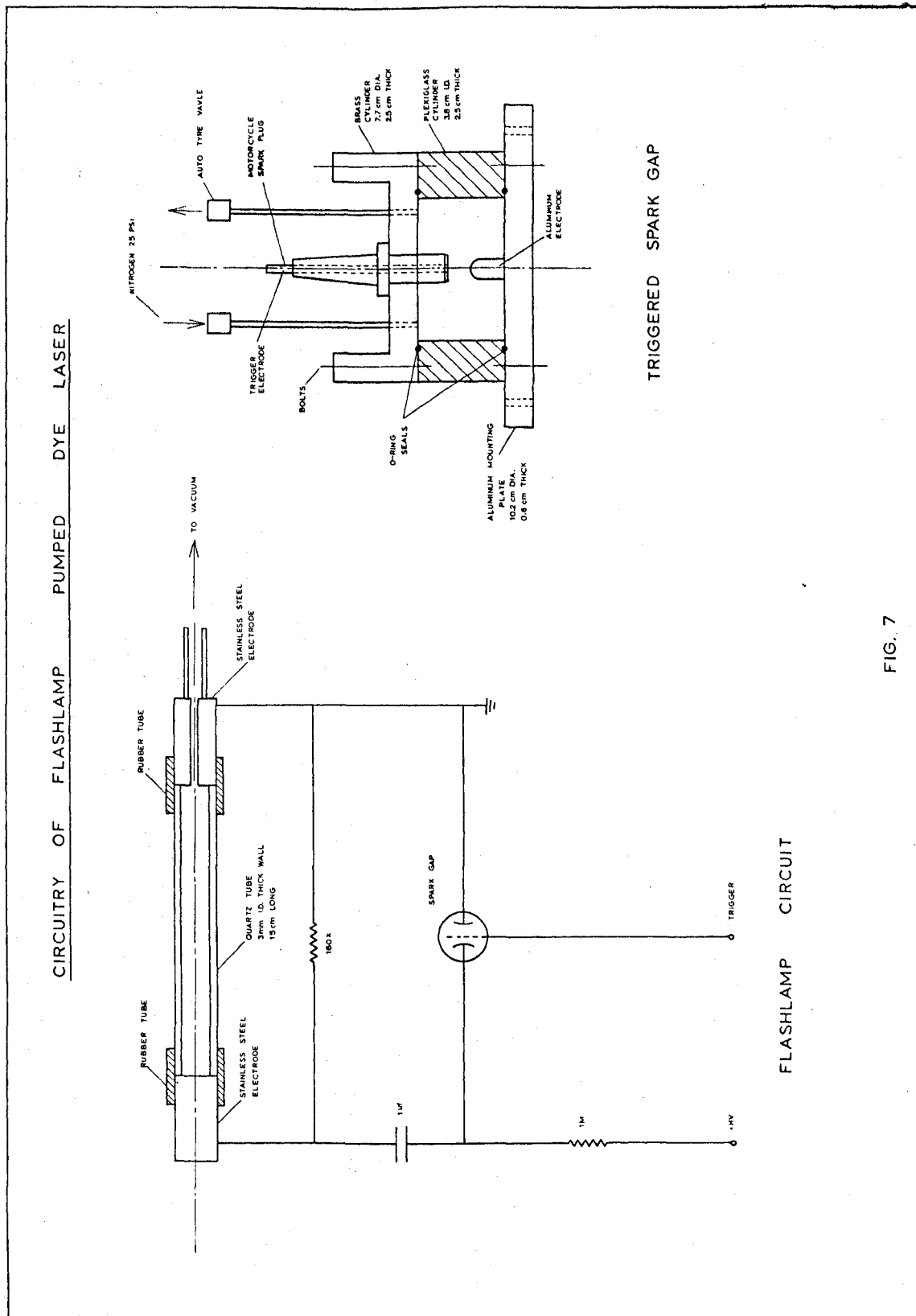


FIG. 7

For values of $C = 1$ microfarad and $L = 0.1$ microHenry, the explosion energy is about 200 joules. The number of pulses obtainable from the lamp is given by Huth et al (1970) as:

$$\log N = -8.5 \log(E_0/E_x) \quad (20)$$

where N is the number of shots, and E_0 is the input energy. This gives an expected lifetime of 350 to 400 pulses at an input energy of 100 joules. This value is in agreement with the number of shots obtained from this lamp operating at 100 joule input energy.

Some experiments were performed using conventional commercially available linear xenon flashlamps in a double elliptical pumping arrangement (described in the next section). However the number of pulses obtainable from these lamps was approximately the same as the above simple air flashlamp. The xenon lamps did however provide higher peak output powers, but due to the high cost of the xenon flashlamps and the comparable lifetimes to the simple design of Ferrar, most of the experimental work was done with the simple flashlamp system.

5(b). THE OPTICAL PUMPING CAVITY

Organic dye lasers with linear flashlamps have used elliptical, spherical, close coupled and circular pumping geometries. Analyses of the efficiencies and pumping uniformities in elliptical cavities have been made by Bowness (1965) and by Evtuhov and Neeland (1967), and in circular cavities by Wildey (1971).

Both elliptical and circular pumping configurations were used in the construction of the flashlamp-pumped dye lasers described here. The elliptical cavity consisted of a double ellipse with a semi-major axis of 3.5 cm and a semi-minor axis of 2.5 cm. The dye cuvette was 15 cm long, 6 mm in diameter and was located at the mutual foci of both ellipses. This design cavity utilized the commercial xenon flashlamps located at the other two foci. The diameter of the flashlamps was 9 mm with a discharge length of 15 cm. The arrangement of the dye cuvette and the flashlamps is shown in figure 8. From the calculations of Bowness (1965) the efficiency, assuming perfect reflection from the walls, is about 30 percent. The efficiency is defined as the amount of light trapped by the dye cuvette compared to that emitted from the flashlamps. Since the reflectivity of the polished aluminum walls is only about 70 percent, the overall efficiency is only about 20 percent.

Wildey has shown that the efficiencies of the double ellipse and the double circular configuration are almost the same. The double circular cavity has a similar geometry to the double elliptical cavity except that the reflecting surface is circular. The distances between the dye cuvette and the circle centres, and between the

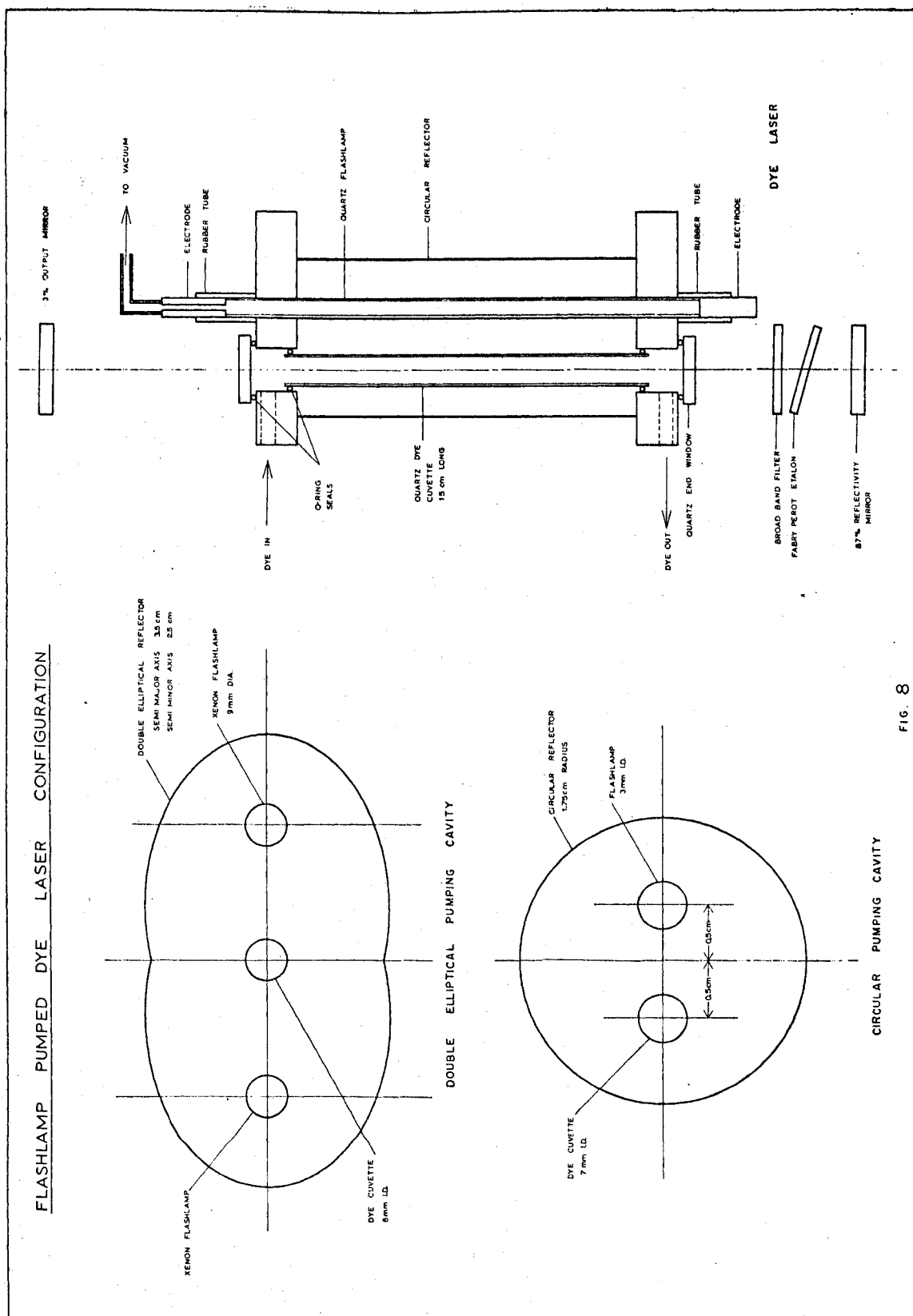


FIG. 8

circle centres and the flashlamps are equal, and in this case have a value of 1.75 cm. For a dye cuvette 6 mm in diameter and a flashlamp 3 mm in diameter, Wildey (1971) indicates the transfer efficiency to be about 30 percent. The reflecting surface is a rear surfaced silvered mirror with a reflectivity of about 80 percent. Thus the overall efficiency will be about 20 to 25 percent.

Actually pumping efficiencies as high as 70 percent can be achieved from the double elliptical design with the appropriate selection of the cavity parameters, lamp and dye cuvette dimensions (Bowness 1965). In contrast, peak efficiencies of only 60 percent can be achieved with the double circular design of Wildey, again with the appropriate cavity, lamp and cuvette dimensions. However, Wildey has shown that the circular design produces an improvement in the pumping uniformity over the elliptical design and since the efficiencies are approximately equal, most of the experimental work was done with the circular reflector and the simple air flashlamp. For simplicity, only a single circular reflector was used. Calculations indicate that the efficiency is somewhat larger, although the pumping uniformity is not as good as the double circular design. Figure 8 shows the circular geometry and the optical cavity and tuning elements for the flashlamp-pumped dye laser.

5(c). THE FLASHLAMP-PUMPED DYE LASER CONFIGURATION

For reasons discussed in the previous sections, the dye laser used for the majority of the experimental work consisted of a flashlamp of the kind described by Ferrar (1969) and a circular pumping cavity of the kind described by Wildey (1971). The dye cuvette was a quartz tube 7mm outside diameter with a wall thickness 1 mm, 15 mm long. The flashlamp was constructed of quartz tubing with a 3 mm bore. The circular reflector was a pyrex tube with a radius of 1.75 cm and coated on the outside with silver, giving a reflectivity of about 80 percent.

A 1 microfarad capacitor, charged to voltages of 14 to 15 kv was discharged through the lamp by a spark gap, which was triggered by an E.G. and G. TM11 trigger module. The inductance of the circuit was kept at a minimum by mounting the spark gap directly on the end of the capacitor, both of which were mounted inside a brass cylinder to provide a coaxial current return path. The connections to the flashlamp were also made in a coaxial manner to keep the inductance minimal.

The dispersive element consisted of a mica spaced Fabry-Perot etalon of the type described by Dobrowolski (1959) together with a broad band filter (FWHM 3.0 nm). This arrangement allowed only one of the Fabry-Perot resonance lines to oscillate, as the free spectral range of the etalon was about 1.6 nm. The linewidth for this filter combination was 0.25 nm as measured with a 0.75 metre Jarrall-Ash spectrograph.

5(d). EXPERIMENTAL DATA

Experimental performance characteristics are given for operation near 600.0 nm using a 2×10^{-4} M/litre solution of rhodamine 6G in methanol.

The output beam exhibited a divergence of 5 milliradians. The output power of the dye laser was measured with a calibrated SGD-100A photodiode, after attenuation of the beam with neutral density filters. An energy output of about 10 millijoules was measured, which corresponds to peak powers of 3 to 5 kw. This corresponds to a conversion efficiency of about 0.01 percent since the energy stored in the capacitor was 100 joules. The flashlamp-pumped dye laser pulse shape was measured using the SGD-100A diode and a Tektronix 551 oscilloscope. The results indicate a pulse with a duration of 5 to 10 microseconds. The pulse shape is shown in figure 9 along with the flashlamp pulse. The bandwidth for the tuned output was measured using a Fabry-Perot etalon with an instrumental bandwidth of 0.003 nm. The results indicate an output bandwidth of about 0.01 nm at an output power of 1 kw with an estimated error of 10 percent. This is in good agreement with the calculated results from the rate equations. The output of the laser with no tuning element in the cavity was also measured. The untuned linewidth was 3.0 nm. This is to be compared to 2.6 nm as calculated by the rate equations.

Repetition rates of 1 to 2 pulses per second were achieved with this laser. By the use of water cooled flashlamps and rapidly circulating dye solutions, repetition rates as high as 20 pulses per second have been demonstrated for a flashlamp-pumped dye laser by Ioth et al (1972).

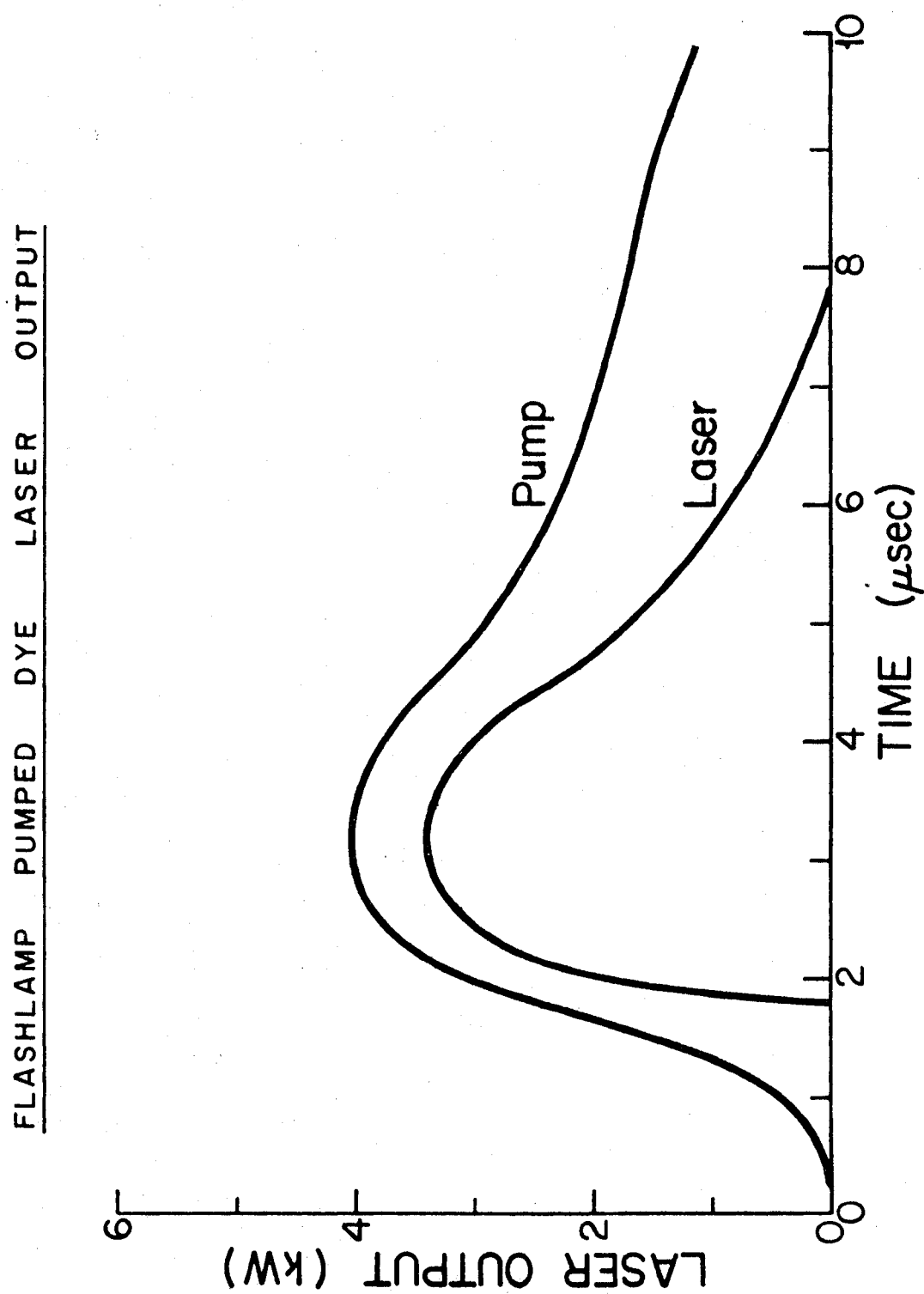


FIG. 9

However, it was found that it was difficult to excite the near ultra-violet and blue laser dyes with the type of flashlamps described previously as they did not produce the rapid risetimes necessary to overcome the triplet state losses described earlier. Also, in order to achieve relatively fast repetition rates (>20 pulses per second), the flashlamps must be water cooled. Both of these criteria make it desirable to obtain an alternative method for pumping the dye laser. For the above reasons it was decided to use a molecular nitrogen laser to pump the dye laser. This choice was made because the nitrogen laser-pumped dye laser design is simple, reliable, has a relatively fast repetition rate and can be tuned over the entire visible spectrum. The short pulse duration (≈ 10 nanoseconds) make this laser ideal for transient studies such as atomic or molecular collisions and lifetime measurements. The next section describes the design and the construction of the molecular nitrogen laser and the nitrogen laser-pumped dye laser.

6. THE NITROGEN LASER

Laser action from the electronic transitions of molecular nitrogen was first observed in the first positive bands by Mathias and Parker (1963) and in the second positive bands by Heard (1963). The laser constructed for pumping the dye laser was based on the superradiant laser line 337.1 nm which is the 0-0 vibrational transition in the second positive band ($C^3\Pi_u \rightarrow B^3\Pi_g$). Calculations of the saturated laser power density at 337.1 nm were first made by Gerry (1965) assuming direct excitation to the laser levels by electron impact and later refined by Ali et al (1967) to include the collisional mixing of the laser levels by electron impact and by ionizations from the upper laser level, $C^3\Pi_u$. In order to determine the dependence of the laser power density and its duration on various circuit and physical parameters, the rate equations for the nitrogen laser will be presented. These will be solved for the inversion criterion and a description of the construction and operation of the laser and the electrical circuits will be given. Detailed description of the rate equation solutions for the various design parameters has been given by Ali (1969) and will not be presented.

6(a). THE RATE EQUATIONS FOR THE NITROGEN LASER

Let N_1 , N_2 and N_3 denote the population densities of the ground state, the lower and upper laser levels respectively, and let X_{ij} denote the rate of collisional excitation by electron impact from level i to level j where $i < j$; Y_{ji} is the rate of collisional de-excitation from level j to level i and $(\tau_{ji})^{-1}$ is the rate of radiative decay from level j to level i . Let R_{ji} denote the rate of induced emission, which includes the Einstein's B coefficients, the linewidth and the energy density. The processes involved are shown in figure 10 (Gleason et al 1972). The rate equations are:

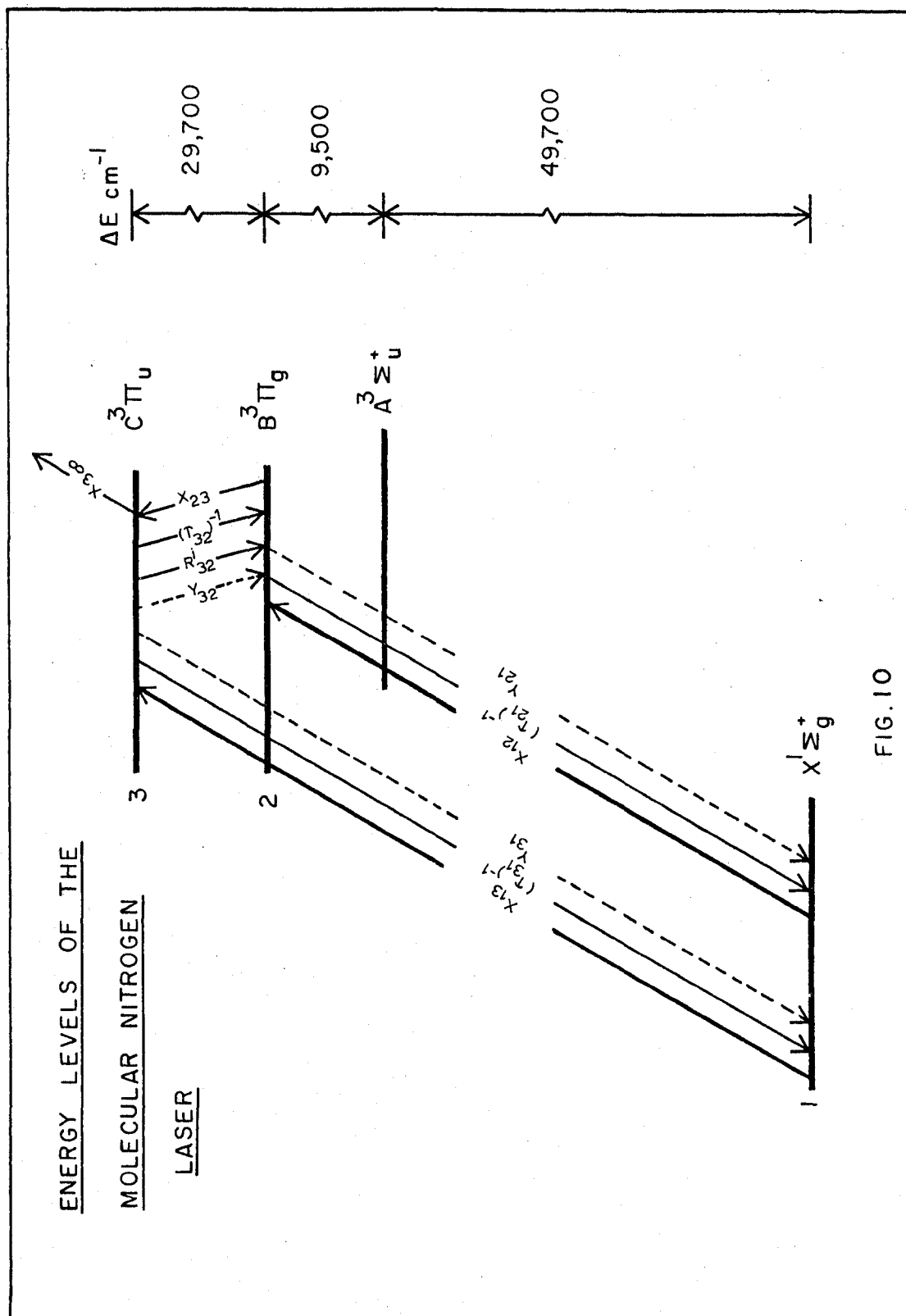
$$\frac{dN_3}{dt} = X_{13}N_1 + X_{23}N_2 - (Y_{31} + Y_{32} + \tau_{31}^{-1} + \tau_{32}^{-1})N_3 - R_{32}^i(N_3 - (g_3/g_1)N_2) \quad (21)$$

$$\frac{dN_2}{dt} = X_{12}N_1 + (\tau_{32}^{-1} + Y_{32})N_3 - (\tau_{21}^{-1} + Y_{21} + X_{23})N_2 + R_{32}^i(N_3 - (g_3/g_2)N_2) \quad (22)$$

$$\frac{dN_1}{dt} = -(X_{12} + X_{13})N_1 + (\tau_{21}^{-1} + Y_{21})N_2 + (\tau_{31}^{-1} + Y_{31})N_3 \quad (23)$$

The energy density Q_L at the laser frequency is given by:

$$(1/E_L)dQ_L/dt = N_3\tau_{32}^{-1} + R_{32}^i(N_3 - (g_3/g_2)N_2) \quad (24)$$



where g_3 and g_2 are the statistical weights of the upper and lower laser levels respectively, and $E_\ell = h\nu$ is the energy of a laser photon. Using the fact that $\tau_{31} \gg \tau_{32}$ (since the intermultiplet transitions have much smaller transition probabilities compared to those among each set), $X_{13} > X_{12}$ according to the Franck-Condon principle, and $\tau_{21} \gg \tau_{32}$ ($\tau_{32} \approx 40$ nsec while $\tau_{21} \approx 10^{-5}$ second (Ali 1967)) the sum of equations (21) and (22) can be written as:

$$d(N_2 + N_3)/dt = X_{13} N_1 \quad (25)$$

which has the solution:

$$N_3 + N_2 = X_{13} N_1 t \quad (26)$$

Equations (26) and (21) will give:

$$dN_3/dt = X_{13} N_1 + (X_{13} N_1 t - N_3) X_{23} - \beta N_3 \quad (27)$$

where $\beta = (\tau_{32}^{-1} + Y_{32})$. The solution to (27) is given as:

$$N_3 = (N_1 X_{13} / \alpha^2) (Y_{32} + \tau_{32}^{-1}) - (N_1 X_{13} / \alpha^2) (Y_{32} + \tau_{32}^{-1}) \exp(-\alpha t) + (N_1 X_{13} X_{23} t / \alpha) \quad (28)$$

where $\alpha = \beta + X_{23}$. For small times the exponential can be expanded in terms up to t^2 giving:

$$N_3 = N_1 X_{13} t - N_1 X_{13} (Y_{32} + \tau_{32}^{-1}) t^2 / 2 \quad (29)$$

Equations (26) and (29) yield:

$$N_2 = \frac{1}{2} N_1 X_{13} (Y_{32} + \tau_{32}^{-1}) t^2 \quad (30)$$

The condition for inversion will be that $N_3 > N_2$ and therefore:

$$2 / (Y_{32} + \tau_{32}^{-1}) > t \quad (31)$$

which implies that inversion takes place in times small compared to $(Y_{32} + \tau_{32}^{-1})^{-1}$. Ali et al (1967) have shown that if electron impact ionization is taken into account, equation (31) should be modified to include the rate of collisional ionization $X_{3\infty}$ as shown in figure 10. Equation (31) then becomes:

$$2 / (Y_{32} + \tau_{32}^{-1} + X_{3\infty}) > t \quad (31)$$

The above quantity is about 15 to 20 nanosecond (Ali et al 1967) and thus the population inversion must occur in the first few nanoseconds after the start of excitation. This implies that the electrical circuits used to produce the discharge in the nitrogen gas must be capable of producing pulses with risetimes of a few nanoseconds.

Since the laser must be constructed with an electrical circuit capable of producing excitation pulses with risetimes in the range of a few nanoseconds, the cross field excitation method was chosen

(Leonard 1965). In the cross field or transverse discharge the discharge occurs between two electrodes which are placed each side of the laser channel along its entire length. This enables long laser tubes to be used with short interelectrode spacings, so that appropriate electric field strengths are produced by comparatively low voltages (~ 10 to 20kv). It has been shown by Ali(1969) that if the discharge is instantaneous along the entire length of the chamber, one has to consider the time history of the power density when designing the length of the laser cavity. In most nitrogen lasers, the laser pulse density terminates in about 5 to 10 nanoseconds. This implies that the cavity length must be no longer than about 1 to 2 metres ($d = ct$) because the lower laser level is a long lived state (10 microseconds) and hence it will absorb the laser light. However, if one utilizes travelling wave excitation along the length of the laser cavity (Shipman 1967), the excitation pulse is synchronized with the arrival of the laser light from the preceding section and in principle the laser cavity can be made as long as desired.

6(b). GENERAL DESCRIPTION OF THE NITROGEN LASER

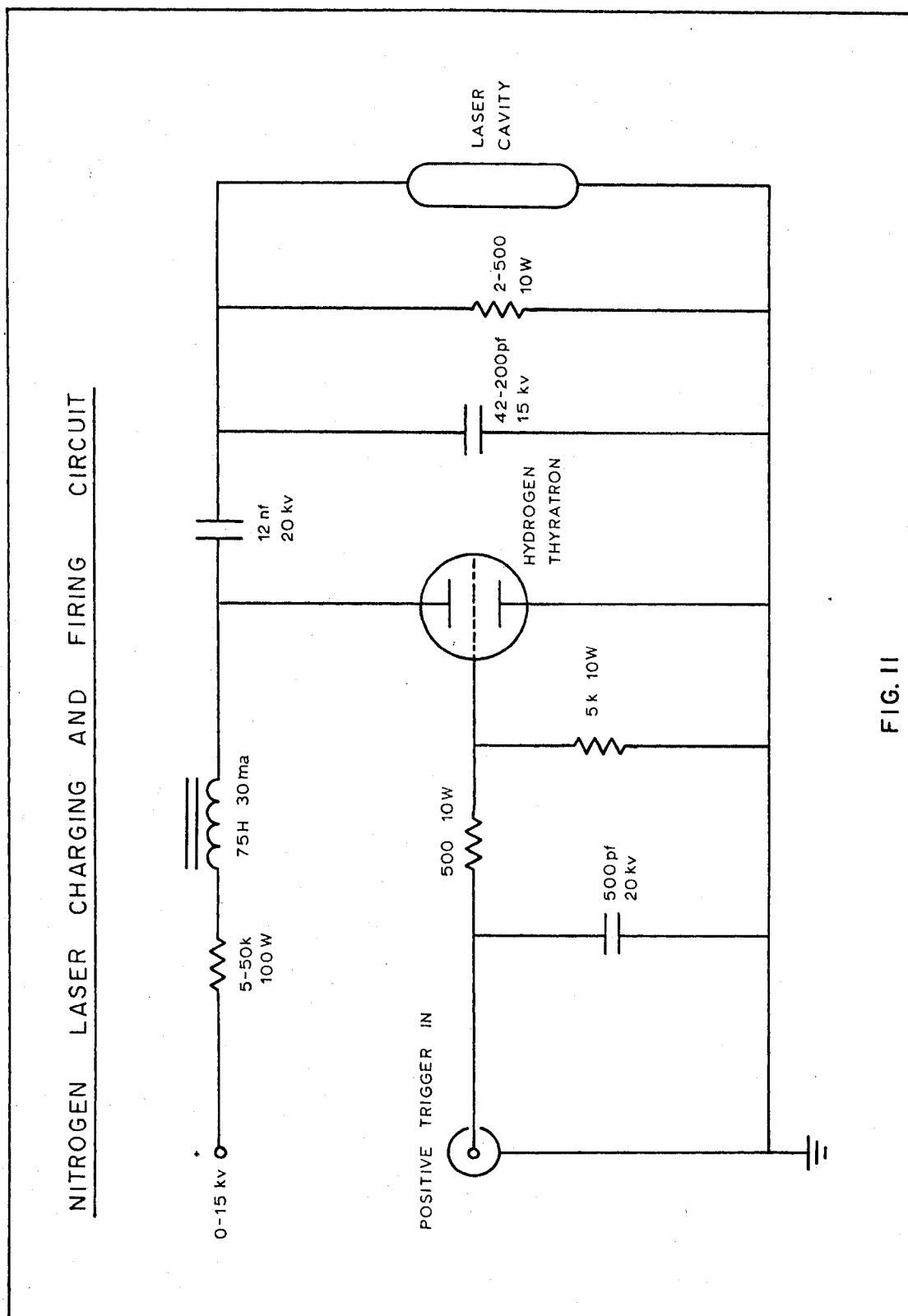
The laser channel consists of two plates of glass supported by an aluminum U-channel which serves both for support and as the grounded anode. The cathode side of the laser channel consists of an aluminum bar and a band saw blade electrode. Both the aluminum bar and the U-channel are water cooled. Forty two dumping capacitors

are mounted in parallel along the laser channel. These are connected to the cathode by a copper bus bar. The dumping capacitors are also connected to a low inductance storage capacitor by an aluminum bus bar placed over the copper bus bar (see figure 12).

The storage capacitor is charged to 10 to 15 kv through a bleeder resistor. When the thyatron switch closes grounding the positive side of the floating storage capacitor, the other side is established at a high negative voltage. Its charge then flows on the bus bar to the dumping capacitors which provide the energy for the discharge in the nitrogen. When the dumping capacitors reach the nitrogen gas breakdown voltage, the discharge is initiated and the dumping capacitors rapidly discharge. The electrical circuit is constructed in a coaxial arrangement to minimize the inductance and provide the fast risetimes necessary to cause a population inversion in the nitrogen gas. The pulsed molecular nitrogen laser electrical discharge circuit is shown in figure 11.

6(c). MECHANICAL CONSTRUCTION OF THE LASER

The base of the laser channel is a one metre length of aluminum U-channel 4.8 x 6.2 cm with a thickness of 1.3 cm (see figure 12). Four double strength tempered glass plates (Shenck 1973) form the side walls of the laser channel. Each side is formed by two plates, one 0.5 x 5.6 x 99 cm, the other 0.3 x 6.3 x 100 cm, which are sealed to the aluminum U-channel using General Electric silicon sealant



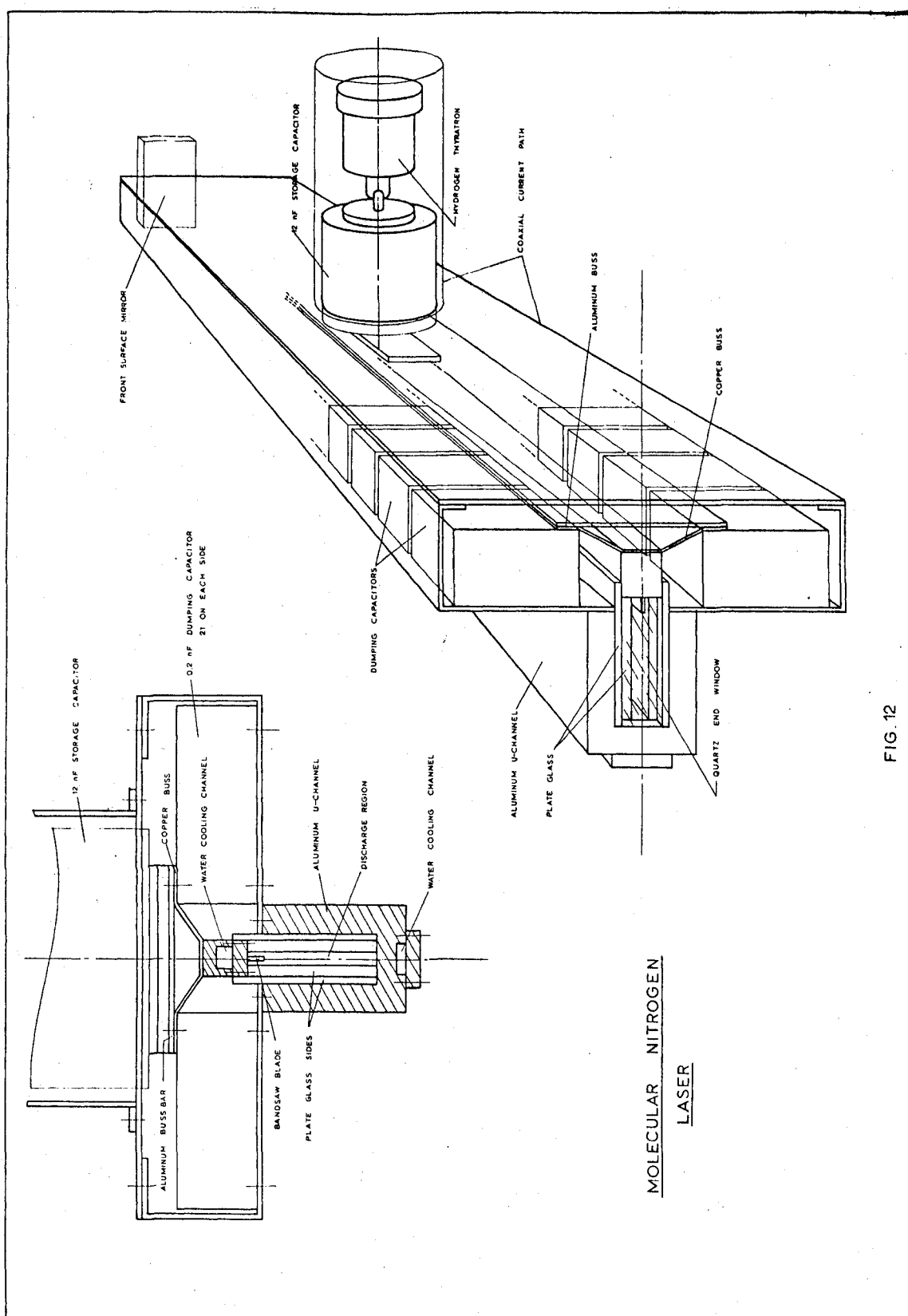


FIG. 12

(RTV102). The silicon sealant alleviates the problem of mechanical construction because it is easily applied and stays flexible when cured. A good vacuum seal is not important because the operating pressure of the flowing nitrogen in the laser is 15 to 20 Torr. The dumping capacitors are mounted on each side of the U-channel as shown in figure 12. Two 3 mm holes centred in the bottom of the U-channel are used to admit and withdraw the nitrogen.

The band saw blade is about 1 mm thick, 15 mm wide, with very little set and teeth every 2mm. It was 1 cm shorter than the laser channel to prevent the discharge from contaminating the end windows. The ends of the channel are sealed with optical grade quartz windows 2 mm thick, which are attached to the ends of the glass walled U-channel with silicon sealant. The entire laser channel was mounted in an aluminum box 110 x 56 x 34 cm. This provides mechanical support for the electrical components and an adjustable front silvered mirror as well as providing electrical shielding. The nitrogen flow system contains a standard fore pump to pump dry tank nitrogen with a nominal purity 99.997 percent, through the laser channel. The pressure is monitored by an Edwards C.G.3 speedivac gauge and regulated by a Hoke 233454B needle valve in the input line.

6(d). ELECTRICAL CONSTRUCTION OF THE LASER

The complete circuitry of the molecular nitrogen laser is shown in figures (13) and (14). The circuit incorporates a unijunction

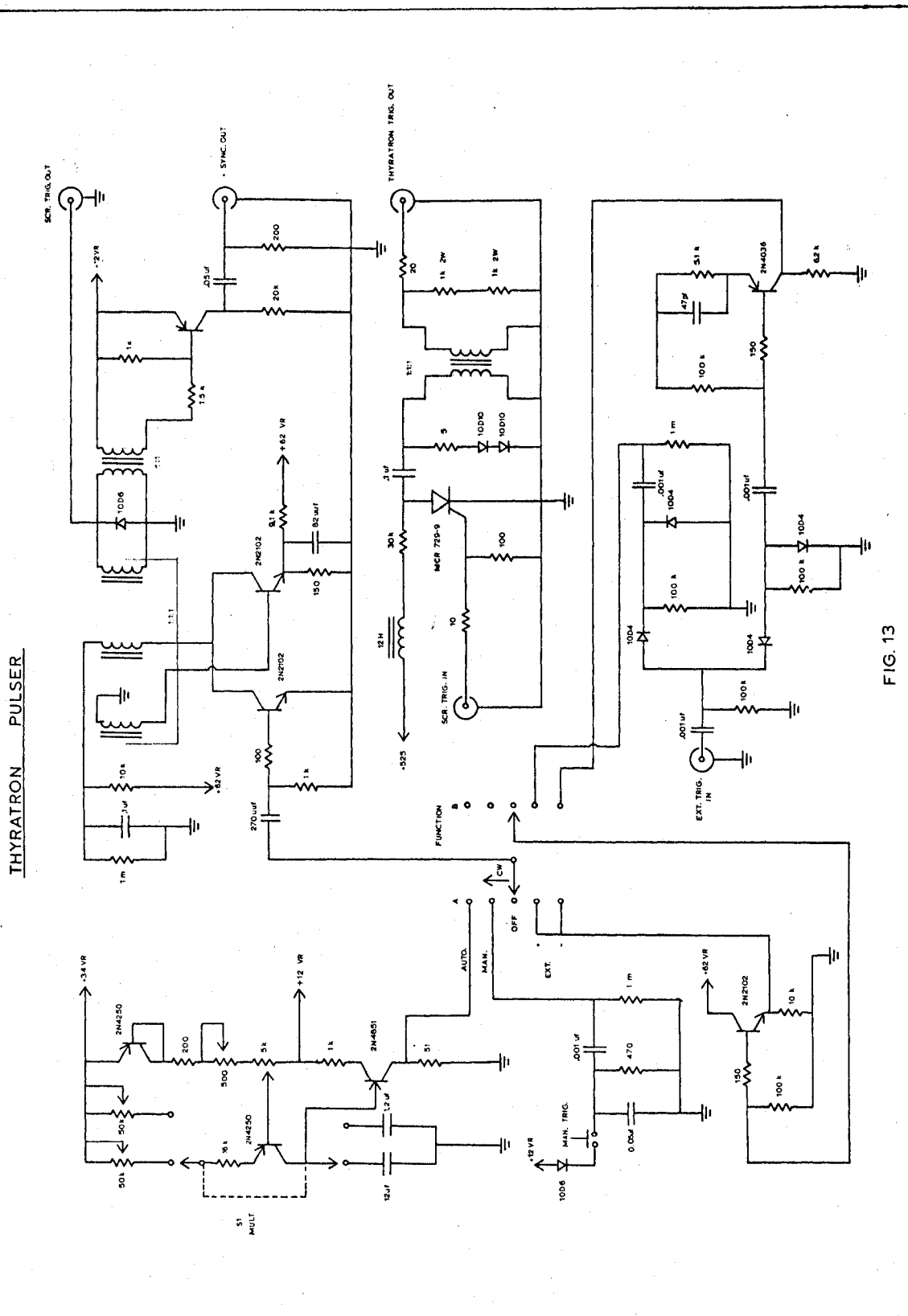
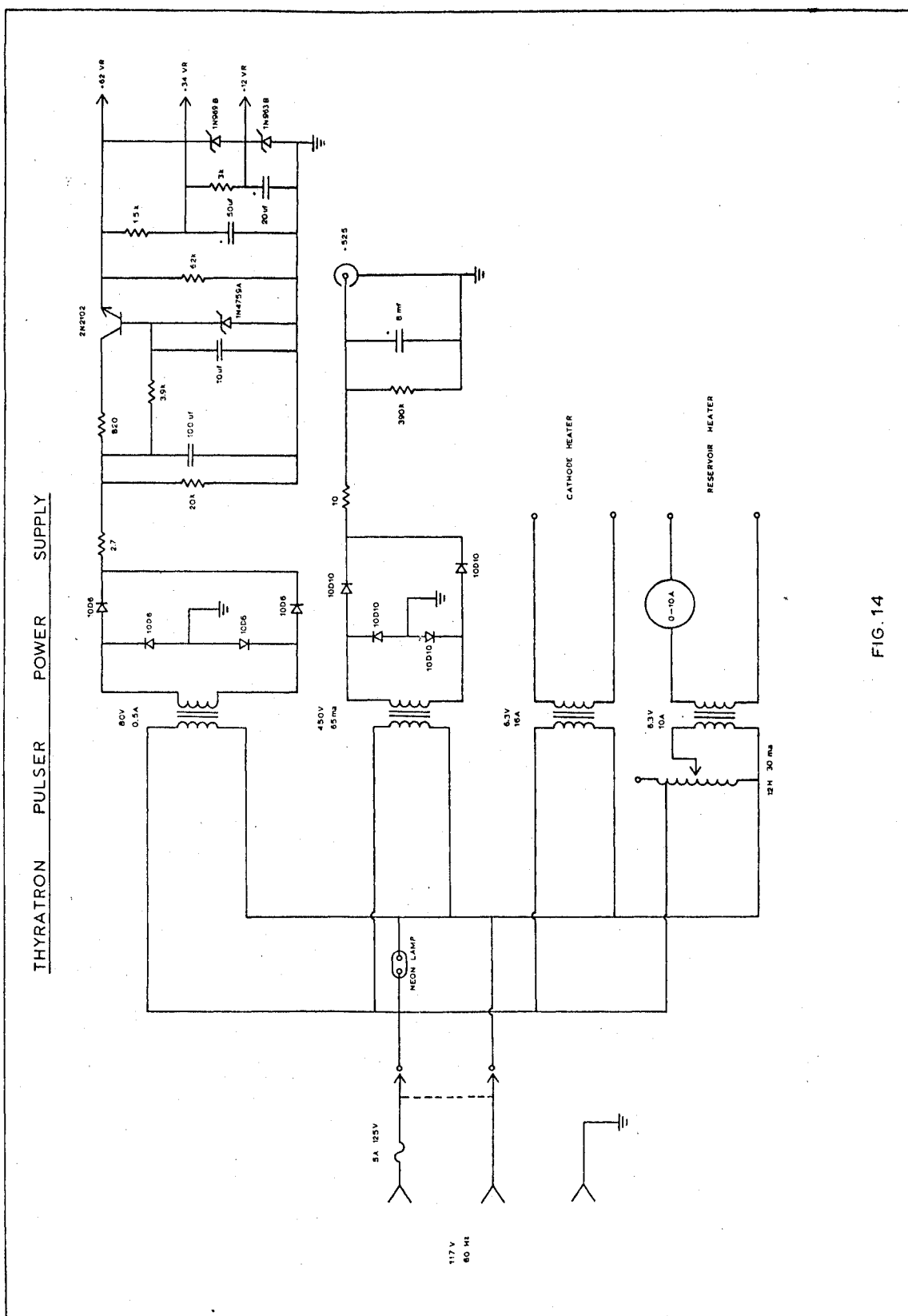


FIG. 13



oscillator and an SCR to fire the thyatron through a trigger transformer. The thyatron is a hydrogen filled E.G. and G. HV35 which will switch the high voltage when provided with a 1000 volts pulse to the grid. In order to prevent high voltage grid flashback, which will destroy the triggering circuitry, a negative voltage must be applied to the grid to shut off the thyatron. This is provided by a filter between the grid and the triggering transformer, so that the back voltage produced by its reactance turns off the thyatron. The oscillator section has provisions for manual, automatic and external positive or negative trigger pulses at a repetition rate of from 0 to 100 pulses per second. A reference pulse is also provided for external use.

The storage capacitor is a low inductance, 12 nanofarad, 20 kv capacitor. The low inductance is necessary as the transfer of charge must be accomplished early in the breakdown of the nitrogen. The storage capacitor is mounted on the aluminum bus bar, both for mechanical support and to make the electrical connection to the dumping capacitors. The thyatron is mounted on the end of the storage capacitor, separated from it by a heat dissipative fin. The ground end of the thyatron is connected to the U-channel by a metal cylinder that fits coaxially around the storage capacitor and the thyatron. The discharge system is thus coaxial minimizing the inductance.

The high voltage was supplied by a Universal Voltronics 25 kv supply. The laser required about 5 milliamperes when operating at 20 pulses per second and 13 kv.

6(e). OPERATION AND PERFORMANCE

The use of the band saw blade as a multiple electrode structure resulted in a very uniform discharge in the nitrogen laser cavity over a pressure range of 10 to 20 Torr. The pulse-to-pulse uniformity of the laser was about ± 10 percent. The threshold of the laser's operation was about 9 kv at a pressure of 17 Torr. At an input voltage of 13 kv, the output power was about 110 kW (measured by an SGD-100A photodiode). The pulse duration was measured using a delayed coincidence technique (eg. Phaneuf 1973) and found to be about 10 nanoseconds. This gives an energy of about 0.4 to 0.5 millijoules per pulse. The efficiency is thus, about 0.05 percent since the energy stored in the 12 nanofarad capacitor is 1 joule. Figure 15 shows the pulse shape as measured by the delayed coincidence technique, along with the pulse shape calculated from the rate equations as solved by Ali (1969) and figure 16 shows the peak output power for various nitrogen pressures. It can be seen that the optimum operating pressure is about 17 Torr for an initial voltage on the storage capacitor of 13 kv.

The power decreased drastically if the first surface mirror is removed or misaligned. Removal of the mirror increases the beam divergence and produces a very inhomogeneous beam. The spectral output (Massone et al 1972) is a composite of lines in a 0.1 nm band about 337.1 nm. The laser will operate with air flowing through the cavity, but with a reduced output and pulse uniformity.

NITROGEN LASER OUTPUT PULSE

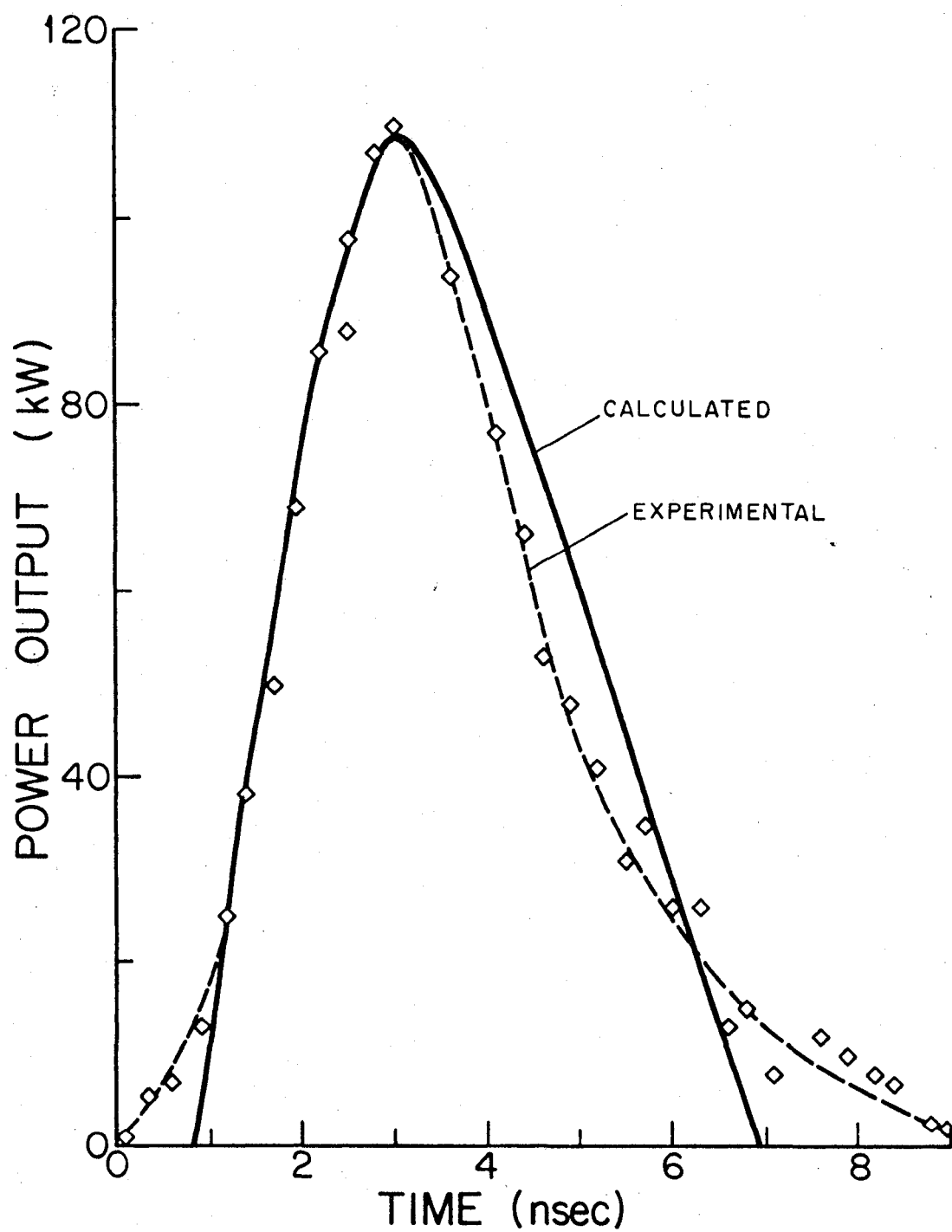


FIG. 15

NITROGEN LASER OUTPUT POWER AS A
FUNCTION OF NITROGEN PRESSURE

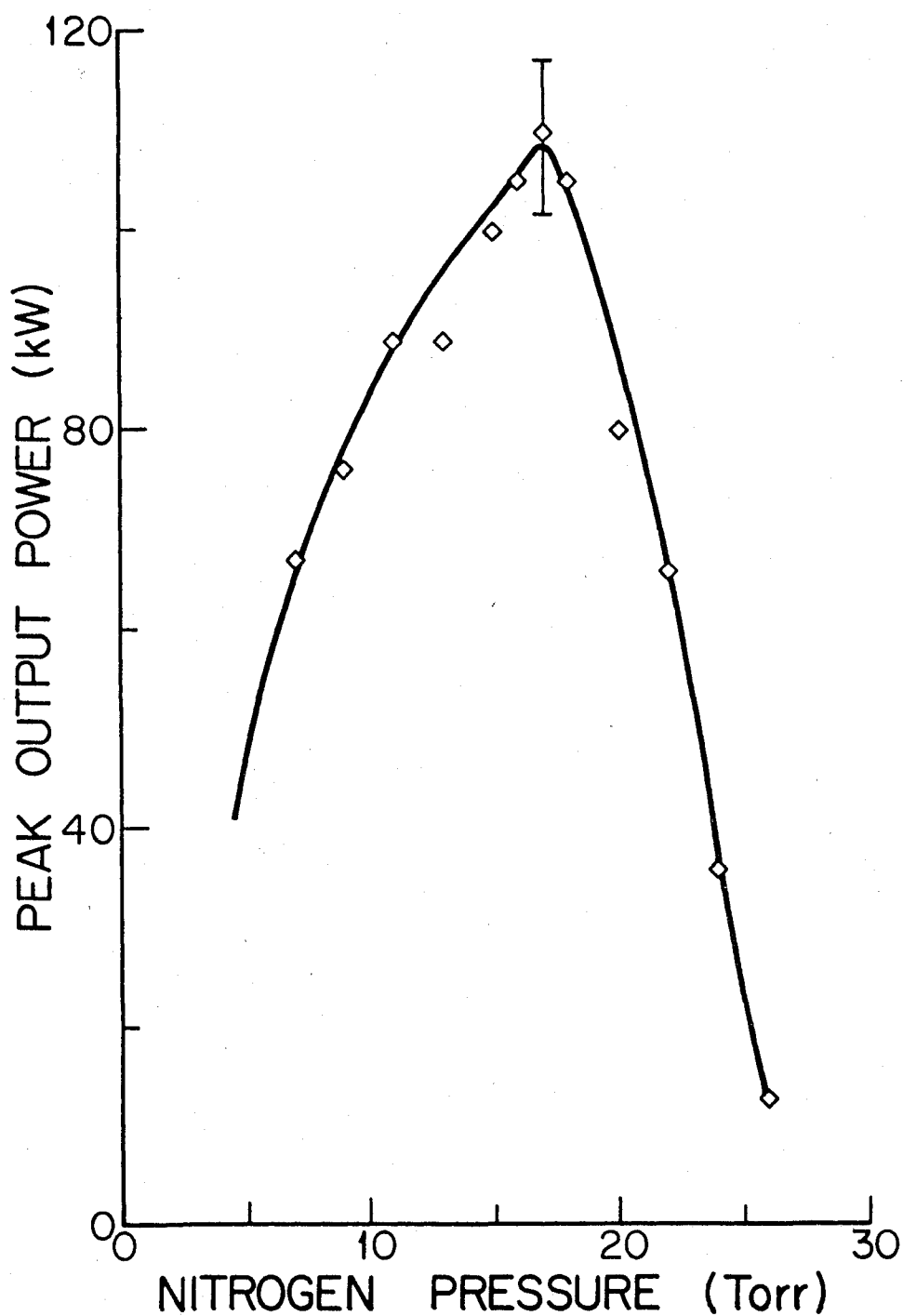


FIG. 16

7. THE NITROGEN LASER-PUMPED DYE LASER

Pulsed molecular nitrogen lasers operating at 337.1 nm have been used to stimulate dyes to lase with broad band outputs in various regions of the spectrum by many authors (eg. Capelle and Phillips 1970, Broida and Haydon 1970, Meyer et al 1970, 1970a). A list of dyes and their lasing ranges when pumped by the molecular nitrogen laser have been summarized by Capelle and Phillips (1970a). Examples of the different methods of obtaining tunable narrow band emission from organic dye lasers by inserting dispersive elements into the cavity have been reported by Soffer and McFarland (1967), Gibson (1969), Bradley et al (1968), Walther and Hall (1970) and by Taylor et al (1971). As has been shown in section II.4(a), long-pulse flashlamp-pumped dye lasers exhibit substantial line narrowing and the spectral width of the output can be a fraction of a nanometre using a dispersive element of low wavelength dispersion. In dye lasers pumped by a molecular nitrogen laser, bandwidths below 1.0 nm are more difficult to achieve. As shown in section II.4(b), the output linewidth of the nitrogen laser-pumped dye laser should not be significantly different from the bandpass of the dispersive element inserted into the laser cavity. Capelle and Phillips (1970a) used a high dispersive grating, but could only achieve a linewidth of 0.5 nm. This is partly due to the short pulse duration and the small beam diameter of the dye laser. The use of a thick holographic grating reduced the linewidth to 0.04 nm (Kogelnik et al 1970) and single

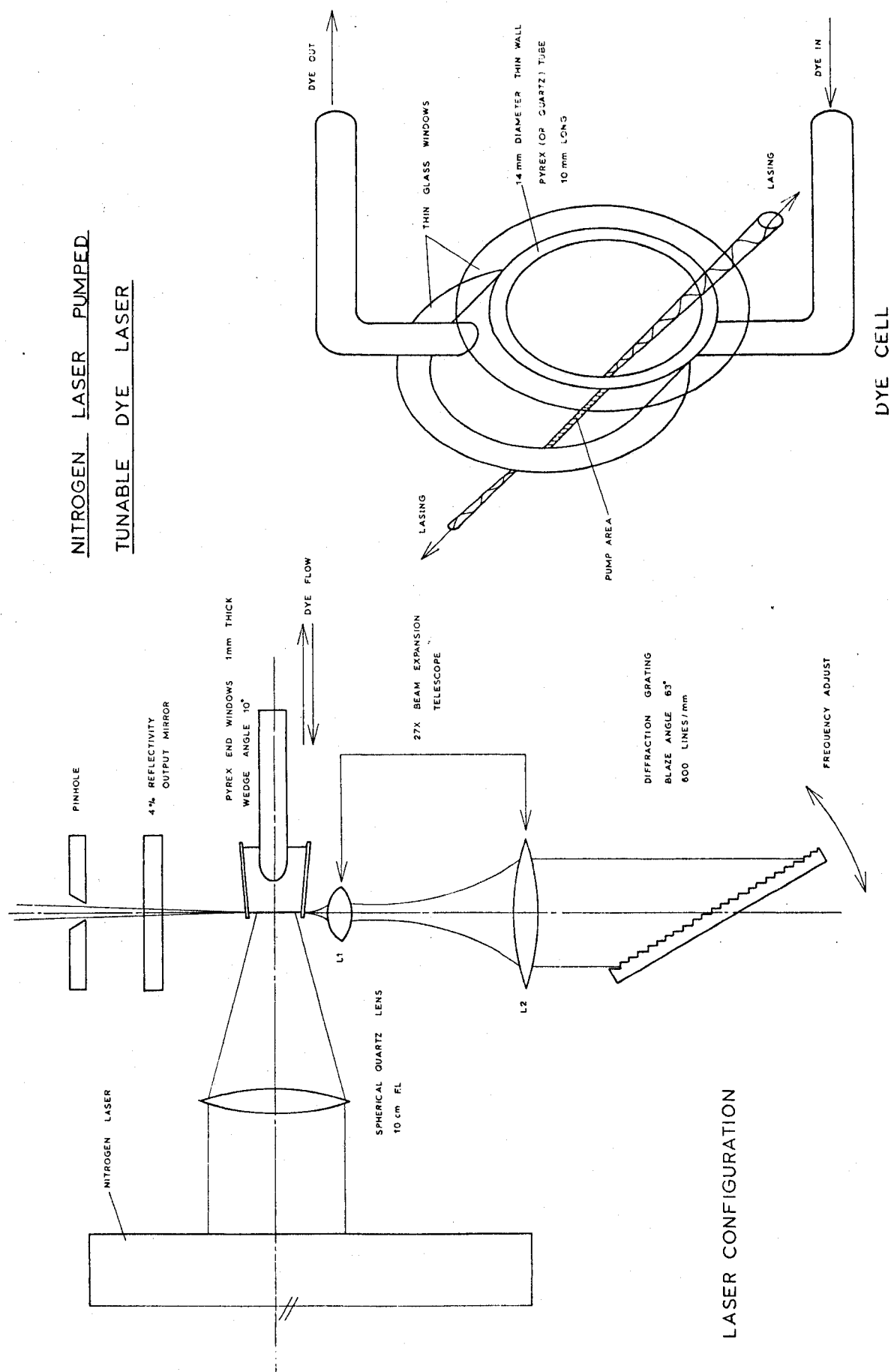
axial mode operation of a nitrogen laser-pumped dye laser with a linewidth of 0.001 nm has been achieved with a holographic grating and a Lyot filter (Hänsch and Schawlow 1970) or a grating and a Fabry-Perot etalon (Hänsch and Schawlow 1970, Itzkan and Cunningham 1971). However the wavelength reproducibility of the last two methods was unsatisfactory.

Stable narrow band emission (0.0004 nm FWHM) of a nitrogen laser-pumped dye laser has been described by Hänsch (1972). In this design, an intracavity beam expansion telescope together with a diffraction grating in a Littrow mount and a tilted Fabry-Perot etalon provided convenient, highly reproducible wavelength tuning with good stability. Peak output powers in the kilowatt range can be generated with pulse lengths in the 5 to 100 nanoseconds range at repitition rates up to 100 pulses-per-second. Since this design proved to be a reliable narrow band dye laser, the laser constructed was based on the design of Hänsch. Futhermore, since the sensitized fluorescence experiments that were done with this laser did not require linewidths as narrow as 0.0004 nm. the Fabry-Perot etalon was not used. This resulted in some inefficiency in exciting the alkali vapours, as the resulting linewidth of the dye laser was about a factor of ten larger than the Doppler widths of the alkalis that were studied. However, it ensured a thermal velocity distribution of excited atoms as the exciting line is much wider than the absorbing line, and reduced the problem of maintaining the dye laser wavelength at the centre of the absorption peak.

7(a). GENERAL DESCRIPTION

Since an unsaturated single pass power gain of 1000 over a pathlength of a few millimetres can be easily achieved in a dye laser pumped by a nitrogen laser (Shank et al 1970, Hänsch et al 1971), one can use very narrow band wavelength selective devices, despite their losses.

The basic components of the dye laser based on the above criteria are shown in figure 17. A side pumped dye cell is placed in a cavity 30 cm long using a diffraction grating as a wavelength selective end reflector. Since only a thin layer near the inner wall of the dye cell is excited by the pump light from the nitrogen laser (see figure 17), diffraction causes a substantial angular spread of the emerging light, which would limit the resolution obtainable from the angle dependent grating (Born and Wolf 1970). In addition only a small portion of the grating would be illuminated, further limiting the resolution. As a result an inverted telescope is placed inside the cavity to ensure that the beam illuminating the grating is well collimated and covers a large area to ensure good resolution. Fine tuning is achieved by mechanically changing the angle of incidence of the diffraction grating. All parts of the dye laser head were mounted rigidly on an optical bench. The output mirror and the diffraction grating were supported in precision angular orientation devices with adjustments controlled by micrometer screws.



7(b). THE DYE LASER AMPLIFIER

The dye cell is 10 mm long and constructed from pyrex tubing of 14 mm outside diameter. Pyrex end windows were sealed to the cell under a wedge angle of about 10 degrees to avoid internal cavity effects. The seals were made with epoxy glue or RTV102. Dye solutions that contained methyl alcohol dissolved the epoxy and in this case the silicone sealant was used. A quartz cell with quartz windows was also constructed using Vitta¹ quartz transfer tapes to make the seal. The dye solution is transversely circulated at a rate of approximately 1 litre per minute using a small centrifugal pump.

The ultraviolet light (337.1 nm) from the molecular nitrogen laser was focused by a spherical quartz lens of 10 cm focal length into a line approximately 0.07 mm wide at the inner cell wall. To provide a nearly circular cross section, the dye concentration was adjusted so that the penetration of the pump light from the nitrogen laser was about 0.07 mm. This means that the dye solutions will be relatively insensitive to small amounts of impurities, as the concentrations used were about 5×10^{-3} M per litre to achieve the above conditions. By solving the rate equations of section II.2 it can be shown that the relative density of the excited singlet state can reach 20 percent under these conditions.

Even though the pumping energies are high (several Joules per

1. Vitta Corporation, Wilton Conn.

cm^3), no thermal optical distortions are observed during the short excitation pulse, thus the amplifying medium remains very homogeneous during the pulse. The thermal schlieren effects occur with a time delay after the absorption of the pumping light (Hänsch 1971a). The return to optical uniformity before the next pumping pulse is ensured by circulating the dye solution.

Most of the previous nitrogen laser-pumped dye lasers used longer dye cells (Myer et al 1970, Capelle and Phillips 1970a, Kogelnik et al 1970, Capelle and Phillips 1970). In this situation the small signal gain is so high that gain saturation is reached in a single pass and the tuning element has no effect. This saturation of the dye medium by amplified unfiltered spontaneous emission is called superradiance. In addition it is difficult to match the active volume to a diffraction limited beam due to the large angular divergence resulting from the small active cross section.

7(c). OUTPUT MIRROR AND BEAM EXPANSION TELESCOPE

A plane mirror is mounted at one end of the cavity as an output mirror. For use with high gain dyes such as rhodamine 6G, POPOP and 4 methyumbelliferone, an uncoated quartz surface with 4 percent reflection is sufficient. However for dyes with relatively low gain, a higher reflectivity mirror should be used.

Spontaneous fluorescence emitted into the near axial directions in the active region is amplified. Part of this light is reflected

by the plane output mirror back into the dye cell, where it is further amplified and emerges as a narrow beam at the other end. The angular divergence of the beam is essentially diffraction limited (Hänsch 1972). If one assumes a Gaussian beam profile with radial intensity distribution given by:

$$I = I_0 \exp(-2r^2/\omega^2) \quad (34)$$

with waist size ω_1 at the centre of the active volume, the diffraction limited angular divergence of the emerging beam is given by (Kogelnik 1965) as:

$$\Delta\theta_1 = \lambda/\pi\omega_1 \quad (35)$$

At a waist size of 0.07 mm and a wavelength in the 500.0 to 600.0 nm range, the divergence angle $\Delta\theta_1$ is about 2.4 milliradians.

The cavity telescope consists of two lenses L_1 and L_2 of focal lengths $f_1 = 3$ mm and $f_2 = 80$ mm. Both are antireflection coated multielement systems. The separation between the dye cell and L_1 is about 2 cm. The telescope is mounted in such a manner that it can be moved freely in all directions using micrometre adjusting screws.

The waist diameter ω_2 of the expanded beam at optimum collimation can be calculated according to Kogelnik (1965) to be:

$$\omega_2^2 = (f_2^2/f_1^2) \{ \omega_1^2 + (f_1 - d_1)^2 (\lambda/\pi\omega_1)^2 \} \quad (36)$$

The initial waist size of 0.07 mm is thus enlarged by the telescope to about $\omega_2 = 4$ mm (if λ is about 500.0 nm), and the divergence is reduced to:

$$\Delta\theta_2 = \lambda/\pi\omega_2 = 0.04 \text{ mrad.} \quad (37)$$

7(d). THE DIFFRACTION GRATING

The high order diffraction grating (blaze angle 63 degrees, 600 lines/mm) is held in a precision angular orientation mount with a mechanical resolution of 0.02 arc-second. If the angle of incidence is ϕ , the angular dispersion of a diffraction grating in a Littrow mount is given by Born and Wolf (1970):

$$d\phi/d\lambda = (2 \tan\phi)/\lambda \quad (38)$$

Since the attainable resolution is proportional to the number of grooves, the grating must be at least as large as the oblique beam cross section $2\omega_2/\cos(\phi)$. If the back reflected beam is displaced by one beam waist at the dye cell active volume, it will not be transmitted and thus further amplified. The deflection angle at the grating will thus be at least equal to the beam divergence $\Delta\theta_2$. The corresponding wavelength deviation is given by equations (37) and (38):

$$\Delta\lambda_g = \lambda^2/2\pi\omega_2 \tan(\phi) \quad (39)$$

Under the above conditions the estimated linewidth of the nitrogen laser-pumped dye laser will be about 0.01 nm. From the earlier discussions, the resultant linewidth of the nitrogen laser-pumped dye laser should also be about 0.01 nm.

7(e). OPERATION AND EXPERIMENTAL DATA

Experimental performance characteristics of the dye laser are given for operation near 600.0 nm using a 5×10^{-3} M per litre solution of rhodamine 6G in methanol. Similar data has been obtained in other regions of the spectrum with POPOP in toluene and 4-Methylumbelliferone in methanol.

The output beam exhibits a near diffraction limited divergence of about 2.4 milliradians. Some weak side maxima, which arise due to the nonuniform transverse gain distribution in the side pumped configuration, are easily eliminated by the insertion of an external pinhole. The output power of the dye laser was measured with a calibrated SGD-100A photodiode. An energy output of 50 microjoules was measured which corresponds to peak powers of 5 to 10 kw, assuming a dye laser pulse FWHM of about 4 nanoseconds. This corresponds to a conversion efficiency of about 10 to 15 percent as the molecular nitrogen laser output energy is about 0.04 millijoule per pulse. The dye laser pulse shape and duration were measured using a delayed coincidence technique (eg. Phaneuf 1973). The results indicate a

pulse with a duration of about 10 nanoseconds (see figure 18).

The bandwidth was measured using a Fabry-Perot etalon with a free spectral range of 0.02 nm and an instrumental bandwidth of 0.004 nm at 600.0 nm. The results indicate a bandwidth of about 0.01 nm FWHM. This result is in good agreement with the theoretical value discussed previously.

It has been shown (Hänsch 1972) that the fluctuations in the frequency are less than 0.001 nm, in the absence of undue temperature variations and mechanical vibrations. However the variation in the peak output power was measured to be about ± 15 to 20 percent. This fluctuation is indicated in figure 18.

This design of tunable laser is capable of operation up to 100 pulses per second. The spectral purity, nearly diffraction limited beam divergence and reproducible wavelength tunability render this laser a powerful tool for optical spectroscopy. The short pulse duration (10 nanoseconds) make this laser an ideal instrument for dynamic studies, such as the measurement of relaxation rates, lifetimes and collisional processes. It has also proven to be useful for nonlinear spectroscopy techniques and high resolution spectroscopy of Doppler broadened transitions (Hänsch et al 1971b). In the remainder of this report the description and results of two atomic collision experiments performed with this laser will be discussed.

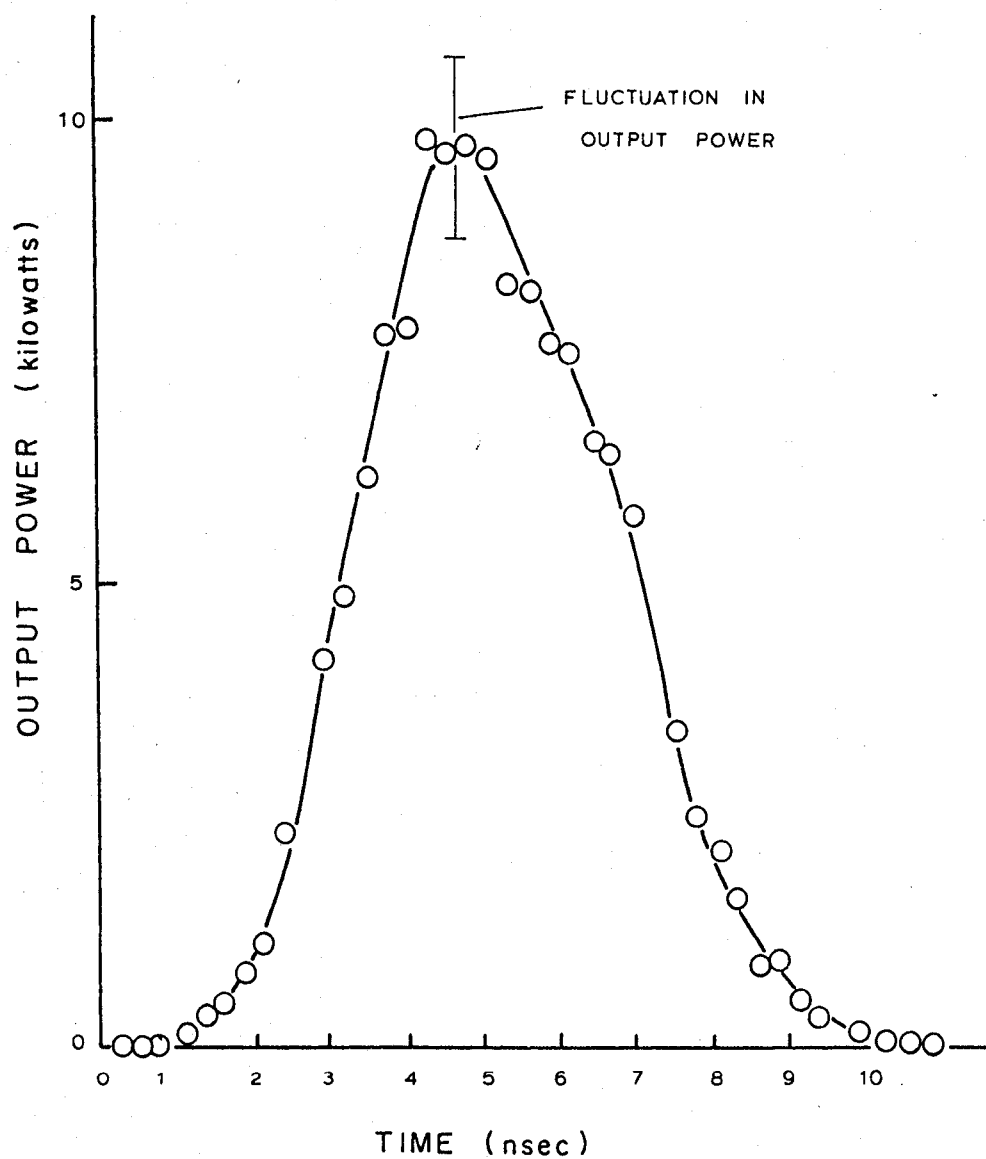
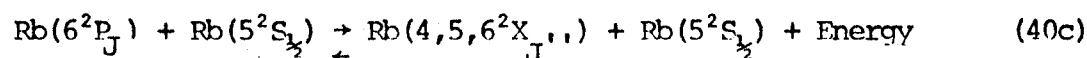
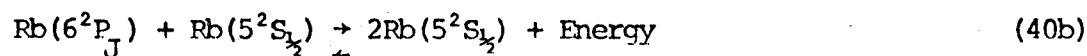
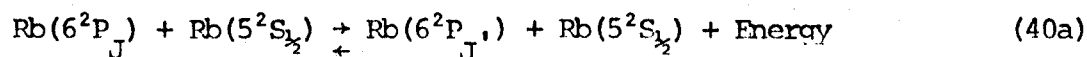
NITROGEN LASER PUMPED DYE LASERTEMPORAL LINESHAPE

FIG. 18

III. TRANSFER OF ELECTRONIC EXCITATION BETWEEN THE $6^2P_{3/2}$ AND THE $6^2P_{1/2}$ STATES OF RUBIDIUM AND THE $7^2P_{3/2}$ AND THE $7^2P_{1/2}$ STATES OF CESIUM INDUCED BY COLLISIONS WITH GROUND STATE ATOMS OF THE SAME TYPE

1. THEORETICAL

The processes that ensue when one fine structure state of the n^2P alkali doublet is irradiated with a short pulse (≈ 10 nanoseconds) of light are shown schematically in figure 19. The energy levels are taken from the tables of Moore (1952). The inelastic interactions of interest for rubidium may be represented by:



where J or J' is $1/2$ or $3/2$ and J'' is $1/2, 3/2$ or $5/2$ depending on whether X represents the states S, P or D . Similar equations can be written for cesium involving the $6^2S_{1/2}$ ground state and the 7^2P doublet. Equation (40a) describes the mixing of the 2P_J substates and is the primary subject of this investigation. In addition to the mixing processes, quenching to the $^2S_{1/2}$ ground state and transfer of excitation

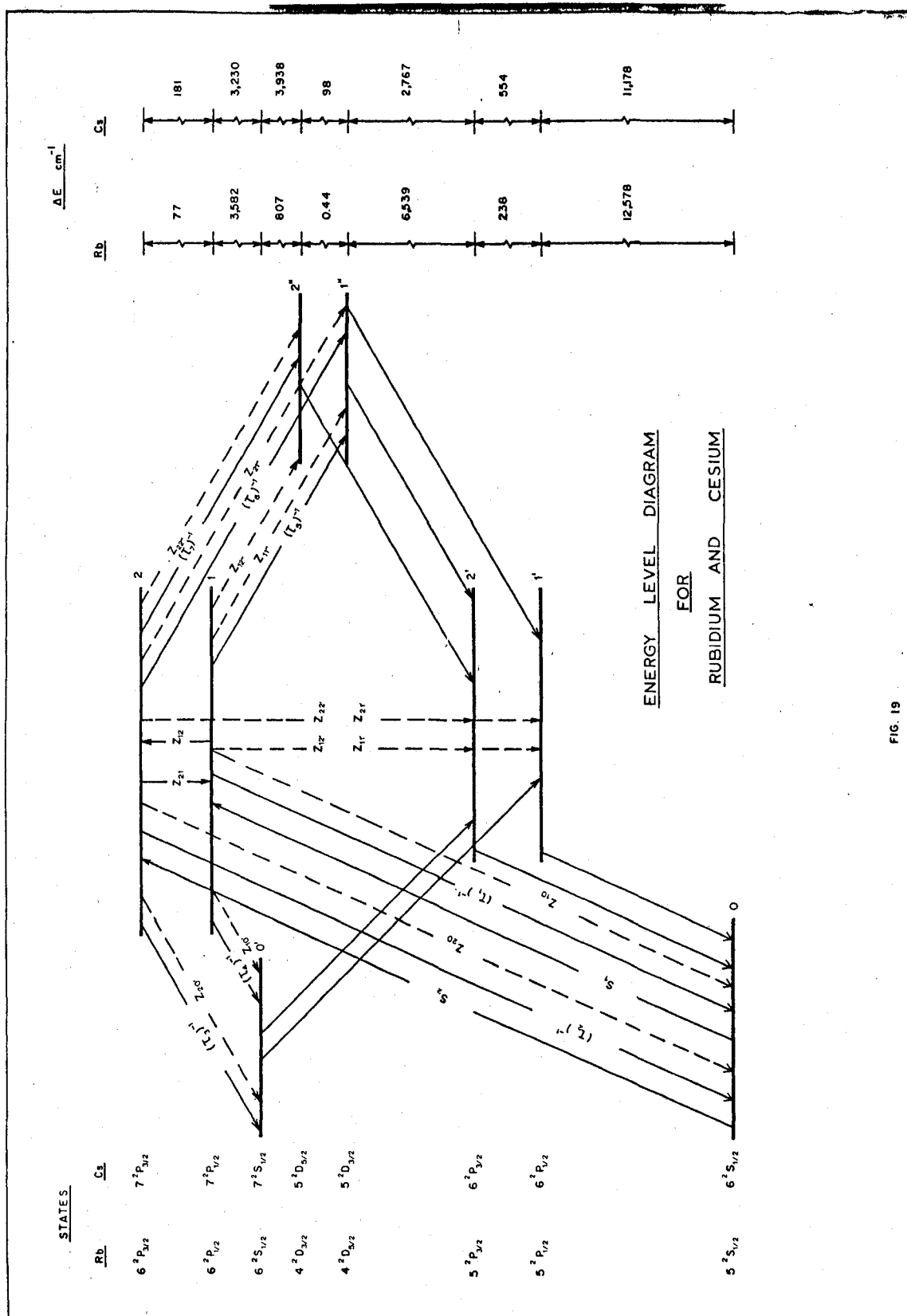


FIG. 19

to the lower lying 2S , 2D and 2P states, described by equations (40b) and (40c) respectively, may also occur. The latter processes jointly manifest themselves as the total effective quenching of the 2P states. In figure 19, the mixing collisions in the lower lying 2D and 2P states have been neglected, since although they will be present, they will not influence the measurements. If we represent the $6^2P_{3/2}$ state of rubidium (or the $7^2P_{3/2}$ state of cesium) by the subscript 2, and the $6^2P_{1/2}$ state of rubidium (or the $7^2P_{1/2}$ state of cesium) by the subscript 1, and define the pumping rate to state 2 as $s_2(t)$ and to state 1 as $s_1(t)$, we can write the following rate equations for the P states (the following arguments apply to both rubidium and cesium):

$$\dot{N}_2 = s_2(t) + N_1 Z_{12} - N_2 (1/\tau_2 + 1/\tau_3 + 1/\tau_7 + 1/\tau_6 + Z_{20} + Z_{21} + Z_{20'} + Z_{22''} + Z_{21'}) \quad (41)$$

$$\dot{N}_1 = s_1(t) + N_2 Z_{21} - N_1 (1/\tau_1 + 1/\tau_4 + 1/\tau_5 + Z_{12} + Z_{10} + Z_{21'} + Z_{11''}) \quad (42)$$

If we now write :

$$1/\tau_{3/2} = 1/\tau_2 + 1/\tau_3 + 1/\tau_6 + 1/\tau_7 \quad (43)$$

$$1/\tau_{1/2} = 1/\tau_1 + 1/\tau_4 + 1/\tau_5 \quad (44)$$

and letting:

$$\Gamma_2 = 1/\tau_{3/2} + Z_{21} + (Z_{20} + Z_{20'} + Z_{22''} + Z_{21''}) \quad (45)$$

$$\Gamma_1 = 1/\tau_{1/2} + Z_{12} + (Z_{10} + Z_{21'} + Z_{11'}) \quad (46)$$

we get the following equations:

$$\dot{N}_2 = s_2(t) + N_1 Z_{12} - N_2 \Gamma_2 \quad (47)$$

$$\dot{N}_1 = s_1(t) + N_2 Z_{21} - N_1 \Gamma_1 \quad (48)$$

where N_1 and N_2 represent the density of atoms in the levels 1 and 2 respectively.

Previous work on collisional mixing between the fine structure states of the alkalis has been performed with continuous excitation by either $s_1(t)$ or by $s_2(t)$. The solutions for N_1 and N_2 are then constants together with transients that depend on the initial conditions. Neglecting the transients, equations (47) and (48) become:

$$0 = s_2 + N_1 Z_{12} - N_2 \Gamma_2 \quad (49)$$

$$0 = s_1 + N_2 Z_{21} - N_1 \Gamma_1 \quad (50)$$

The solutions to these equations and the relationships between

the measured intensity ratios of the fluorescence and the values of the Z 's are discussed by Siara (1973) and Phaneuf (1973). Equations (47) and (48) can also be integrated over all time for the case of $s_1(t)$ and $s_2(t)$ having a finite duration and assuming that the initial and final values of N_1 and N_2 are zero. Equations (47) and (48) then become:

$$0 = s_2' + N_1' Z_{12} - N_2' \Gamma_2 \quad (51)$$

$$0 = s_1' + N_2' Z_{21} - N_1' \Gamma_1 \quad (52)$$

where the prime indicates the value of the time integrated quantity (eg. $N_2' = \int_0^\infty N_2(t) dt$).

The similarities between (49), (50) and (51), (52) are obvious and by measuring the time integrated-fluorescence intensities, Z_{12} and Z_{21} can be determined by the same formulae as were used in the continuous excitation method that was used by the above authors.

Unfortunately measurements of the total time integrated fluorescence are not possible because of the presence of laser light that is scattered by the glass surfaces of the fluorescence cell. In order to eliminate the errors due to this scattered, unabsorbed laser light, the detection system was gated on after the termination of the laser excitation pulse. The values of the time integrated populations, as calculated from the equations (47) and (48), now depend on the Γ 's, the Z 's and also on the exact time dependence of $s_1(t)$ and $s_2(t)$.

The intensity of the fluorescence at the photodetector can be written as:

$$I = k_{ab} h\nu_{ab} N_a A_{ab} \quad (53)$$

where k_{ab} is a factor that depends on the geometry of the detection system and the transmission of the optical elements, $h\nu_{ab}$ is the energy of a photon of frequency ν_{ab} where a is the upper state and b is the lower state, N_a is the population of radiating level a , and A_{ab} is the Einstein A coefficient for the transition $a \rightarrow b$. The integrated signals from the detector corresponding to the fluorescence from each level can be written as:

$$D_1 = k_{12} h\nu_{10} \bar{N}_1 A_{10} ; D_2 = k_{21} h\nu_{20} \bar{N}_2 A_{20} \quad (54)$$

where the k 's are apparatus constants to be determined and \bar{N}_1 and \bar{N}_2 are defined by:

$$\bar{N}_1 = \int_{t_g}^{\infty} N_1 dt ; \bar{N}_2 = \int_{t_g}^{\infty} N_2 dt \quad (55)$$

with t_g being the gate turn on time.

The A values for the transitions are derived from the measured values of the lifetimes and the theoretical branching ratios. The lifetimes for rubidium are:

$$\tau(6^2P_{1/2}) = 11.4 \times 10^{-8} \text{ second (Bucka et al 1966)}$$

$$\tau(6^2P_{3/2}) = 11.68 \times 10^{-8} \text{ second (Gallagher 1969)}$$

and for cesium:

$$\tau(7^2P_{1/2}) = 15.5 \times 10^{-8} \text{ second (Altman and Kazantsev 1970)}$$

$$\tau(7^2P_{3/2}) = 12.2 \times 10^{-8} \text{ second (Markova et al 1967)}$$

The branching ratios for rubidium are:

$$6^2P_{1/2} \rightarrow 5^2S_{1/2} \quad 0.27 \quad (\text{Heavens 1961})$$

$$6^2P_{3/2} \rightarrow 5^2S_{1/2} \quad 0.31 \quad (\text{Heavens 1961})$$

and for cesium the branching ratios are the average values taken from the calculations of Heavens (1961) and Warner (1968) and are:

$$7^2P_{1/2} \rightarrow 6^2S_{1/2} \quad 0.27$$

$$7^2P_{3/2} \rightarrow 6^2S_{1/2} \quad 0.41$$

The ratio of the sensitized to resonance fluorescence signals is defined by:

$$\mu_1 = \frac{k_{12} v_{10} \bar{N}_1 A_{10}}{k_{20} v_{20} \bar{N}_2 A_{20}} \quad (s_1 = 0) \quad (56)$$

$$\mu_2 = \frac{k_{21} v_{20} \bar{N}_2 A_{20}}{k_{10} v_{10} \bar{N}_1 A_{10}} \quad (s_2 = 0) \quad (57)$$

μ_1 and μ_2 are the measured quantities and their values depend on the collision numbers together with the Γ 's, A values, t_g and the time dependence of s_1 and s_2 . The method of obtaining the Z values from the measured μ_1 and μ_2 was as follows. The dye laser pulse and thus $s_1(t)$ or $s_2(t)$ could be represented quite accurately by $s_{1,2}(t) = a_{1,2} \sin \omega t$ for $t \leq t_0$ where $\omega t_0 = \pi$ and t_0 is the duration of the laser pulse. The solution to the rate equations when $s_1(t)$ and $s_2(t)$ have this form has been discussed by Copley (1969) and will be presented here for completeness.

For the dye laser used in the experiments, $t_0 \approx 10$ nanoseconds, thus the rate equations (47) and (48) can be solved to give the following results:

$$N_1(t) = A_1 \exp(-r_1 t) + A_2 \exp(-r_2 t) + A_3 \sin \omega t + A_4 \cos \omega t \quad (58)$$

$$N_2(t) = B_1 \exp(-r_1 t) + B_2 \exp(-r_2 t) + B_3 \sin \omega t + B_4 \cos \omega t \quad (59)$$

The coefficients can be derived from the initial conditions

$$N_1(0) = N_2(0) = 0 \text{ and } dN_1(0)/dt = s_1(0) \text{ and } dN_2(0)/dt = s_2(0).$$

Using these conditions we get:

$$A_1 = (r_2 A_4 + \omega A_3) / (r_1 - r_2) \quad (60)$$

$$A_2 = (r_1 A_4 + \omega A_3) / (r_2 - r_1) \quad (61)$$

$$A_3 = \{(\Gamma_1 \Gamma_2 - Z_{12} Z_{21} - \omega^2)(Z_{21} a_2 + \Gamma_2 a_1) + \omega^2(\Gamma_1 + \Gamma_2) a_1\} / \{(\Gamma_1 \Gamma_2 - Z_{12} Z_{21} - \omega^2)^2 + \omega^2(\Gamma_1 + \Gamma_2)^2\} \quad (62)$$

$$A_4 = \{(\Gamma_1 \Gamma_2 - Z_{12} Z_{21} - \omega^2) a_1 \omega - \omega(\Gamma_1 + \Gamma_2)(Z_{21} a_2 + \Gamma_2 a_1)\} / \{(\Gamma_1 \Gamma_2 - \omega^2 - Z_{21} Z_{12})^2 + \omega^2(\Gamma_1 + \Gamma_2)^2\} \quad (63)$$

$$B_1 = (r_2 B_4 + \omega B_3) / (r_1 - r_2) \quad (64)$$

$$B_2 = (r_1 B_4 + \omega B_3) / (r_2 - r_1) \quad (65)$$

$$B_3 = \{(\Gamma_1 \Gamma_2 - Z_{12} Z_{21} - \omega^2)(Z_{12} a_1 + \Gamma_1 a_2) + \omega^2(\Gamma_1 + \Gamma_2) a_2\} / \{(\Gamma_1 \Gamma_2 - Z_{12} Z_{21} - \omega^2)^2 + \omega^2(\Gamma_1 + \Gamma_2)^2\} \quad (66)$$

$$B_4 = \{(\Gamma_1 \Gamma_2 - Z_{12} Z_{21} - \omega^2) \omega a_2 - \omega(\Gamma_1 + \Gamma_2)(Z_{12} a_1 + \Gamma_1 a_2)\} / \{(\Gamma_1 \Gamma_2 - Z_{12} Z_{21} - \omega^2)^2 + \omega^2(\Gamma_1 + \Gamma_2)^2\} \quad (67)$$

and r_1 and r_2 are given by:

$$r_1 = (\Gamma_1 + \Gamma_2)/2 + \frac{1}{2}\{(\Gamma_1 - \Gamma_2)^2 + 4Z_{12}Z_{21}\}^{\frac{1}{2}} \quad (68)$$

$$r_2 = (\Gamma_1 + \Gamma_2)/2 - \frac{1}{2}\{(\Gamma_1 - \Gamma_2)^2 + 4Z_{12}Z_{21}\}^{\frac{1}{2}} \quad (69)$$

After excitation ceases at $t = t_0$ yielding $a_1 = a_2 = 0$, the initial conditions for the decay become $N_{10} = N_1(t_0)$ and $N_{20} = N_2(t_0)$.

The rate equations for the decay become:

$$\dot{N}_1 = N_2 Z_{21} - N_1 \Gamma_1 \quad (70)$$

$$\dot{N}_2 = N_1 Z_{12} - N_2 \Gamma_2 \quad (71)$$

These have the solutions:

$$N_1(t) = A'_1 \exp(-r_1 t) + A'_2 \exp(-r_2 t) \quad (72)$$

$$N_2(t) = B'_1 \exp(-r_1 t) + B'_2 \exp(-r_2 t) \quad (73)$$

Where the coefficients are given by:

$$A'_1 = \{N_{20} Z_{21} + N_{10} (r_2 - \Gamma_1)\} / (r_2 - r_1) \quad (74)$$

$$A'_2 = \{N_{20} Z_{21} + N_{10} (r_1 - \Gamma_1)\} / (r_1 - r_2) \quad (75)$$

$$B'_1 = \{N_{10} Z_{12} + N_{20} (r_2 - \Gamma_2)\} / (r_2 - r_1) \quad (76)$$

$$B'_2 = \{N_{10} Z_{12} + N_{20} (r_1 - \Gamma_2)\} / (r_1 - r_2) \quad (77)$$

The values of μ_1 and μ_2 as calculated from the above set of equations, were then compared to the measured values of the μ 's and the Z 's adjusted until agreement was reached.

In the above analysis it has been assumed that collisional transitions to the lower lying S,P and D states are negligible. This is a reasonable assumption in view of the large energy separations between the P states of interest and the lower lying states (Siara 1973). Collisional quenching to the ground state would manifest itself as a departure from linearity of the plots of collisional numbers Z against rubidium or cesium density (Siara 1973). As will be seen, the plots are linear to within the statistical errors. We can therefore assume that quenching to the ground state is of negligible importance in alkali - alkali collisions.

The average effective collision cross section Q_{ef} , describing the collisional transfer $e \rightarrow f$, is related to the differential cross section for this process by the equation (Pimbert 1972):

$$Z_{ef} = N_0 \int_0^{\infty} q_{ef}(v) v f(v) dv \quad (78)$$

where N_0 is the density of ground state atoms, $q_{ef}(v)$ is the differential cross section and $f(v)$ is the velocity distribution

of the colliding atoms. Since the function $q_{ef}(v)$ is not known, an average or effective Q_{ef} is taken by writing equation (78) in the form:

$$Z_{ef} = N_0 Q_{ef} \bar{v} \quad (79)$$

where \bar{v} is the mean relative velocity of the colliding partners assuming a Maxwell-Boltzmann distribution of velocities. \bar{v} is related to the temperature of vapour by $\bar{v} = (8kT_0/\pi\bar{m})^{1/2}$ where \bar{m} is the reduced mass of the colliding partners and T_0 is the absolute temperature of the vapour.

In this manner, by exciting the atoms with each component of the 2P doublet in turn and measuring the corresponding fluorescence intensity ratios μ_1 and μ_2 it is possible to determine independently the mixing cross sections Q_{12} and Q_{21} . According to the principle of detailed balancing, the cross sections should be related by:

$$Q_{12}/Q_{21} = (g_2/g_1) \exp(-\Delta E/kT_0) \quad (80)$$

where $g_1 = 2$ and $g_2 = 4$ are the statistical weights of the $^2P_{1/2}$ and the $^2P_{3/2}$ states respectively and ΔE is the energy splitting of the fine structure states, amounting to 77 cm^{-1} for the 6^2P states of rubidium and 181 cm^{-1} for the 7^2P states of cesium.

2. EXPERIMENTAL

2(a). DESCRIPTION OF THE APPARATUS

The arrangement of the apparatus is shown in figure 20. The light from the dye laser was focussed to a line in the corner between the entrance and exit windows of a quartz fluorescence cell (Krause 1966). The cell is similar to the original design of Wood (1914). The fluorescence emerging at right angles to the exciting beam was collimated and detected by a pair of photomultiplier tubes, which were adjusted to have the same sensitivity. Each phototube viewed the same volume element of radiating gas (Ocheltree and Storey 1973). With this arrangement, both the sensitized and resonance fluorescence can be observed simultaneously by placing the appropriate wavelength selectors in front of the phototubes. In this experiment one phototube was used to observe the sensitized transition using a monochromator as a wavelength selective device, while the other phototube observed the total radiation emitted from the observed volume. Since the sensitized fluorescence is weaker than the resonance fluorescence by a factor of 10^3 to 10^4 , the total emitted radiation essentially corresponds to the resonance transition.

The reasons for measuring both the sensitized and the resonance transitions simultaneously are twofold. Firstly it shortens the data acquisition time and secondly it minimizes inaccuracies due to fluctuations in the output intensity and frequency of the dye laser. It was found that the pulse-to-pulse reproducibility of the dye

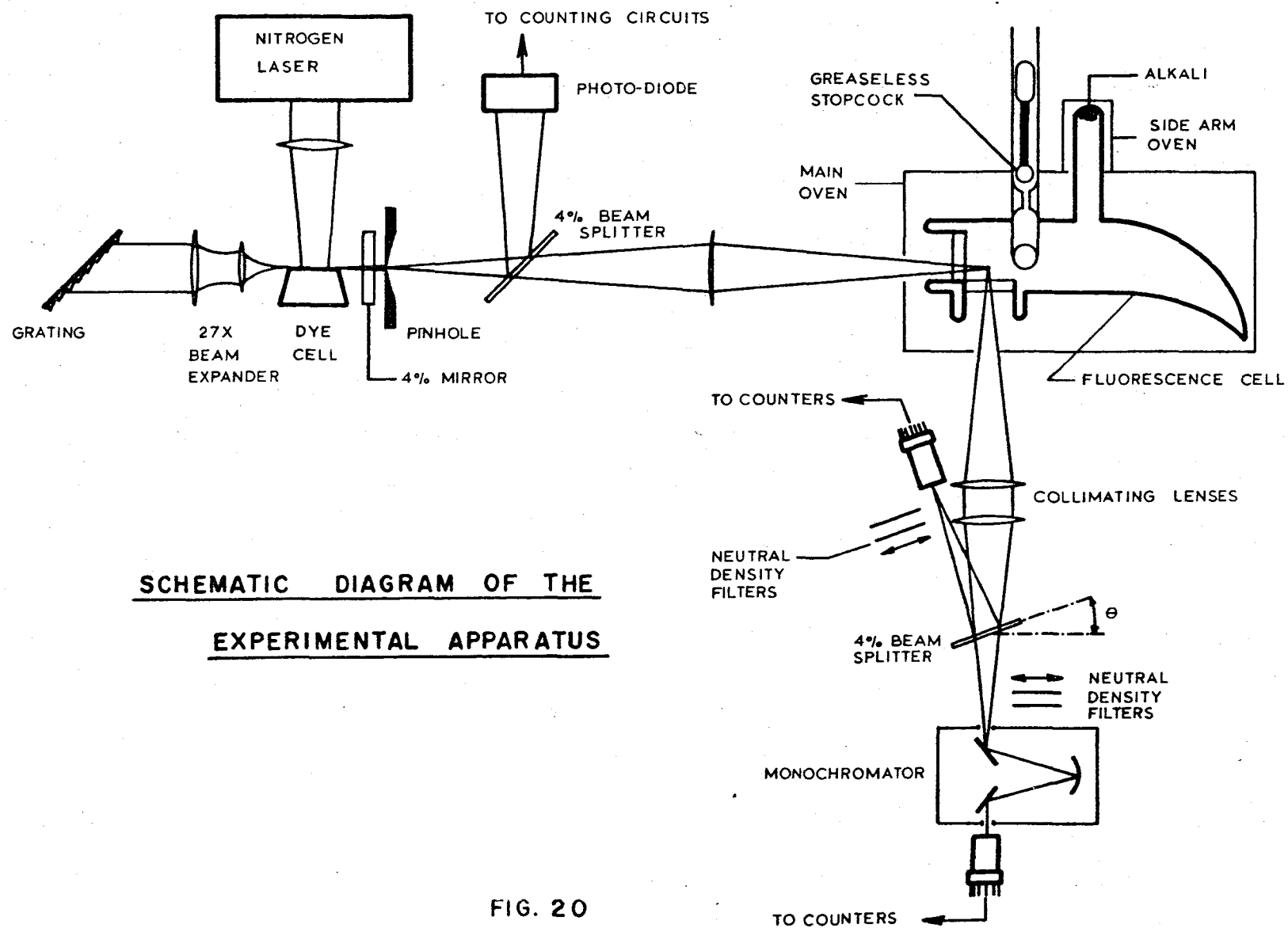


FIG. 20

laser was only ± 20 percent, and the output intensity tended to decrease with time. This decrease was attributed to heating and photo-bleaching of the dye. The frequency jitter was smaller than the laser linewidth, but still caused small fluctuations of the alkali fluorescence intensities.

Since the frequency selection of the dye laser was performed by a diffraction grating, the output tended to be polarized parallel to the direction of the grooves in the grating. If we refer to figure 20, this means the laser output was partially linearly polarized in a plane normal to the plane of the diagram. In the case of the alkalis, if we excite the $n^2P_{3/2}$ state, the fluorescence from this state will be partially polarized in the same direction as the exciting light. However, the sensitized fluorescence from the $n^2P_{1/2}$ state will not be polarized (Feofilov 1961). With increasing alkali density, collisions will tend to depolarize the resonance $n^2P_{3/2}$ state. This effect can be very large for resonance depolarization between atoms of the same kind (Feofilov 1961). Therefore, if the resonance radiation detector is polarization sensitive, the signal from this detector will not be a true measure of the population of the $n^2P_{3/2}$ state.

To enable both phototubes to view the same volume element of fluorescing vapour, a beam splitter was placed in the output from the fluorescence cell. This introduces polarization sensitive detection into the system, since the beam splitter preferentially reflects light polarized in a plane perpendicular to the plane defined by the incident and the reflected rays (Shurcliff 1962). However,

for a dielectric beam splitter near zero incidence, calculations using Fresnel's equations for reflection and transmission coefficients (Corson and Iorrain 1962) indicate all polarization directions are reflected with almost equal intensity. Thus, provided the angle θ in figure 20 is small, very little error will be introduced in measuring the $n^2P_{3/2}$ transition. For this experiment, θ was about 8 to 9 degrees. Since the sensitized radiation is always depolarized, no error should be introduced by the beam splitter or the monochromator. When the $n^2P_{1/2}$ state is excited by the laser, both the resonance and the sensitized lines should be depolarized (Foefilov 1961), and no errors will be introduced by the beam splitter.

I.T.T. FW130 photomultiplier tubes with S-20 spectral responses were used. Power to the phototubes was supplied by independent Fluke 412-B power supplies. The outputs of the phototubes were sent to the counting circuits described in the next section. The monochromator used to isolate the sensitized lines was a 0.25 metre Jarrall-Ash instrument with a dispersion of 1.6 nm per mm. The output optical system, which included the two phototubes, the monochromator, collimating lenses and the beamsplitter was enclosed in a light tight wooden box.

A glass vacuum system, evacuated by an Edwards E02 oil diffusion pump and backed by an ES35 rotary pump was used to evacuate the fluorescence cell through a greaseless stopcock placed inside the oven. The vacuum in the system was measured with a C.V.C. model GIC-110-B ionization gauge equipped with a GIC-016-C ion gauge head (10^{-3} to 10^{-8} Torr). With this arrangement, pressures below 10^{-7} Torr could be obtained consistently.

A side-arm 2 cm in diameter and 5 cm long served as the reservoir for the rubidium or the cesium metal, whose temperature determined the vapour density in the cell. The side arm was heated by circulating oil through a copper coil placed around the side-arm. Thermal contact was ensured by using silicon grease between the coils and the side-arm. The fluorescence cell was mounted in a doubled-walled oven consisting of an outer transite box and an inner aluminum box. The transite box was equipped with pyrex windows. The inner box was heated by two G.E. JX2B1 strip heaters. The power to the strip heaters was supplied by a Powerstat variable autotransformer (0 to 120 volts), connected to a regulated AC line. The inner surfaces of the transite box were lined with aluminum foil and the space between the inner aluminum box and the outer transite box was packed with fibre wool to reduce heat losses and to improve the uniformity of the temperature within the oven. The temperature of the inner oven was maintained at about 440 degrees K. Calibrated copper-constantan thermocouples, used in conjunction with a Leeds and Northrup millivolt potentiometer permitted temperature measurements at various locations in the oven and side-arm with an accuracy of ± 0.1 degree K. The temperature of the main oven was uniform to within ± 2 degrees K and remained stable to ± 1 degree K for the duration of the experiments.

2(b). THE PULSE COUNTING SYSTEM

The lifetimes of the excited states of the alkalis of interest are about 100 nanoseconds and a computer simulation shows that 99.8 percent of the integrated fluorescence intensity will occur within 1 microsecond. For a typical laser repetition rate of 20 pulses per second, the duty cycle of the signal detection system is therefore 2×10^{-5} . In the next section it will be seen that for the counting system, a collection rate of less than 1 signal pulse in 10 dye laser pulses should be maintained. Hence the signal collection rate is less than 2 pulses per second, whereas the dark current for the phototubes is about 100 pulses per second. In order to improve the signal-to-noise ratio, the phototubes were turned on for approximately 1 microsecond. This does not change the average signal count rate, but it reduces the average dark count rate to 2×10^{-3} pulses per second and the signal-to-noise ratio rises to a reasonable value. Furthermore, gating the phototubes on after the termination of the laser pulse eliminates the pulses due to laser light that is scattered from the glass surfaces of the cell. A narrower spectral linewidth of the laser output would be an advantage, since the light would be absorbed in a short distance within the cell. However, a narrower linewidth also requires a more stable wavelength control and the elimination of vibration in the optical components.

A number of methods have been used to gate phototubes (Albach and Meyer 1973). Pulsing one of the dynodes tends to produce spurious noise transients, while pulsing the cathode and/or first dynode gives rise times in the response of more than 20 nanosecond. Pulsing the last dynode does not give good cut-off ratios and all these methods require pulses in the range 100 to 200 volts. For these reasons the output of the phototubes was sent through a simple electronic gate and the phototubes were left on continuously.

The electronic gate system consisted of a pulse amplifier, a TTL SN7408 AND gate, a Signetics NE555 timer used as a pulse shaper, and E.G. and G. SGD-100A photodiode and a Universal AD-YU Electronics model 20A1 delay line. The arrangement of the components is shown in figure 21 and the electronic schematics are shown in figure 22. The pulse amplifier, which has a gain of 200 and a bandwidth of 10 MHz is used to amplify the phototube pulses to a level of 1 volt which is sufficient to activate the AND gate.

The system works as follows. The output pulse of the dye laser is sampled using a 4 percent beam splitter and the photodiode. The output of the photodiode is sent through the delay line. This allows positioning of the gate pulse to accept only fluorescence pulses and to reject the scattered, unabsorbed laser light. The pulse from the diode is then shaped in the NE555 timer to give a square pulse of 1 microsecond duration, 4.5 volts peak and a rise time of 40 nanoseconds. This pulse is sufficient to activate the AND gate such that the effective time resolution of the circuit is a few nanoseconds.

DETECTION AND COUNTING APPARATUS

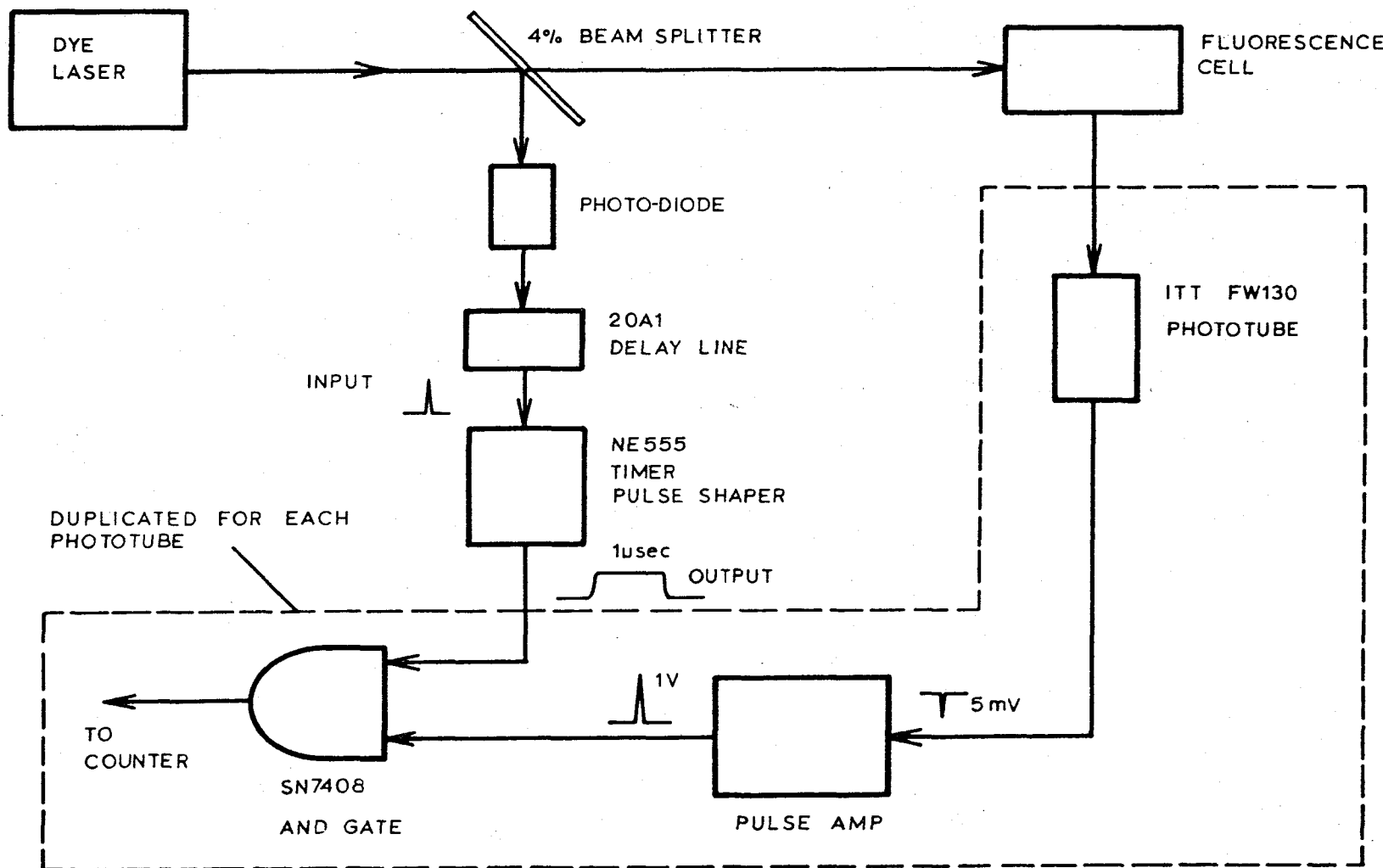
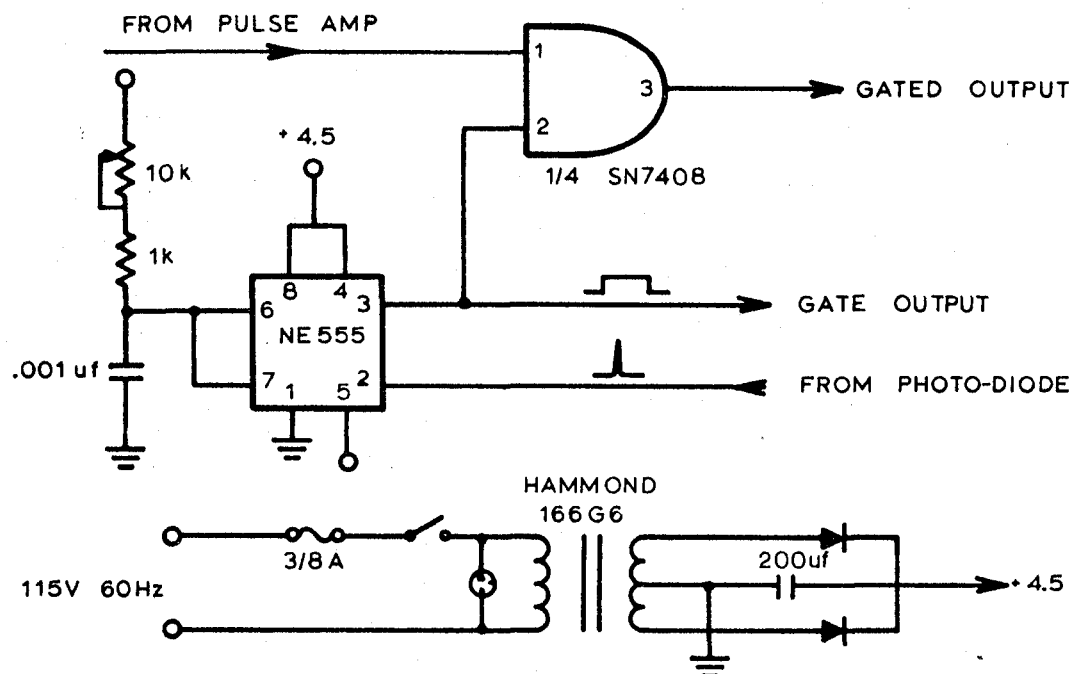


FIG. 21

POWER SUPPLY, AND GATE and TIMER



PULSE AMPLIFIER

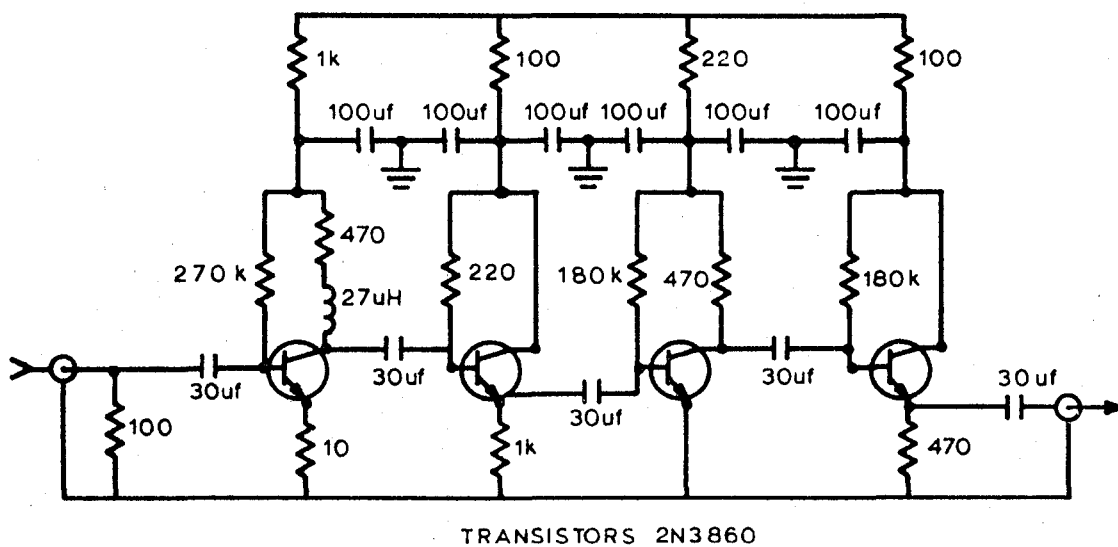


FIG. 22

The AND gate operates such that it will only produce an output pulse if the pulse from the phototube arrives during the time interval that the pulse from the timer is at the AND gate, otherwise no output is seen.

Duplicate circuits were constructed for each phototube. The outputs of the two gates were fed to Philips PW4230 scalers and the counts were recorded on a printer.

In order to obtain meaningful results the ratio k_{12}/k_{21} in equations (56) and (57) must be evaluated. This was accomplished by tuning the monochromator to the resonance transition so that both phototubes simultaneously viewed the same signal. Neutral density filters were then inserted to reduce the counting rates of both phototubes to values such that corrections for the dead time of the scalers could be made as described in the next section. The response of both the monochromator and the phototubes is essentially the same for both fine structure lines according to the manufacture's specifications and hence the ratio k_{12}/k_{21} (or k_{21}/k_{12}) was simply determined from the counting rates and the transmission factors of the neutral density filters. The latter were measured on a Carey double-beam¹ spectrophotometer.

-
1. Gratitude is expressed to Dr. M. Schlesinger for performing the measurements on the neutral density filters.

2(c). COUNTING LIMITATIONS

The counter used in the experiment has a non-paralysable dead time of approximately 1 microsecond. This places certain limitations on the mean number of pulses per counting interval since the counter can only register one pulse during one microsecond. We must therefore ensure that m , the mean number of pulses per counting interval is small enough that the probability of more than one pulse in the counting interval is very small and can be corrected in a simple statistical manner. This can be done in practice by inserting neutral density filters in front of the phototubes until the counting rate is at the desired level.

Poisson statistics apply to events which have a small but constant probability of occurrence. The probability of a photon being emitted at any instant is proportional to the number of atoms in the upper state corresponding to the transition. We therefore do not have a constant probability of detecting a photon during the counting interval. However, the total number of excited atoms that exist during the counting interval is constant to within the fluctuations of the laser intensity. The probability that a photon will be observed during the counting interval is therefore constant from interval to interval and the probabilities for observing zero, one, two, etc. photons in the interval will therefore obey Poisson statistics.

Let m be the true mean number of pulses per counting interval.

The probability of observing n pulses is:

$$P(n) = m^n \exp(-m)/n! \quad (81)$$

where $n!$ means n factorial. The ratio of the probability for observing more than one pulse to the probability of observing one pulse is given by:

$$\exp(-m) \sum_2^{\infty} m^n/n! / \{m \exp(-m)\} = \sum_2^{\infty} m^{n-1}/n! \quad (82)$$

For small m , the first term dominates and the ratio is $m/2$. For an error of less than 5 percent this means m must be less than 0.1.

It is possible to make corrections to the observed mean number of pulses per counting interval to obtain the true mean m . If we have N counting intervals, the true number of pulses is given by:

$$N \sum_0^{\infty} nP(n) = Nm \quad (83)$$

The measured number of pulses is given by:

$$R = N \sum_1^{\infty} P(n) + N P(0) \sum_1^{\infty} P'(n) \quad (84)$$

$P(0)$ is the true probability of zero signal pulses and $P'(n)$ is the probability of n dark current or scattered light pulses. The second term has this form because only those dark current pulses that occur when there are no signal pulses will add to the counts. We can

measure $P'(n)$ in a separate experiment by tuning the laser off the absorption line and measuring the counts. Since the dark current and the scattered light obey Poisson statistics we have:

$$P'(n) = \exp(-r)r^n/n! \quad (85)$$

where r is the mean number of noise pulses per interval. In the dark current measurement, the total number of counts registered is given by:

$$N' \sum_1^{\infty} P'(n) = N' \{1 - P'(0)\} = N' \{1 - \exp(-r)\} \quad (86)$$

where N' is the total number of counting intervals over which the measurements occur. Hence $\sum_1^{\infty} P'(n)$ can be evaluated. The measured number of pulses (signal + dark noise etc.) can be written as:

$$N\{1 - P(0)\} + NP(0) \sum_1^{\infty} P'(n) = R \quad (87)$$

Rearranging gives:

$$P(0) = (1 - R/N) / \{1 - \sum_1^{\infty} P'(n)\} \quad (88)$$

Since $P(0) = \exp(-m)$, m and hence the true number of pulses in N counting intervals can be calculated.

The error in m arises from the fluctuations in both the signal and dark count rates. For true Poisson distributions, the variance

of the mean value is equal to the mean value, with the error normally being understood as the square root of the variance. Although the statistics are not exactly Poisson, they are close enough to take the variance of R to be R and hence the error in R is $R^{\frac{1}{2}}$. Similarly we can measure the error in $\sum_{n=1}^{\infty} P'(n)$ from the dark current counts. Denoting $\sum_{n=1}^{\infty} P'(n)$ as W we have:

$$P(0) = (1 - R/N)/(1 - W) \quad (89)$$

therefore:

$$\begin{aligned} \Delta P(0)/P(0) &= \Delta(1 - R/N)/(1 - R/N) + \Delta(1 - W)/(1 - W) \\ &= \Delta R/(N - R) + \Delta W/(1 - W) \end{aligned} \quad (90)$$

Since $P(0) = \exp(-m)$, it is easy to show that $\Delta m = \Delta P(0)/P(0)$ and the error in the true mean number of counts is $N\Delta m = N\Delta P(0)/P(0)$. For most practical purposes $\Delta P(0)/P(0) = \Delta R/(N - R)$, thus:

$$N\Delta m = N\Delta R/(N - R) \approx \Delta R/(1 - R/N) \approx \Delta R = R^{\frac{1}{2}} \quad (91)$$

The use of the above formulae enables faster count rates to be used and still preserve the linearity of the system. Values of m of approximately 0.1 to 0.2 were used, which give rise to corrections of about 5 to 10 percent. Since the error is of the order of $R^{\frac{1}{2}}$, we require R to be 1000 for an error of about 3 percent. For a laser pulser rate of 20 pulses per second and $m = 0.1$, the data will be

acquired in about 8 to 10 minutes.

2(d). EXPERIMENTAL PROCEDURE

In preparation for the experiments, the fluorescence cell was attached to the vacuum system through the greaseless stopcock and was outgassed at approximately 600 degrees K for several days under a vacuum of better than 10^{-7} Torr. A glass ampoule containing either rubidium (99.99% pure) or cesium (99.95% pure), supplied by the A.D. McKay Company, was broken under vacuum and a small quantity of the metal was distilled into the side arm, which was then sealed off. In order to reduce the reflections and improve the temperature uniformity, the cell was coated with Aquadag colloidal graphite. After a small portion of the alkali metal was distilled into the cell it was then baked at 600 degrees K with the side arm at 300 degrees K for several days. This ensured that all the metal was now in the side arm.

When aligning the optical system, the focused laser beam was placed as closely as possible to the corner formed by the two cell windows, without producing spurious reflections. This reduced the optical path length of the observed fluorescence to about 2 mm.

As described in section II.7 the dye laser produced a pulse with a duration of about 10 nanoseconds, with peak powers of a few kilowatts at a repetition rate of 20 pulse per second. The dye used for the rubidium experiments was POPOP (2,2'-p-Phenylenebis(5-phenyloxazole)) which lases in the region around 420.0 nm, and the dye

used for the cesium experiments was 4-Methylumbelliferone which lases in the region around 450.0 nm. Both these dyes were mixed in concentrations of 5×10^{-3} M per litre. The solvent used for the POPOP was toluene while that used for the 4-Methylumbelliferone was methyl alcohol with a pH of about 9.

The fluorescence cell was kept at a temperature of 440 degrees K for the rubidium experiments and 443 degree K for the cesium experiments. The temperature of the side arm containing the liquid alkali was varied to alter the vapour pressure of the metal in the cell. The vapour pressure of the liquid alkali metals may be represented by (Nesmeyanov 1963):

$$\log_{10} P(\text{Torr}) = A - B/T(^{\circ}\text{K}) + CT(^{\circ}\text{K}) + D \log_{10} T(^{\circ}\text{K}) \quad (92)$$

For rubidium:

$$A = 15.88, \quad B = 4529, \quad C = 0.0005866, \quad D = -2.991$$

and for cesium:

$$A = 8.22, \quad B = 4006, \quad C = -0.0006019, \quad D = -0.1962$$

and T is the temperature of the side arm. The vapour pressure is related to the alkali density by:

$$N_0 (\text{cm}^{-3}) = 9.656 \times 10^{18} P(\text{Torr})/T_0 (^{\circ}\text{K}) \quad (93)$$

where N_0 is the density of alkali atoms and T_0 is the temperature of the vapour.

It has been assumed that there is no radiation trapping.

Imprisonment of radiation, if present, would cause an increase in the effective lifetime of the doublet states (D'Yakonov and Perel' L 1965) and would result in errors in the cross sections. Radiation trapping was avoided by working at rubidium vapour densities below 6×10^{12} atoms per cm^3 and cesium vapour densities below 10^{13} atoms per cm^3 . Below these densities the graphs of μ against alkali density were linear, indicating the absence of trapping.

Four other factors which could influence the measurements of the intensity ratios should also be mentioned. The first is the polarization of the incident light. This has already been discussed. A second consideration involves the possibility of saturating the $^2P_{1/2,3/2} \leftarrow ^2S_{1/2}$ transitions. Numerical solutions to the rate equations (47) and (48) show that, for photon densities typical of the dye laser, saturation and a considerable reduction of the ground state atomic density is possible. When this occurs, the Z values are reduced since N_0 in equation (79) is less than that indicated by equation (93). Since smaller values of Z will produce smaller μ values, care was taken to reduce the incident photon density so that the values of the μ 's were independent of the incident photon density. The third consideration involves the possibility of photoionization from the excited states as discussed by Popescu et al (1973,1974). Under conditions present in the experiments, it is possible to photoionize atoms from all the excited states of both cesium and rubidium. The subsequent recombination will populate all the excited states to an amount depending upon the recombination coefficients. Any cascading

to the second 2P levels which were not optically excited directly will lead to larger values of μ . The possible importance of this was determined both experimentally and theoretically. Since the probability of photoionization depends on the incident photon density, the constancy of the values of μ with respect to the incident photon density was taken as evidence that the effect was negligible. As a check that the effects of photoionization and saturation were not simply cancelling each other, the rate equations for the populations including the effects of photoionization were solved. The photoionization cross sections were calculated using the quantum defect method of Burgess and Seaton (1960). The total number of ions that were produced was calculated to be negligible compared to the excited state populations, even under conditions of saturation and hence the effect could be neglected.

Finally there is the possibility of errors caused by line broadening. The ratio Q_{12}/Q_{21} should correspond to the detailed balance ratio as given by equation (80) regardless of the pressure of the alkali vapour. Thus the violation of this ratio for mixing due to collisions with inert gases as reported by Krause (1966) has been interpreted by Gallagher (1968) as being caused by the non-Lorentzian red wing of the collisionally broadened resonance lines. The radiating $^2P_{3/2}$ line is broadened due to collisions and the intensity received by the detector centred on the $^2P_{1/2}$ transition will have a component that is due to the $^2P_{3/2}$ line. This component will be proportional to the pressure and thus cause an error in the measured cross sections. Although only a very small portion of the

broadened resonance line is detected as sensitized signal, there is also only a very small proportion of the excited atoms that are collisionally transferred to the sensitized state. Because the densities are very low in these experiments compared to those in the experiments with the inert gases, pressure broadening will be negligible.

3. RESULTS AND DISCUSSION

The graphs of the fluorescence intensity ratios μ_1 and μ_2 plotted against alkali metal density are shown in figure 23 for rubidium and in figure 24 for cesium. In both cases the gate delay time t_g was 170 nanoseconds. As expected from equations (54) and (79) the plots are linear and have a slope proportional to the cross section σ_{21} and σ_{12} . The error bars shown are the standard deviations of the number of counts plus the error in the calibration of the optical system. The experimental data for the intensity ratios against alkali densities are given in Appendix A. As will be shown the intercept in figures 23 and 24 is in good agreement with the value expected on the basis of measuring the scattered light and finite resolution of the monochromator. This value is about 1.2×10^{-3} with an error of about 4 percent. The intercepts from all the experimental curves fell within this range, and thus in the results presented in figure 23 and 24 all the curves were adjusted to have the same intercept.

Linear least squares analyses were performed on the values of μ_1 and μ_2 in relation to the vapour densities, and the values of the resulting slopes were used in the equations of section III.1 to evaluate the total mixing cross sections σ_{21} and σ_{12} . The entire analysis of the experimental data was performed on a Digital PDP-8/L laboratory computer, including the statistical corrections to the number of counts of sensitized and resonance fluorescence signals.

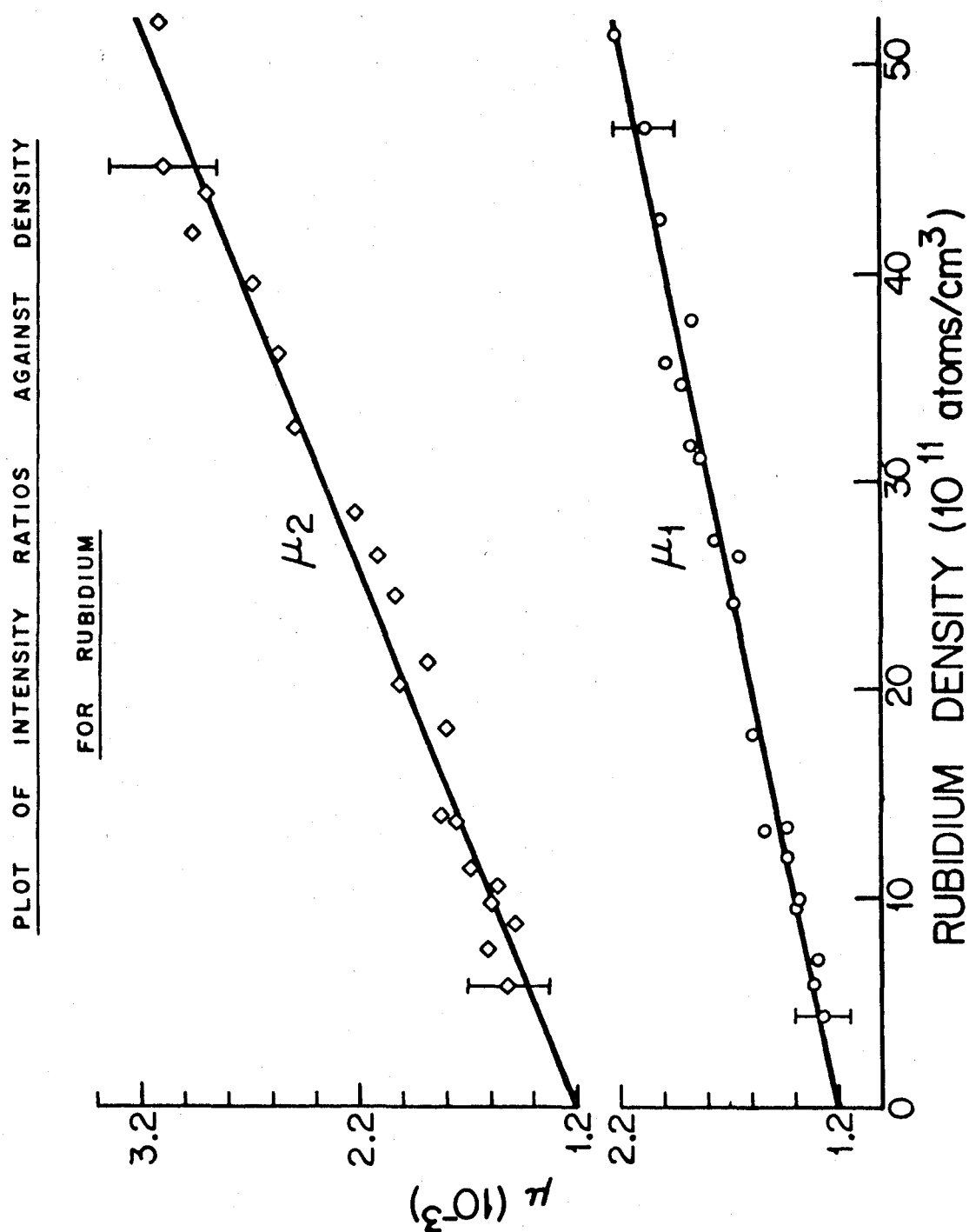


FIG. 23

GRAPH OF INTENSITY RATIOS AGAINST DENSITY FOR CESIUM

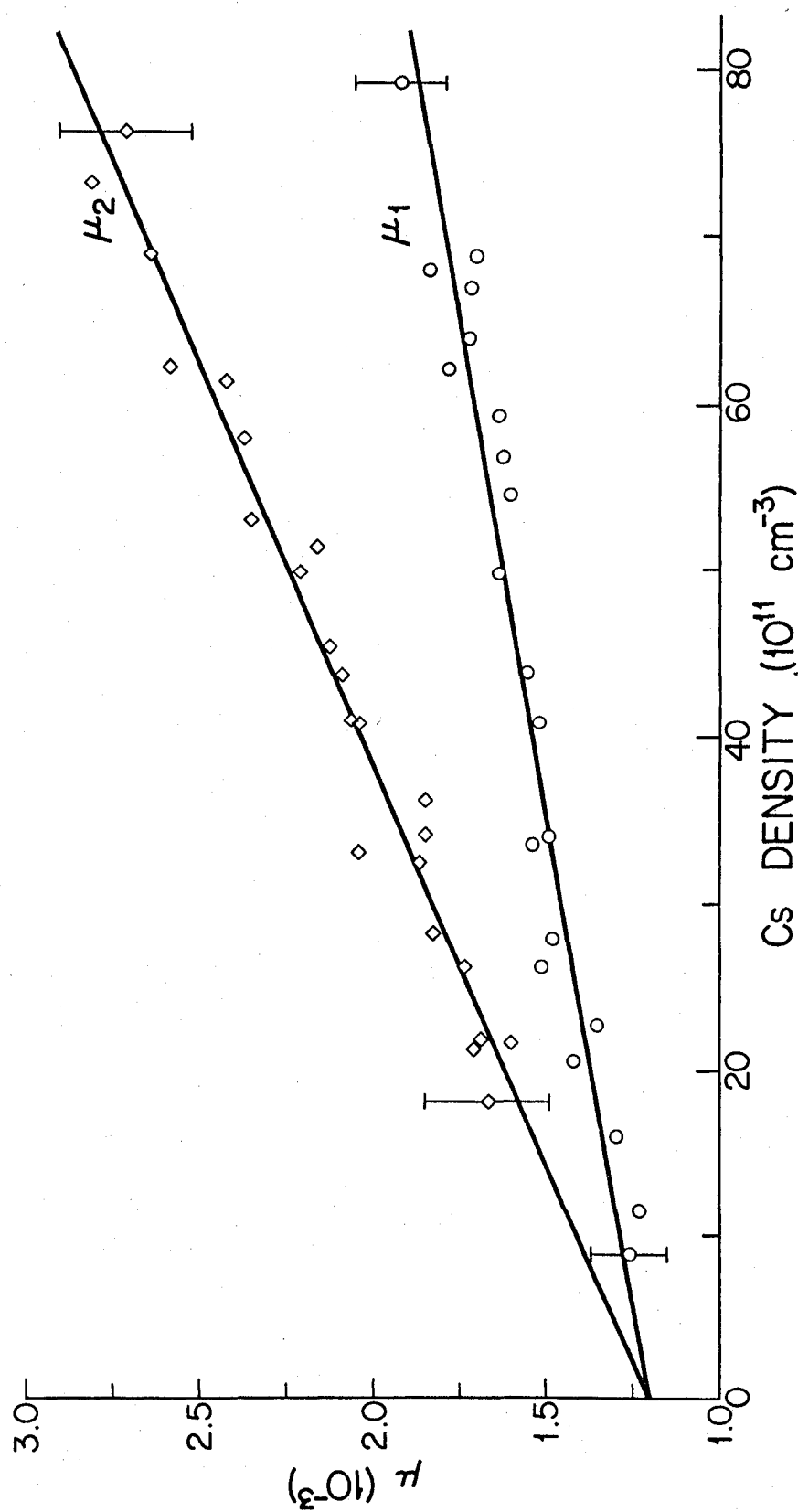


FIG. 24

The results of the analysis gives the following values for the mixing cross sections:

$$\text{Rb: } Q_{12} (6^2P_{1/2} \rightarrow 6^2P_{3/2}) = 245 \text{ A}^2$$

$$\text{Rb: } Q_{21} (6^2P_{1/2} \leftarrow 6^2P_{3/2}) = 163 \text{ A}^2$$

$$\text{Cs: } Q_{12} (7^2P_{1/2} \rightarrow 7^2P_{3/2}) = 121 \text{ A}^2$$

$$\text{Cs: } Q_{21} (7^2P_{1/2} \leftarrow 7^2P_{3/2}) = 107 \text{ A}^2$$

The following sources of error were inherent in the experiments:

- 1) Uncertainties in the lifetimes of the alkali metals.

For Cs the error is about 5% and for Rb the error is about 11%.

- 2) Errors in the temperature measurements of about 3%.

- 3) Uncertainties in the least squares analysis. In this case the errors in the standard deviations of the slopes for Rb are about 4% and for Cs the errors are about 5%.

- 4) Uncertainty in the turn on time t_g of the phototube gate of about 8%.

- 5) Uncertainties in the transmissions of the neutral density filters estimated to be about 5% maximum.

As the above sources of error are uncorrelated, they can be combined in quadrature to give uncertainties in the cross sections of about 16% for Rb and about 12% for Cs. At the temperature at which the experiments were performed, the ratio Q_{12}/Q_{21} from equation (80) should be 1.55 for Rb and 1.12 for Cs. The measured values were 1.50 ± 0.48 for Rb

and $1.13 \pm .27$ for cesium. Both these values are in good agreement with the principle of detailed balance.

The general behaviour of the alkali*-alkali mixing cross sections can be interpreted in terms of the 'adiabatic criterion' (Massey 1971). A collision is designated adiabatic if its duration τ_c is considerably larger than $h/2\pi\Delta E$, where ΔE is the energy to be transferred in the collision. Therefore in an adiabatic collision we have:

$$\tau_c \gg h/2\pi\Delta E \quad (\text{adiabatic}) \quad (94)$$

In this case the relative motion of the atoms is slow enough to allow the electronic motion to adjust to small changes in the inter-nuclear separation. The orbital angular momentum vector \vec{L} and the spin angular momentum vector \vec{S} remained coupled and any change in the total electronic angular momentum vector \vec{J} requires that there be a change in \vec{S} . The cross section for a 'spin flip' transition is very small and thus the probability for occurrence of fine structure transitions in adiabatic collisions is very small.

On the other hand, when the duration of the collision is considerably smaller than $h/2\pi\Delta E$, the collision is termed 'non-adiabatic' and we have:

$$\tau_c \ll h/2\pi\Delta E \quad (\text{non-adiabatic}) \quad (95)$$

In this case \vec{S} remains fixed in the collision and \vec{L} is reoriented. After the collision \vec{L} and \vec{S} recouple to give the resultant \vec{J} whose

magnitude can assume any value between $|L - S|$ and $|L + S|$. Since the magnitude of the cross section for the reorientation of \vec{L} is the same order as the disorientation cross section ($\approx 10^{-14} \text{ cm}^2$) the cross sections for fine structure mixing should be large.

Whether a fine structure mixing collision is adiabatic or non-adiabatic depends on the relative velocity of the colliding partners as well as on ΔE . This accounts for the dependence of the mixing cross sections on ΔE . If we examine the results of Krause (1966) for the first excited states of Na and K ($\Delta E = 17 \text{ cm}^{-1}$ and 57 cm^{-1} respectively), we find that the collisions are non-adiabatic and according to the above criterion the cross sections should be of the order of 10^{-14} cm^2 . However for the first excited states of rubidium and Cs ($\Delta E = 238 \text{ cm}^{-1}$ and 554 cm^{-1} respectively) the collisions are adiabatic and the above criterion states that the cross sections should be much smaller than 10^{-14} cm^2 . In fact the cross sections vary in a continuous manner in passing from Na to Cs. The results presented in this report confirm the importance of the role played by ΔE , the energy difference between the fine structure levels. Table I gives all the measured values of the cross sections for alkali*-alkali mixing collisions as determined by the various authors. It should be noted that Pimbert only measured Q_{12} and the principle of detailed balance was used to determine Q_{21} . In the case of sodium, only Q_{21} could be measured and the same method was used to obtain the other cross section. The verification of the principle of detailed balancing for the higher excited states of rubidium and cesium is thus of importance. Figure 25 shows the relationship between the value

TABLE I
ALKALI-ALKALI COLLISION CROSS SECTIONS

Collision Process	ΔE_1 (cm^{-1})	Experimental Cross Section (\AA^2)		Q_{12}/Q_{21}	$\frac{g_2}{g_1} e^{-\Delta E/kT}$	Author
		Q_{12}	Q_{21}			
$\text{Cs}(6^2\text{P}_{1/2} \rightleftharpoons 6^2\text{P}_{3/2})$	554	6.4 ± 1	31 ± 3	0.21 ± 0.06	0.27	Krause
$\text{Cs}(8^2\text{P}_{1/2} \rightarrow 7^2\text{D}_{5/2})$	360	20 ± 5	-	-	0.82	Pimbert
$\text{Cs}(8^2\text{P}_{1/2} \rightarrow 7^2\text{D}_{3/2})$	339	21 ± 5	-	-	0.59	Pimbert
$\text{Rb}(5^2\text{P}_{1/2} \rightleftharpoons 5^2\text{P}_{3/2})$	238	53 ± 6	68 ± 9	0.78 ± 0.2	0.85	Krause
$\text{Cs}(7^2\text{P}_{1/2} \rightleftharpoons 7^2\text{P}_{3/2})$	181	121 ± 15	107 ± 13	1.13 ± 0.27	1.12	Present Investigation
$\text{Cs}(8^2\text{P}_{1/2} \rightarrow 8^2\text{P}_{3/2})$	83	190 ± 57	-	-	1.62	Pimbert
$\text{Rb}(6^2\text{P}_{1/2} \rightleftharpoons 6^2\text{P}_{3/2})$	77	245 ± 39	163 ± 26	1.50 ± 0.48	1.55	Present Investigation
$\text{K}(4^2\text{P}_{1/2} \rightleftharpoons 4^2\text{P}_{3/2})$	58	370 ± 37	250 ± 75	1.48 ± 0.59	1.60	Krause
$\text{Na}(3^2\text{P}_{1/2} \rightleftharpoons 3^2\text{P}_{3/2})$	17.2	-	283 ± 28	-	1.88	Krause

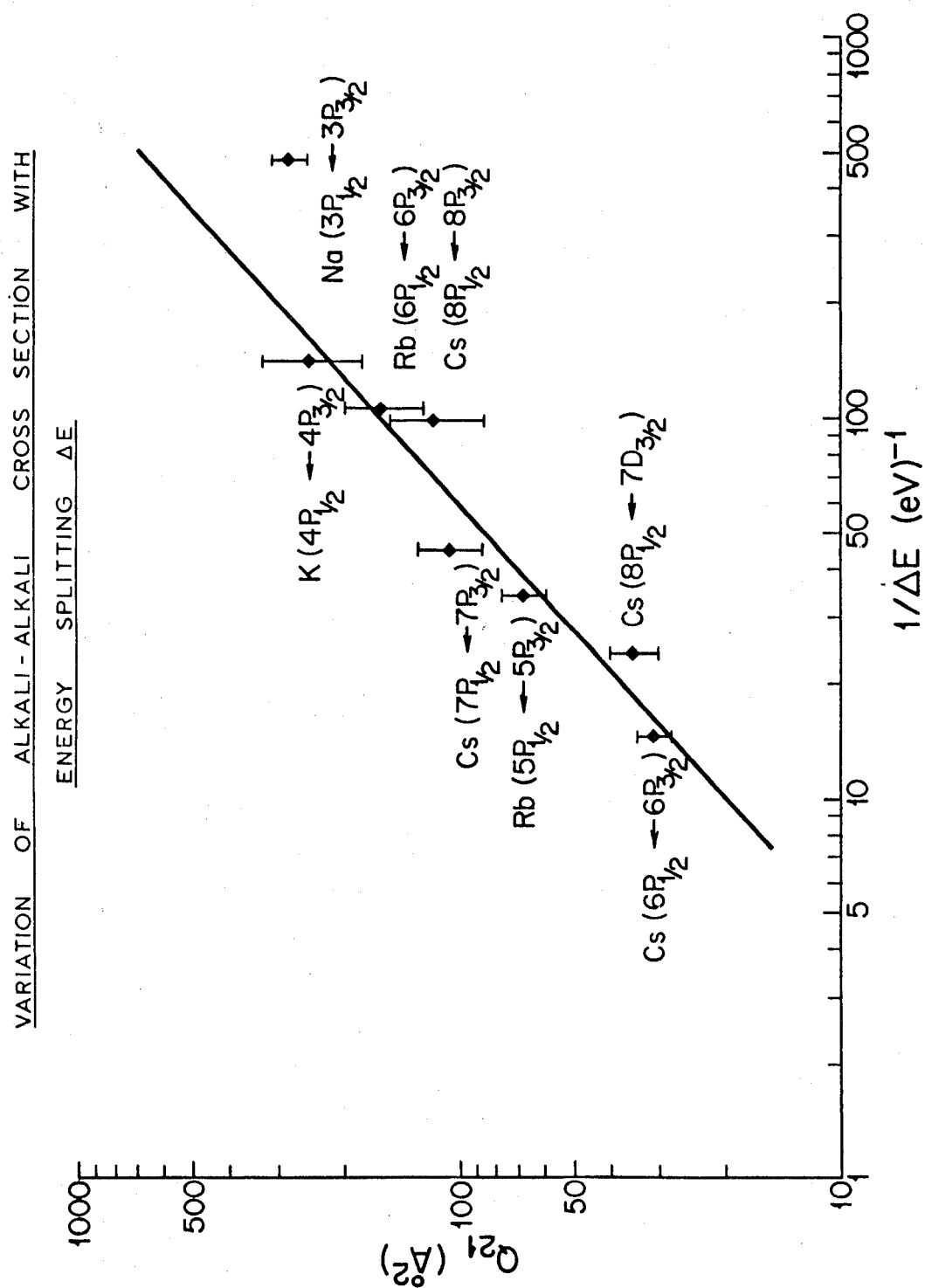


FIG. 25

of Q_{21} for the different systems as a function of ΔE^{-1} . The value of Q_{21} is chosen rather than Q_{12} since it is the more fundamental of the two. No energy is required to cause the transition from level 2 to level 1 and thus the velocity distribution of the ground state atoms plays a lesser role in the value of Q_{21} compared to Q_{12} as the cross sections are velocity averaged. For all the transitions except sodium, the graph indicates an essentially linear relationship between Q_{21} and ΔE^{-1} and thus Franck's rule is obeyed (Franck 1929). For sodium, ΔE is so small that it does not influence the cross section significantly (Krause 1966) and thus it does not fit the linear relationship.

Unfortunately there are no theoretical calculations of the cross sections for the excitation transfer between the second excited states of rubidium and cesium, induced by collisions with ground state atoms of the same kind. The cross sections calculated by Zembekov and Nikitin (1971) for the mixing of the third excited states of cesium due to collisions with ground state cesium atoms are a factor of two smaller than the experimental results. The work of Dashevskaya et al (1969) and Lewis (1971) on the first excited states of the alkalis also produce results that are too small. It is hoped that the results presented here will assist in producing a better theoretical model of the interactions between the alkali atoms.

Finally it is of interest to compare the results obtained using the dye laser excitation method to attempts made using a resonance lamp as the excitation source. Figure 26 shows a scan across the resonance and sensitized fluorescence lines for the second excited

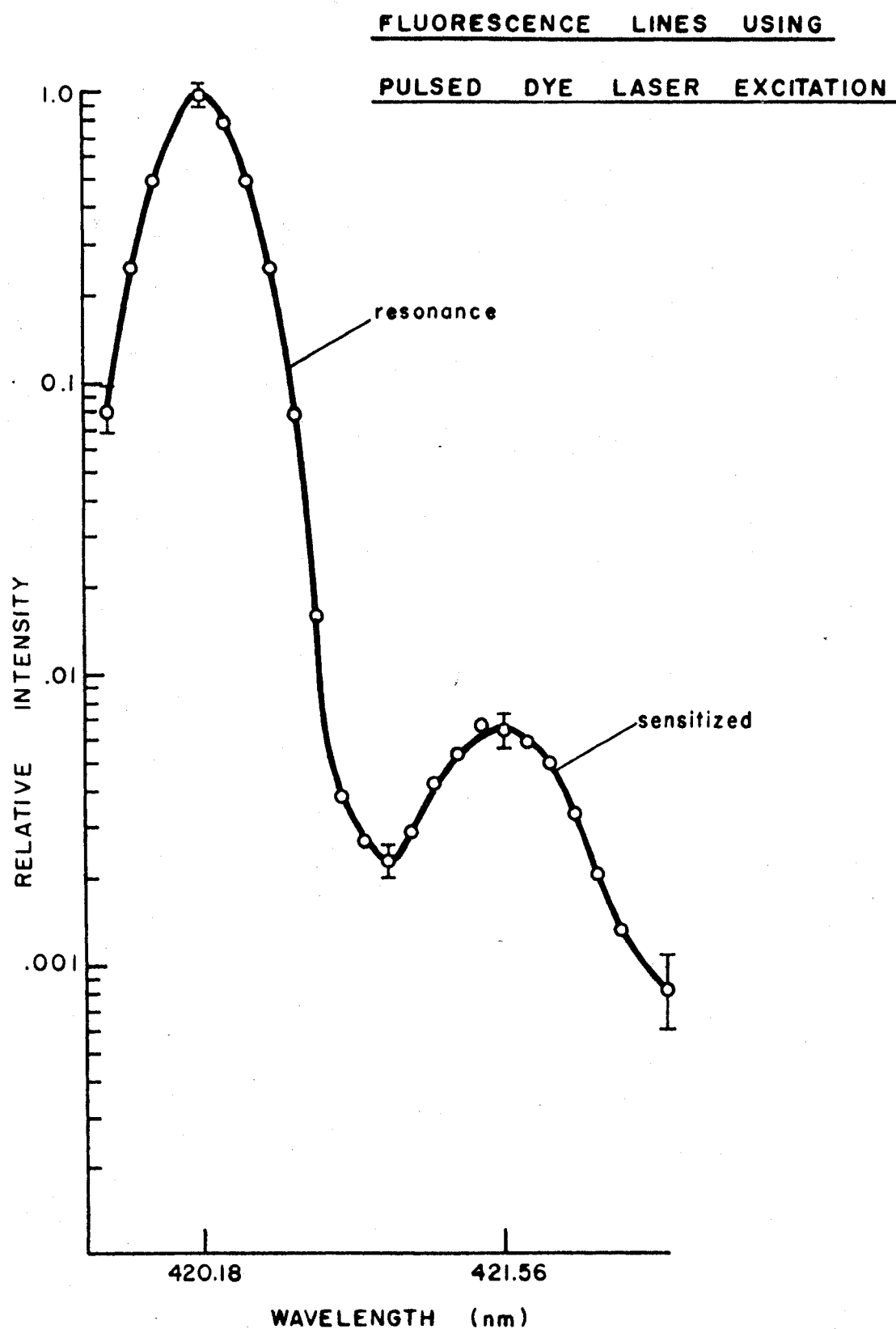


FIG. 26

states of rubidium using the dye laser as the excitation source. The spectral resolution was limited by the monochromator. The density of rubidium was adjusted to give a peak-to-peak intensity ratio of about 0.0066 ± 0.0007 . As can be seen from figure 26, the scattered light and finite resolution of the monochromator indicate that the intercept on the graph of sensitized to resonance intensity ratio against alkali density should be about 1.2×10^{-3} . This is in agreement with the value actually measured. For the same experimental conditions, the resonance lamp excitation method produced a statistical error of about 70 percent compared to an error of less than 10 percent on the above measurement. Furthermore this value of the intensity ratio is very close to the limits of detection using the resonance lamp as an excitation source in the higher excited states.

At present, it is difficult to estimate the ultimate sensitivity of the apparatus. Using the present system, a sensitized to resonance intensity ratio as small as 10^{-4} to 10^{-5} can be measured. However by using a monochromator with better resolution and with less scattered light, ratios as small as 10^{-6} to 10^{-7} may be measured.

IV. CONCLUSIONS

This report has discussed the theory and construction of an organic dye laser and the apparatus suitable for a sensitized fluorescence experiment. For the first time, the collisional energy transfer cross sections between the second excited states fine structure doublet of rubidium and cesium, colliding with ground state atoms of the same type, have been measured. In addition, the upward and the downward transition cross sections have been determined independently.

In the first part of this investigation the dye laser was discussed on the basis of the rate equation formalism. A set of rate equations describing the dye laser were developed and solved numerically to give the dye laser pulse shape, along with the output lineshape as a function of the intracavity wavelength selector bandwidth. The investigation has led to the following conclusions:

- 1) For long pulse flashlamp excited dye lasers, line narrowing down to a fraction of a nanometre can be achieved with optical filters of low dispersion.
- 2) For short pulse laser excited dye lasers, little or no 'gain narrowing' occurs. This means that the output linewidth of the laser-pumped dye laser will be essentially the same as the linewidth of any inserted filter.
- 3) The dye laser constructed for the purpose of doing a sensitized fluorescence experiment was based upon a nitrogen laser pumped dye laser. This choice was made because the

nitrogen laser pumped design is simple, reliable, has a relatively fast repetition rate and can be tuned over the entire visible spectrum.

In the second part of this investigation, the technique of sensitized fluorescence has been employed to determine the fine-structure mixing cross sections in the second excited states of rubidium and cesium induced in collisions with ground state atoms of the same type. In order to utilize the dye laser effectively, a pulse counting apparatus was developed to measure the alkalis' fluorescence. This detection system has the advantages of a large signal-to-noise ratio and the capability of measuring very small sensitized to resonance intensity ratios. The results obtained in this experiment together with the results obtained by other authors for the transitions between the first excited states and the third excited states, induced in collisions with ground state atoms of the same type indicate the following:

- 1) The alkali-alkali mixing cross sections exhibit a strong dependence on the splitting energy ΔE . In fact the dependence was found to be a smooth function of $1/\Delta E$.
- 2) The values of the cross sections calculated by the theory of Zembekov and Nikitin (1971) for the third excited states mixing in cesium do not agree with the experimental results. The work of Dashevskaya et al (1969) and Lewis (1971) on the first excited states of the alkalis also produces results that are too small. In these analyses, resonance dipole-dipole interactions, polarization interactions, exchange

interactions and intra-atomic spin-orbital interactions have been taken into account. Since the theoretical results are smaller than the experimental values by at least a factor of two, it would seem possible that additional interaction forces should be included into the formalism, or at least a re-evaluation of the above contributions is necessary.

An extension of the present study would be an investigation of the quenching and depolarization properties of the higher excited S and D states of the alkali metals. Quenching of the higher S, P and D states of sodium has been measured in a sensitized fluorescence experiment by Czajkowski et al (1972); however, by using a double resonance technique (Agárbeiceau et al 1963), or a two photon excitation process (Pritchard et al 1974, Levenson and Bloembergen 1974), previously inaccessible higher excited alkali states could be studied by the method of delayed coincidences (eg. Phaneuf et al 1971, Deech and Baylis 1971, Deech et al 1971). It would also be possible to study mixing collisions in highly excited 2D states by exciting the vapour by two photon excitation.

Another possible experiment would be an investigation of the multi-photon ionization processes that ensue when an alkali vapour is optically excited with light of sufficient energy to cause photo-ionization from the first and higher excited states. These processes have been studied by Collins et al (1973) and Popescu et al (1973) for the higher excited states of cesium; however, further study is necessary to understand the mechanisms involved in these complex processes. With the development of the dye laser it should now be

possible to study photoionization processes in several alkali metals.

APPENDIX A

EXPERIMENTAL DATA FOR CESIUM SECOND

EXCITED STATES MIXING CROSS SECTIONS

Density ($\times 10^{11} \text{ cm}^{-3}$)	μ_1 ($\times 10^{-3}$)	Density ($\times 10^{11} \text{ cm}^{-3}$)	μ_2 ($\times 10^{-3}$)
8.143	1.248(.110)	16.904	1.632(.186)
10.621	1.217(.110)	19.995	1.672(.144)
15.009	1.285(.121)	20.331	1.565(.152)
19.338	1.412(.108)	20.672	1.652(.166)
21.371	1.346(.106)	24.792	1.702(.148)
24.792	1.501(.101)	26.903	1.789(.164)
26.468	1.472(.104)	31.126	1.833(.113)
32.144	1.535(.110)	31.631	2.006(.113)
32.664	1.482(.120)	32.664	1.814(.130)
39.540	1.509(.102)	34.823	1.810(.137)
42.780	1.542(.106)	39.540	2.005(.144)
48.472	1.624(.145)	39.540	2.032(.163)
53.189	1.590(.108)	42.113	2.054(.119)
55.702	1.616(.143)	44.141	2.088(.150)
59.223	1.627(.124)	48.472	2.174(.135)
61.058	1.772(.104)	49.999	2.122(.143)
62.947	1.711(.151)	51.572	2.316(.150)
65.879	1.703(.125)	56.563	2.342(.162)
66.883	1.832(.150)	60.134	2.386(.182)
67.903	1.692(.139)	61.058	2.554(.152)
78.905	1.906(.138)	67.903	2.604(.185)
		72.122	2.775(.191)
		75.444	2.674(.189)
		80.089	2.983(.199)

EXPERIMENTAL DATA FOR RUBIDIUM SECOND
EXCITED STATES MIXING CROSS SECTIONS

Density ($\times 10^{11} \text{ cm}^{-3}$)	μ_1 ($\times 10^{-3}$)	Density ($\times 10^{11} \text{ cm}^{-3}$)	μ_2 ($\times 10^{-3}$)
4.063	1.264(.095)	5.543	1.486(.135)
5.643	1.298(.099)	7.221	1.571(.130)
6.733	1.270(.084)	8.441	1.462(.102)
9.198	1.381(.063)	9.357	1.560(.150)
9.682	1.365(.058)	10.189	1.535(.128)
11.666	1.422(.074)	11.091	1.652(.150)
12.899	1.522(.081)	13.337	1.725(.145)
13.116	1.400(.079)	13.560	1.787(.144)
17.644	1.573(.088)	17.934	1.761(.154)
23.952	1.662(.111)	20.085	1.975(.143)
26.339	1.639(.106)	21.079	1.843(.094)
27.183	1.752(.111)	24.335	1.990(.117)
31.292	1.816(.079)	26.339	2.074(.099)
31.783	1.860(.104)	28.493	2.252(.236)
34.875	1.904(.134)	32.785	2.456(.179)
38.244	1.855(.116)	36.524	2.539(.214)
43.199	1.986(.123)	40.037	2.621(.188)
48.012	2.058(.139)	42.549	2.932(.232)
52.522	2.206(.126)	44.526	2.861(.218)
		45.892	3.069(.254)
		53.311	3.076(.239)

BIBLIOGRAPHY

- Agárbiceau, I.I., Popescu, I.M., Cucurezeanu, I., Vasilu, V.
1963. C.R. Acad. Sci. 257, 2264
- Albach, G.G., Meyer, J. 1973. Rev. Sci. Inst. 44, 615
- Ali, A.W., Klob, A.C., Anderson, A.D. 1967. Appl. Optics 6, 2115
- Ali, A.W. 1969. Appl. Optics 8, 993
- Altman, E.L., Kazantsev, S.A. 1970. Opt. Spect. 28, 432
- Bass, M., Deutsch, T.F., Weber, M.J. 1971. 'Dye Lasers' in Lasers
Vol.3, A.K. Levine and A.J. DeMaria Ed.
New York: Marcel Dekker, pp 274-278
- Baylis, W.E., Walentynowicz, E., Phaneuf, R.A., Krause, L. 1973.
Phys. Rev. 31, 741
- Birks, J.B. 1970. Photophysics of Aromatic Molecules
London: Wiley-Interscience, pp 29-32, 103-235
- Born, M., Wolf, E. 1970. Principles of Optics, Oxford:
Pergamon Press
- Bowness, C. 1965. App; . Optics 4, 103
- Bradley, D.J., Durrant, A.J.F., Gale, G.M., Moore, M., Smith, P.D.
1968. IEEE J. Quant. Elec. QE-9, 707
- Bradley, D.J., Nicholas, J.V., Shaw, J.R.D. 1971. Appl. Phys.
Lett. 19, 172
- Brock, E.G., Czavinsky, P., Hormats, E., Nedderman, H.C., Stirpe, D.,
Unterleiter, F. 1961. J.Chem.Phys. 35, 759

- Broida, H.P., Haydon, S.C. 1970. Appl. Phys. Lett. 16, 142
- Bucka, H., Grosswendt, B., Sshüssler, H.A. 1966. Z.Phys. 194, 193
- Burgess, A., Seaton, M.J. 1960. Monthly Notices of Royal Ast.
Soc. 120, 121
- Capelle, G., Phillips, D. 1970. Appl. Optics 9, 517
- Capelle, G., Phillips, D. 1970a. Appl. Optics 9, 2742
- Claesson, S., Lindqvist, L. 1958. Arkviv Kemi 12, 1
- Collatz, L. 1966. The Numerical Treatment of Differential
Equations, New York: Springer-Verlag
- Collins, C.B., Johnson, B.W., Popescu, D., Musca, G., Pasu, M.L.,
Popescu, I. 1973. Phys.Rev. A8, 2197
- Copley, G.H. 1969. Ph.D. Thesis, University of Windsor
- Corson, D.R., Lorrain, P. 1962. Introduction to Electromagnetic
Waves and Fields, San Francisco: W.H. Freeman
and Company
- Cuvellier, J., Fournier, P., Gouanand, F., Berlande, J. 1973.
C.R. Acad. Sci. B276, 855
- Czajkowski, M., Krause, L., Skardis, G.M. 1973. Can. J. Phys.
51, 1582
- Dashevskaya, E.I., Voronin, A.I., Nikitin, E.E. 1969. Can. J. Phys.
47, 1237
- Deech, J.S., Baylis, W.E. 1971. Can. J. Phys. 49, 90
- Deech, J.S., Pitre, J., Krause, L. 1971. Can. J. Phys. 49, 1976
- Drobrowolski, J.A. 1959. J. Opt. Soc. Am. 49, 794
- Evtuhov, V., Neeland, J.K. 1967. Appl. Optics. 6, 437
- Feofilov, P.P. 1961. The Physical Basis of Polarized Emission
New York: Consultants Bureau

- Ferrar,C.M. 1969. Rev. Sci. Inst. 40, 1436
- Franck,J. 1929. Naturwissenschaften 14, 211
- Gallagher,A. 1968. Phys. Rev. 172, 88
- Gallagher,J.H. 1969. Ph.D. Thesis, University of Colorado.
- Gerry,E.T. 1965. Appl. Phys. Lett. 7, 6
- Gleason,T.J.,Willett,G.S.,Curnutte,R.M.,Kruger,J.S. 1972.
Appl. Phys. Lett. 21, 276
- Gibson,A.J. 1969. J. Sci. Inst. 2, 802
- Hänsch,T.W.,Schawlow,A.L. 1970. Bull. Am. Phys. Soc. 15, 1638
- Hänsch,T.W.,Varsangi,F.,Schawlow,A.L. 1971. Appl. Phys. Lett.
18, 108
- Hänsch,T.W.,Shahnin,I.S.,Schawlow,A.L. 1971a. Phys. Rev. Lett.
27, 707
- Hänsch,T.W. 1972. Appl. Optics 11, 895
- Hänsch,T.W.,Shahnin,I.S.,Schawlow,A.L. 1972. Nature Phys.
Sci. 235, 63
- Heard,H.G. 1963. Nature 200, 667
- Heavens,O.S. 1961. J. Opt. Soc. Am. 51, 1058
- Heller,A. 1968. J. Mol. Spect. 28, 101
- Heller,A. 1968a. J. Mol. Spect. 28, 208
- Hercher,M.,Pike,H.A. 1971. Optics Commun. 3, 172
- Holzrichter,J.F.,Schawlow,A.L. 1970. Annals of New York Acad.
Sci. 168, 703
- Hrycyshyn,E.S.,Krause,L. 1969. Can. J. Phys. 47, 223
- Huth,B.G.,Kagan,M.R.,Farmer,G.I. 1970. IBM Tech. Report
AFAL-TR-70-294, Wright-Patterson Air Force Base

- Itzkan, I., Cunningham, F.W. 1971. IEEE J. Quant. Elec. QE-7, 14
- Keller 1970. IEEE J. Quant. Elec. QE-6, 411
- Kogelnik, H. 1965. Bell Systems. Tech. J.
- Kogelnik, H., Li, T. 1966. Appl. Optics 5, 1550
- Kogelnik, H., Shank, C.V., Sosnowski, T.P., Dienes, A. 1970.
Appl. Phys. Lett. 16, 499
- Krause, L. 1966. Appl. Optics 5, 1375
- Kuhl, J., Marowsky, G. 1971. Opt. Commun. 4, 125
- Lempicki, A., Samelson, H. 1966. 'Organic Laser Systems' in
Lasers, A.K. Levine Ed. pp. 181-252
- Leonard, D.A. 1965. Appl. Phys. Lett. 7, 4
- Levenson, M.D., Bloembergen, N. 1974. Phys. Rev. Lett. 32, 645
- Lewis, E. 1971. Phys. Lett. 35A, 387
- Loth, C., Astier, R., Meyer, Y.H. 1972. J. Phys. E. 5, 169
- Mack, M.E. 1968. J. Appl. Phys. , 2483
- Markova, G., Khostenko, G., Chaika, M. 1967. Opt. Spect. 23, 456
- Massey, H.S.W. 1971. Electronic And Ionic Impact Phenomena III
Oxford: Clarendon Press, pp 1925-1928
- Massone, C.A., Garavaglia, M., Gallardo, M., Calatroni, J.A.E.
Tagliaferri, A.A. 1972. Appl. Optics 11, 1317
- Mathias, L.E.S., Parker, J.T. 1963. Appl. Phys. Lett. 3, 16
- McGillis, D.A., Krause, L. 1968. Can. J. Phys. 46, 1051
- Moore, C.E. 1952. Atomic Energy Levels, Vol.2
Washington: NBS
- Myer, J.A., Johnson, C., Sharma, R., Itzkan, I. 1970. Appl. Phys.
Lett. 16, 1

- Myer, J.A., Itzakan, I., Kierstead, E. 1970a. *Nature* 225, 594
- Nesmeyanov, N. 1963. *Vapour Pressure of the Elements*,
New York: Academic Press
- Ocheltree, S.L., Story, R.W. 1973. *Rev. Sci. Instr.* 44, 367
- Peterson, O.G., Tuccio, S.A., Snavely, B.B. 1970. *Appl. Phys. Lett.*
17, 245
- Phaneuf, R.A. 1970. M.Sc. Thesis, University of Windsor
- Phaneuf, R.A. 1973. Ph.D. Thesis, University of Windsor
- Phaneuf, R.A., Pitre, J., Hammond, K., Krause, L. 1973. *Can. J. Phys.*
51, 724
- Pimbert, M. 1972. *Journal de Physique* 23, 331
- Pitre, J., Krause, L. 1969. *Can. J. Phys.* 45, 2671
- Pitre, J., Krause, L. 1968. *Can. J. Phys.* 46, 125
- Popescu, D., Pascu, L., Collins, C.B., Johnson, B.W., Popescu, I.
1973. *Phys. Rev.* A8, 1666
- Popescu, D., Collins, C.B., Johnson, B.W., Popescu, I. 1974.
Phys. Rev. A9, 1182
- Pritchard, D., Apt, J., Ducas, T.W. 1974. *Phys. Rev. Lett.* 32, 641
- Rautain, S.G., Sobel'mann, I.I. 1961. *Opt. Spect.* 10, 65
- Rocchiccioli, J.L. 1972. *C.R. Acad. Sci.* B274, 787
- Schäfer, F.P., Schmidt, W., Volze, J. 1966. *Appl. Phys. Lett.* 9, 306
- Schmidt, W., Schäfer, F.P. 1967. *Z. Naturforsch.* 22A, 1563
- Shank, C.V., Dienes, A., Silfast, T.W. 1970. *Appl. Phys. Lett.*
17, 307
- Shenck, P. 1973. Private Communication
- Shipman Jr., J.D. 1967. *Appl. Phys. Lett.* 10, 3

- Shurcliff, W.A. 1962. Polarized Light, Cambridge Mass.:
Harvard University Press
- Siara, I., Hrycyshyn, E.S., Krause, L. 1972. Can. J. Phys.
50, 1826
- Siara, I., Krause, L. 1972a. Can. J. Phys. 51, 257
- Siara, I. 1972. Ph.D. Thesis, University of Windsor.
- Siara, I., Kwong, H.S., Krause, L. 1974. Can. J. Phys. (in print)
- Snavely, B.B. 1969. Proc. IEEE 57, 1374
- Snavely, B.B., Schäfer, F.P. 1969a. Phys. Lett. 28A, 728
- Soffer, B.H., McFarland, B.B. 1967. Appl. Phys. Lett. 10, 260
- Sorokin, P.P., Lankard, J.R. 1966. IBM J. Res. Dev. 10, 162
- Sorokin, P.P., Lankard, J.R., Hammond, E.C., Moruzzi, V.L. 1967.
IBM J. Res. Dev. 11, 130
- Sorokin, P.P., Lankard, J.R. 1967. IBM J. Res. Dev. 11, 148
- Sorokin, P.P., Lankard, J.R., Moruzzi, V.L., Hammond, E.C. 1968.
J. Chem. Phys. 48, 4726
- Spaeth, M.L., Bortfield, D.P. 1966. Appl. Phys. Lett. 9, 179
- Stockmann, D.L., Mallory, W.R., Tittel, K.F. 1964. Proc. IEEE
52, 318
- Stupavsky, M., Krause, L. 1968. Can. J. Phys. 46, 2127
- Stupavsky, M., Krause, L. 1969. Can. J. Phys. 47, 1249
- Taylor, D.J., Harris, S.E., Nieh, S.T.K., Hänsch, T.W. 1971. Appl.
Phys. Lett. 19, 269
- Vrehan, O.H.F. 1971. Opt. Commun. 3, 144
- Walther, H., Hall, J.L. 1970. Appl. Phys. Lett. 17, 239
- Warden, J.T., Gough, L. 1971. Appl. Phys. Lett. 19, 345

- Warner,B. 1968. Mon. Not. R. Astr. Soc. 139, 115
- Wildey,C.G. 1971. J. Phys. E. 4, 257
- Winston,H.,Gudmundsen,R.A. 1964. Appl. Optics 3, 143
- Wood,R.W.,Dunoyer,L. 1914. Phil. Mag. 27, 1018
- D'Yakonov,M.I.,Perel',V.I. 1965. JETP 20, 997
- Zembekov,A.A.,Nikitin,E.E. 1971. Chem. Phys. Lett. 9, 213

VITA AUCTORIS

I Was born on October 5, 1946 in Toronto , Ontario. At the age of six my family moved to Brampton, Ontario where I graduated from Brampton High School in 1965. I then enrolled in the Honours Applied Physics program at the University of Waterloo. After graduation in 1970 I enrolled in the Faculty of Graduate Studies at the University of Toronto, Institute For Aerospace Studies. After receiving a M.A.Sc. degree in Aeronautical Engineering in 1971 I enrolled in the Faculty of Graduate Studies at the University of Windsor and proceeded to work towards a degree in experimental atomic and laser physics at the Ph.D. level. During my last two years of study at the University of Windsor I was the holder of a National Research Council of Canada Graduate Scholarship.